EFFECT OF FORMATION WATER AND SURFACTANT CHARACTERISTICS ON RESERVOIR ROCK SURFACE CHARGES AND THEIR ZETA POTENTIALS

AZAD ANUGERAH BIN ALI RASOL

UNIVERSITI TEKNOLOGI MALAYSIA

UNIVERSITI TEKNOLOGI MALAYSIA

DECLARATION OF THESIS AND COPYRIGHT

Author's full name : **AZAD ANUGERAH BIN ALI RASOL**

Date of Birth : **3rd JANUARY 1988**

Title : **EFFECT OF FORMATION WATER AND SURFACTANT CHARACTERISTICS ON RESERVOIR ROCK SURFACE CHARGES AND THEIR ZETA POTENTIALS**

Academic Session : **2020/2021-1**

I declare that this thesis is classified as:

☐	**CONFIDENTIAL**	(Contains confidential information under the Official Secret Act 1972) *
☐	**RESTRICTED**	(Contains restricted information as specified by the organization where research was done) *
☑	**OPEN ACCESS**	I agree that my thesis to be published as online open access (full text)

I acknowledged that Universiti Teknologi Malaysia reserves the right as follows:

1. The thesis is the property of Universiti Teknologi Malaysia
2. The Library of Universiti Teknologi Malaysia has the right to make copies for the purpose of research only.
3. The Library has the right to make copies of the thesis for academic exchange.

SIGNATURE OF STUDENT

PKP153014

MATRIC NUMBER

Date: 28 APRIL 2021

Certified by:

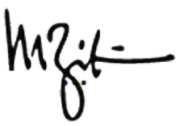

SIGNATURE OF SUPERVISOR

ASSOC. PROF. IR. DR. MOHD ZAIDI JAAFAR

NAME OF SUPERVISOR

Date: 28 APRIL 2021

NOTES: * If the thesis is CONFIDENTAL or RESTRICTED, please attach with the letter from the organization with period and reasons for confidentiality or restriction.

"We hereby declare that we have read this thesis and in our opinion this thesis is sufficient in terms of scope and quality for the award of the degree of Doctor of Philosophy in Petroleum Engineering"

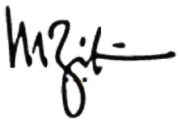

Signature : …….....

Name of Supervisor I : ASSOC. PROF. IR. DR. MOHD ZAIDI JAAFAR

Date : 28 APRIL 2021

Signature : …….....

Name of Supervisor II : EMERITUS PROF. DR. AHMAD KAMAL

Date : 28 APRIL 2021

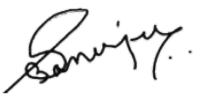

Signature : …….....

Name of Supervisor III : DR. SULALIT BANDYOPADHYAY

Date : 28 APRIL 2021

BAHAGIAN A – Pengesahan Kerjasama*

Adalah disahkan bahawa projek penyelidikan tesis ini telah dilaksanakan melalui kerjasama antara ________________________ dengan ________________________

Disahkan oleh:

Tandatangan : ……………………………….. Tarikh : …………………….

Nama : ……………………………………….

Jawatan : ……………………………………..

(Cop rasmi)

** Jika penyediaan tesis/projek melibatkan kerjasama.*

=:=

BAHAGIAN B – Untuk Kegunaan Pejabat Sekolah Pengajian Siswazah

Tesis ini telah diperiksa dan diakui oleh:

Nama dan Alamat Pemeriksa Luar :

Nama dan Alamat Pemeriksa Dalam :

Nama Penyelia Lain (jika ada) : ……………………………………………..

……………………………………………..

……………………………………………..

Disahkan oleh Timbalan Pendaftar di SPS:

Tandatangan : ………………………………….. Tarikh: …………………

Nama: ………………………………………….

EFFECT OF FORMATION WATER AND SURFACTANT CHARACTERISTICS ON RESERVOIR ROCK SURFACE CHARGES AND THEIR ZETA POTENTIALS

AZAD ANUGERAH BIN ALI RASOL

A thesis submitted in fulfilment of the
requirements for the award of the degree of
Doctor of Philosophy

School of Chemical and Energy Engineering
Faculty of Engineering
Universiti Teknologi Malaysia

APRIL 2021

DECLARATION

I declare that this thesis entitled "*Effects of Formation Water and Surfactant Characteristics on Reservoir Rock Surface Charges and their Zeta Potentials*" is the result of my own research except as cited in the references. The thesis has not been accepted for any degree and is not concurrently submitted in candidature of any other degree.

Signature : .....

Name : AZAD ANUGERAH BIN ALI RASOL

Date : 28 APRIL 2021

DEDICATION

Keeping knowledge to yourself is like keeping salt in the ocean. Too high salt concentration, makes the ocean 'dead'.

ACKNOWLEDGEMENT

In the nama of Allah, the most Gracious and the Most Merciful. Alhamdulillah. All praises to Allah. For all the things You have given to me, I never thanked You once.

I would like to express my sincere gratitude to my supervisor PM. Ir. Dr. Mohd Zaidi Jaafar for all the continuous support of my PhD study, for his patience, motivation, enthusiasm and immense knowledge. His guidance helped me during the research and writing of this thesis. An equal thanks to Prof. Dr. Ahmad Kamal for his continuous guidance, valuable advise and untiring support over these years especially on writing this thesis. Special thanks to Dr. Sulalit from NTNU for his great guidance in understanding fundamental theories in this work, his warm friendship and his fabulous insight in experimental work.

Next on the list, eternal thanks to my wife, Dr. Siti Aminah, for her love and constant support. To my mother, Azimah and father, Ali Rasol, thank you for your prayers, love, support, sacrifices and unwavering belief in me. Thanks also to my brothers and sister who are supportive in whatever I do in my life. A special mention to my in-laws, for your prayers and supports.

I would also like to thank my best friends, Shamsul, Suriani, Amran and Shye for always offering assistance during this time. Last but not least, I would like to record my sincere thanks to the Ministry of Education Malaysia and Universiti Teknologi Malaysia (UTM) for financial support. An extra warm thank you to everyone who helped me in making this study a reality.

ABSTRACT

The loss of injected surfactants in the oil reservoir during a surfactant flooding due to adsorption onto the rock surface weighs heavily on economics. Surfactant adsorption weakens the efficiency for the oil-water interfacial tension reduction. Several factors that influence the surfactant adsorption have been investigated, including the effect of temperature, as well as the concentration and charge of the surfactants. However, the impact of rock surface charge and zeta potential on surfactant adsorption has remained uncertain. This is because the surface charge development of the rock is complex depending on the effect of rock mineralogy, pH, brine salinity, and ionic strength of the ions present. This project aimed to develop an improved understanding of these effects on the rock surface charge and its contribution to the surfactant adsorption. These objectives were achieved through detailed laboratory measurement of surface charge density and zeta potential of silica and kaolinite by electrophoretic light scattering at different pH, brine salinities, and ionic strength. There were three different surfactant types used: anionic, zwitterionic, and non-ionic, which are represented by sodium dodecyl sulphate, coco betaine, and triton X-100, respectively, to investigate their adsorption on the surface of silica and kaolinite. The mineral characterization study shows that SiO_2 and Al_2O_3 were dominant chemical compound in both silica and kaolinite, which reflect their surface charge. The experimental work demonstrates that silica has a negative surface charge for pH exceeding 4.4 at all NaCl concentrations from 0.01M to 1M. However, in $CaCl_2$ solutions, the negative surface charge of silica turns to a positive charge at 0.1M for pH exceeding 8.7 and becomes more positively charged at a concentration of 1M. Different surface charge behavior was observed for kaolinite, which it is negatively charged at all NaCl concentrations from 0.01M to 1M. Moreover, both negative and positive charges were observed in $CaCl_2$ solutions. At pH of less than 10.8, the kaolinite surface indicates a negative charge at both concentrations of 0.01M and 0.1M. The positive charge of kaolinite was observed at a concentration of 1M with pH exceeding 4.4. These results indicate that pH, salt concentration (salinities), and salt types (ionic strength) have a major influence on the surface charge behavior of silica and kaolinite..

ABSTRAK

Kehilangan surfaktan tersuntik di dalam reservoir minyak ketika banjiran surfaktan berikutan penjerapannya pada permukaan batuan memberi impak yang besar terhadap ekonomi. Penjerapan surfaktan mengurangkan kecekapan untuk merendahkan ketegangan permukaan minyak-air. Beberapa faktor yang mempengaruhi penjerapan surfaktan telah dikaji termasuk kesan suhu, kepekatan dan cas surfaktan. Walau bagaimanapun, kesan cas permukaan batuan dan potensi zeta terhadap penjerapan surfaktan masih samar. Puncanya ialah pembentukan cas permukaan pada batuan adalah rumit, yang bergantung pada kesan mineralogi batuan, pH, kemasinan air garam, dan kekuatan ion-ion yang wujud. Projek ini bertujuan untuk menghasilkan pemahaman yang lebih baik tentang pengaruh faktor-faktor terbabit terhadap cas permukaan batuan dan kesannya pada penjerapan surfaktan. Semua objektif ini telah dicapai menerusi kajian makmal terhadap ketumpatan cas permukaan dan potensi zeta silika dan kaolinit, yang telah dilaksanakan secara terperinci dengan mengaplikasi penyerakan cahaya elektroforetik pada pH, kemasinan air garam, dan kekuatan ion yang berbeza. Tiga jenis surfaktan telah diguna: anion, zwiterion, dan bukanion, dengan masing-masing bahan kimia ialah natrium dodesil sulfat, koko betaina, dan triton X-100, bagi mengkaji penjerapan ketiga-tiga surfaktan itu pada permukaan silika dan kaolinit. Kajian pencirian mineral menunjukkan bahawa SiO_2 dan Al_2O_3 ialah sebatian kimia utama yang terdapat pada silika dan kaolinit, yang telah menentukan cas permukaan masing-masing. Data uji kaji menunjukkan bahawa silika mempunyai cas permukaan yang negatif pada pH 4.4 ke atas bagi semua kepekatan NaCl dari 0.01M hingga ke 1M. Walau bagimanapun, dalam larutan $CaCl_2$, cas permukaan negatif silika berubah kepada cas positif pada kepekatan 0.1M dan pH melebihi 8.7, dan seterusnya menjadi cas yang lebih positif pada kepekatan 1M. Tingkah laku cas permukaan yang berbeza belaku pada kaolinit dengan cas negatif terbentuk pada semua kepekatan NaCl dari 0.01M hingga ke 1M. Tambahan lagi, cas negatif dan cas positif telah terbentuk pada larutan $CaCl_2$. Bagi pH kurang daripada 10.8, permukaan kaolinit menunjukkan cas negatif pada kedua-dua kepekatan 0.01M dan 0.1M. Kaolinit bercas positif telah terbentuk pada kepekatan 1M dengan pH yang melebihi 4.4. Hasil kajian ini menunjukkan bahawa pH, kepekatan garam (kemasinan), dan jenis garam (kekuatan ion) mempunyai pengaruh yang besar terhadap tingkah laku cas permukaan silika dan kaolinit.

TABLE OF CONTENTS

LIST OF TABLES

LIST OF FIGURES

LIST OF ABBREVIATIONS

ASP	-	Alkaline surfactant flooding
BET	-	Brunauer-Emmett-Teller
CEOR	-	Chemical enhanced oil recovery
CMC	-	Critical micelle concentration
CPC	-	Critical packing parameter
DLS	-	Dynamic light scattering
EOR	-	Enhanced oil recovery
EDL	-	Electrical double layer
FESEM	-	Field Emission Scanning Electron Microscope
FTIR	-	Fourier Transform Infrared
IFT	-	Interfacial tension
IEP	-	Isoelectric point
IHP	-	Inner Helmholtz Plane
OHP	-	Outer Helmholtz Plane
PZC	-	Point of zero charge
SDS	-	Sodium dodecyl sulphate
SEM	-	Scanning Electron Microscope
TGA	-	Thermal Gravimetric Analysis
XRD	-	X-ray Diffraction
XRF	-	X-ray Fluorescence

LIST OF SYMBOLS

F	-	Force
v	-	Velocity
p	-	Surface charge density
r	-	distance
N_c	-	Capillary number
T	-	Absolute temperature
π	-	pi
V	-	Electric potential
a	-	radius
k_b	-	Boltzmann constant
ε	-	Constant permittivity
H^+	-	Hydrogen ion
OH^-	-	Hydroxyl ion
C_i	-	Ionic strength
Z_i	-	Ion charge
$1/\kappa$	-	Debye length

CHAPTER 1

INTRODUCTION

1.1 Background of Study

> "He has let free the two bodies of owing water, meeting together. Between them is a barrier which they do not transgress." (The Quran) [1]

The above refers to the interface-related phenomena in nature. Interfaces are truly ubiquitous. They play an essential role in diverse areas ranging from the cell to black holes. The unique characteristic of the interface is its interfacial tension (IFT). The manifestation of IFT and its essential role can be observed in everyday life; the demixing of oil and water, coating of ice cream in soft drinks in making ice cream soda, the rising of water when putting a straw in a glass of water and a few other occurrences. All these phenomena are a microscopic demonstration of the force between molecules, which has attracted scientists to explore and expand the knowledge of interfaces. Scientifically, the study of the interface phenomena has a long history; it brings the great name of van der Waals to mind, who was the first to propose the theory of interfaces, which led to the thermodynamic description of a flat interface between a gas and a liquid [2]. In 1908, von Smoluchowski then realized that the interface is rough, corrugated by thermal capillary waves [3]. Their theories continue to inspire other research from a variety of fields to further investigate interfaces.

In the oil industry, enhancing oil production especially in the existing and matured oil fields is a crucial task for oil companies but is challenging because a considerable part of the oil remains trapped by the capillary forces [4]. The cause of capillary forces is due to interfacial phenomena raised between the water and oil in

the porous reservoir rock. Strong oil-water IFT keeps oil immobile and traps in porous media as shown in Figure 1.1**.** This phenomenon is causing about 70% of oil to remain unproducible in the subsurface reservoir rock [5,6]. Thus, IFT plays a vital parameter in controlling oil recovery.

At the microscopic view, the flow of oil in porous rock toward a producing well is subjected to capillary numbers. The capillary number is crucial in determining the remaining oil saturation [7]. Capillary numbers (N_C) is defined as a ratio of viscous forces to the capillary forces [8]. An increase in Nc indicates an increase in oil recovery, which could be achieved either by increasing the viscous power or reducing the capillary forces [9,10]. Lowering oil-water IFT has become central in the reduction of capillary forces; thus, unlocking the trapped oil.

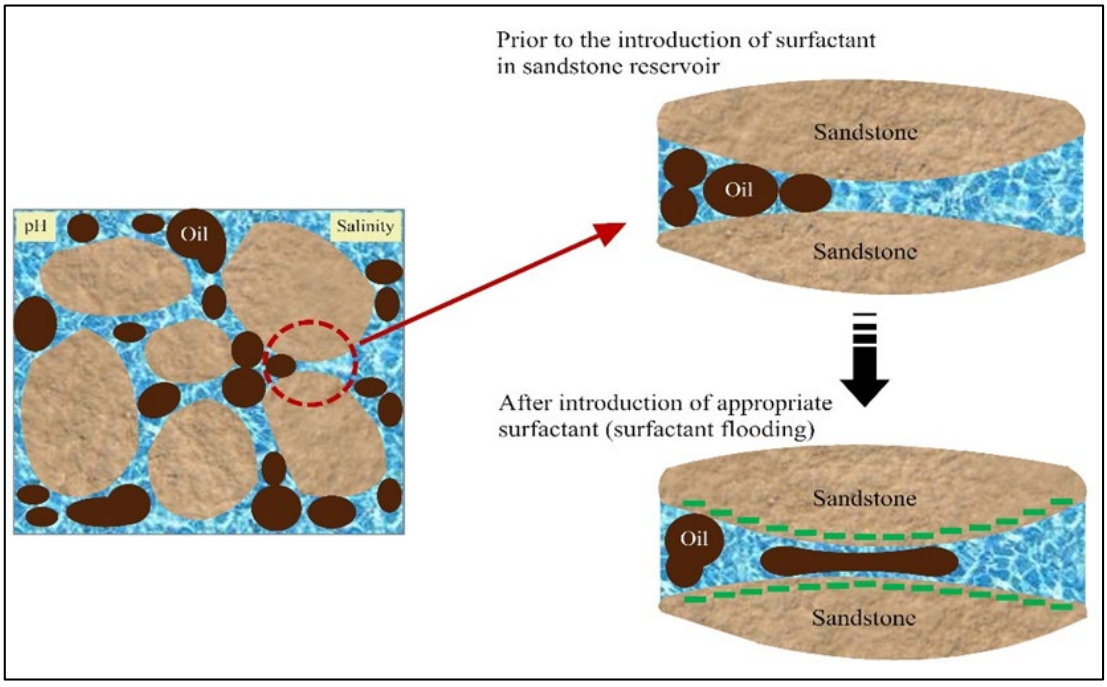

Figure 1.1 The schematic representation of (a) oil trapped within the pore throat (b) oil mobilized by lowering IFT with surfactant solution injection.

To reduce the oil-water IFT, the application of surfactants in the oil industry is introduced. This is known as surfactant flooding [11–13]. Surfactant flooding is a technology that employs surfactant in the injection fluids to lower the oil-water IFT [14–16]. The surfactant flooding process aims to achieve favorable phase behavior of the oil-water interface at ultra-low (0.001mN/m targeted) [17,18] IFT in order to

mobilize the trapped oil [13,19]. Whenever the oil is in contact with water, the surfactants are accumulated at the oil-water interface and formed an adsorbed film, which lowers the IFT between them [20].

Successful implementation of surfactant flooding has been recorded by Gao et al. [21]. They reported that surfactant flooding was implemented in Shengli field since 1922 in over 60 wells. Most surfactant flooding projects showed an increment in oil production and lasted for several years. Likewise, Belhaj et al. [22] documented that successful surfactant flooding has been achieved in other fields in the United States, Germany, Austria, and Canada. However, surfactant flooding shows expensive recovery due to high-cost chemicals.

The high cost of surfactant flooding is associated with surfactant losses during the process. As a result, a substantial amount of surfactant is needed [23]. Surfactant losses occur in the reservoir due to different mechanisms; (1) surfactant adsorption, (2) surfactant precipitation, and (3) surfactant degradation [23,24]. Surfactant losses due to precipitation can be avoided by choosing a surfactant that is tolerant of temperature and salt [22]. However, Kamal et al. [25] and Gogoi et al. [26] reported that surfactant adsorption cannot be avoided but can only be minimized. Surfactant adsorptions [18,27,28] the most dominant factor that controls surfactant losses. Surfactant adsorption on rock surfaces results in a loss, reducing the available surfactant concentration to be used for the oil-water IFT reduction [18,29], thus reduces its feasibility from an economic perspective.

Numerous studies have been done in the past to investigate the mechanism of surfactant adsorption. Various factors were found to affect surfactant adsorption. Azam et al. [30], Paria et al.[31] and Somasundaran [32] reported surfactants concentration, surfactant types, ionic strength, pH, salinity and temperature are the parameters that control the degrees of surfactant adsorption.

To date, the characteristic of surfactant adsorption has been extensively studied for various combination of surfactants such as anionic [33–35], non-ionic surfactant [36–39] zwitterionic surfactant [40–42] and reservoir rock samples

[26,29,34,36,43]. According to Dang et al. [44] in 2011, anionic surfactant adsorption increases with increments in sodium chloride (NaCl) concentration. A similar finding reported by Bera et al.[34] in 2013, in which the amount of sodium dodecyl sulfate (SDS) (anionic) adsorption on the sand surface increases with increased salinity. However, the effect of divalent ion such $CaCl_2$ was remain uncertain.

Additionally, surfactant adsorption studies on silica surface [38,45], quartz [46] and carbonate rock [47,48] are described in detail. The studies show that surfactant adsorption is also dependent on the rock mineralogy and its surface charge. This is supported in a recent study by Rahul et al. [49] and Afeez et al. [50] indicating that the mineralogy of the reservoir and their surface charge significantly controls the surfactant adsorption and the selection of surfactants used. Most of the oil reservoir rock is charged either negatively or positively in nature, depending on the mineralogy of the rock [41,51,52]. Practically the adsorption can be minimized by having a similar charge of surfactant with the rock surfaces. A similar charge causes a repulsive force at surfactant-solid interfaces, thus preventing adsorption from taking place.

The role of surface charge in the adsorption mechanism has been documented by Marek et al. [53]. Besides rock mineralogy, the surface charge is also dependant on the pH and salinity of formation water in the reservoir. The isoelectric point (IEP), zeta potential and ionic strength are used to describe the relationship. IEP is a pH where the zeta potential value is zero, which means the negative and positive charge is in balance. The surface charge is highly dependant on the IEP. When the pH of the solution is over the IEP, the surface charge is negative and vice-versa [54]. At the same time, the zeta potential is also influenced by ionic strength. The presence of different types of salt, such as mono and divalent ions will significantly affect the ionic strength, thus effecting the zeta potential and IEP of the solid surface charge [41,54].

The surfactant adsorption system in porous media is genuinely complex. Even though many research have been done, there are still uncertainties associated

with the interpretation of measurement, especially concerning the role of surface charge, pH, salinity and ionic strength to the surfactant adsorption mechanism. The surface charge is the key to selecting the appropriate surfactant in the surfactant flooding process. Therefore, to understand the surface charge development and its association with adsorption is essential, and it has been the motivation of this study.

1.2 Problem Statement

Finding an excellent model system in describing surfactant adsorption phenomena in an oil reservoir can be a problematic process. Many factors have to be dealt with, and Figure 1.2 helps to break the complexity in understanding the surfactant adsorption mechanism in the oil reservoir rock.

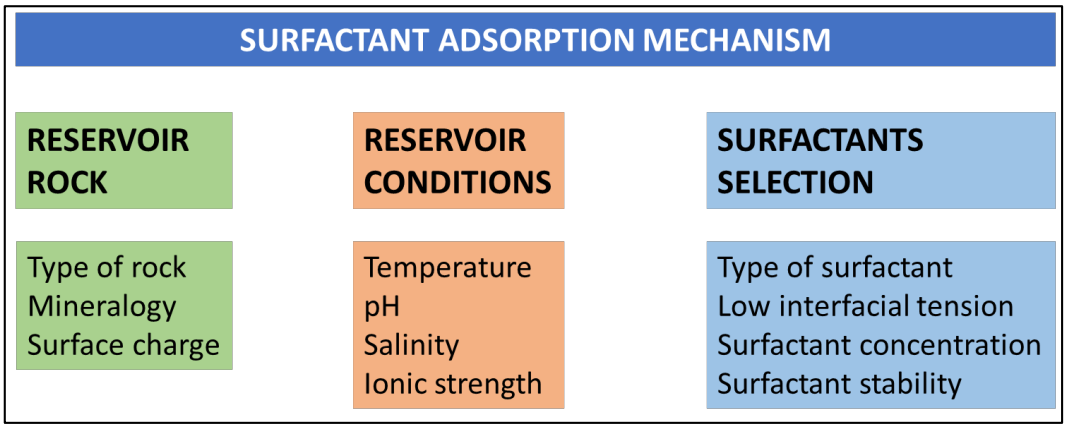

Figure 1.2 The schematic representation of the surfactant adsorption factors.

Surfactant adsorption onto the porous rock is very dependant on the reservoir rock type, reservoir condition, and surfactant types that are used in the surfactant flooding process. The reservoir conditions, especially pH, salinity and ionic strength (due to valent ion) are the central parameters controlling the interaction properties of both reservoir rock and the surfactant.

The interaction between the reservoir fluid and rock surface makes the rock surface positively or negatively charged depending on the mineralogy of the rock. However, the rock mineralogy is not the only factor that controls the rock surface

charge. This is because the pH may significantly affect the surface charge. Modification of the surface charge can vary with different pH. Point zero charge (PZC) is an indication where the surface charge can change from positive to negative or vice-versa. PZC measures the pH where the negative and positive charge is in balance. When the reservoir pH is above the PZC value, it means the rock surface has a negative charge. With this, the surfactant that has a similar charge should be used for surfactant flooding to minimize the surfactant adsorption.

The role of zeta potential and its relation to surfactant adsorption is still a major debate. Zeta potential also varies with pH. The pH where the zeta potential is zero is called an isoelectric point (IEP). The zeta potential may determine the forces involved in surfactant adsorption process either by a repulsive or attractive force. However, the mechanism of these forces needs further investigation because they are related to the salinity and the presence of valent ions in the reservoir fluid. On the other hand, the correlation between the surface charge and the zeta potential is still uncertain.

1.3 Research Goal

The project aims to develop an improved understanding of the surface charge development on different types of reservoir minerals under different reservoir conditions. The study will further investigate how this surface charge influences the selection of surfactant types and the adsorption into reservoir rock. In detail, the objectives of this research are as follows:

i. To characterise the mineralogy of reservoir rock minerals and their physicochemical properties.
ii. To examine the surface zeta potential behavior of the reservoir rock minerals at different pH, salinity, and ionic strength.
iii. To investigate the stability of different surfactant types on different reservoir environment primarily by temperature and salinity.

iv. To investigate the zeta potential behavior at the surface of rock minerals with different types of surfactants and salinity.

1.4 Scope of the Study

To achieve the objectives of the research, several parameters within the study are specified. Firstly, reservoir minerals used in this study are silica and kaolinite. Silica is vital because it is widely found in sandstone. Kaolinite is a clay minerals that are also significant because their existence, even in a small amount, is likely to affect the rock surface charge. Various characterization techniques was used to identify their chemical compounds and also physical properties. The main chemical compound present in the silica and kaolinite was measured by X-ray Diffraction (XRD) analysis. An analysis of Fourier Transform Infrared Spectroscopy (FTIR) was carried out to detect the structure and chemical bonding of the chemical compound. The physical properties such as surface area, pore size, particle size, and surface morphology are also measured.

Secondly, there are three different types of surfactants used in this study: anionic, zwitterion, and non-ionic. Sodium Dodecyl Sulphate (SDS), Coco Betaine, and Triton X-100, respectively. The critical micelle concentration (CMC) of the surfactants was determined by measuring their surface tension values at varying surfactant concentrations and different salinity using a tensionmeter. The surfactant stability at various temperature ranges was measured by thermal gravimetric analysis (TGA).

Thirdly, the determination of the surface charge of reservoir minerals is investigated under various ranges of pH, salinity and ionic strength. Hydrochloric acid (HCl) and sodium hydroxide (NaOH) was used to adjust the desired pH of the solutions from pH 2 to 12. Sodium chloride (NaCl) and Calcium Chloride ($CaCl_2$) was used to produce reservoir formation water at different salinity and ionic strength. The surface charge of the reservoir materials was determined by measuring zeta potential using the electrophoretic light scattering approach. The result of the

pH/salinity/ionic strength versus the surface zeta potential enables the determination of the isoelectric point (IEP) of the reservoir materials, which will be essential to identify the types of surfactants used for the surfactant flooding process.

The last part is the adsorption study. This experimental study was conducted at static conditions. The surfactant was employed based on the surface charge obtained. Zeta potential approach was used to discuss all the surfactant adsorption phenomena together with explanations from published literature.

1.5 Significance of the Study

This study provides a comprehensive understanding of the underlying principle, surfactant adsorption in the surfactant flooding process with regards to the surface charge of the rock, the reservoir condition, and surfactant selection. The findings would benefit the oil industry in the sense of filling the knowledge gap on the role of surface charge for designing an effective surfactant flooding from its losses.

Besides, the adoption of zeta potential measurement not only enables discussion on the adsorption process concerning pH, salinity and ionic strength, but also describes the force involved such as attractive and repulsive forces.

CHAPTER 2

LITERATURE REVIEW

2.1 Overview of Enhanced Oil Recovery

Enhanced oil recovery is a way forward for the oil industry when faced with pressing challenges to increase well productivity to fulfill the increasing demand for oil base energy, particularly in developed and developing countries. The need to maximize the existing well productivity is in conjunction with the limited discovery of new oil fields. Many oilfields are in the mature stage with decreasing production rate. Enhanced oil recovery (EOR), with its various technologies such as chemical enhanced oil recovery (CEOR), gaseous injection and thermal alteration, shows a promising approach to overcome declining oil production. The EOR technologies are, however, very much dependent on the type of reservoir, physical and fluid properties, economic scenario, and also the crude oil price. Therefore, the feasibility of EOR is significantly affected by these factors.

The maximizing of the existing oil well productivity is meant to recover the remaining unproducible oil in the reservoir. The production of oil reservoirs is initiated by their natural energy sources including the initial reservoir pressure, gas cap drive, solution gas drive, natural water drive, fluid and rock expansion, and gravity drainage [13,55]. This production stage is well known as the primary stage (Figure 2.1). The recovery factor of this stage is typically low, ranging from five to 30 percent of the original oil in place [56]. The limitation of this stage is due to the decline in the strength of their energy over the time of production. As a result, the energy is no longer able to pump the oil to the surface. When this stage arrived, the water and gas flooding is introduced namely as a secondary drive, which is mainly used for pressure maintenance and volumetric sweep efficiency. With this external support of energy to the oil reservoir, the recovery factor can increase up to 50 percent [56].

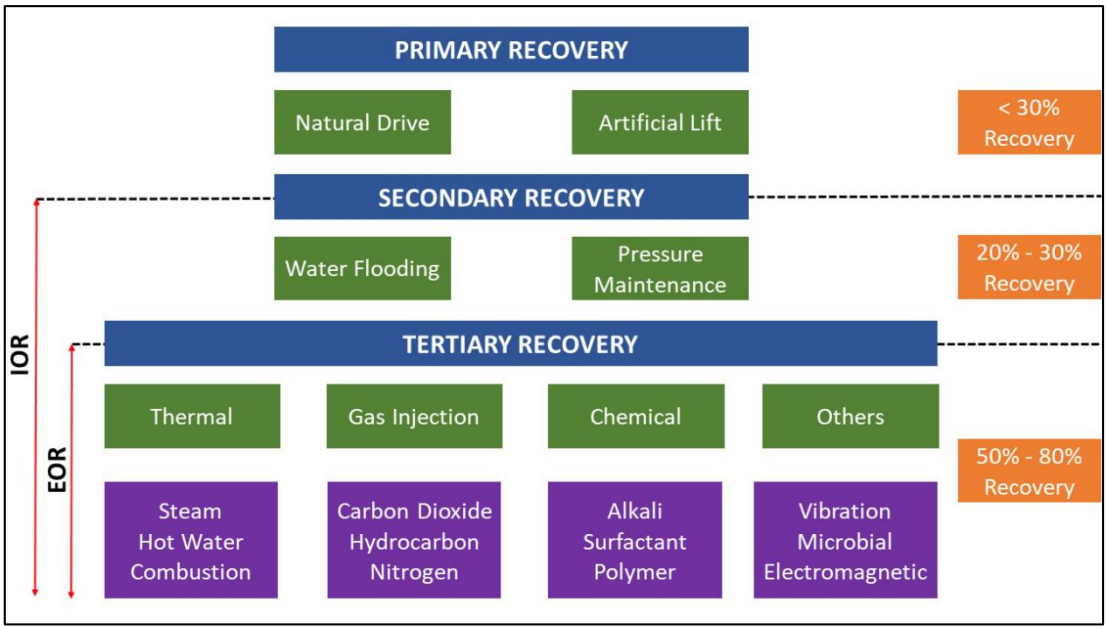

Figure 2.1 Classification of EOR processes.

The challenge with the water flooding at the second recovery process is related to the water production issue [57]. To treat the water produced requires extra cost. The water flooding has become unfeasible when excessive water produced reaches the economy limit whereby the cost of produced water treatment is higher than the profit gained from the oil produced. This leads to about two-thirds of the remaining oil in the oil reservoirs at the end of water flooding. The remaining oil is either trapped by capillary forces (residual oil) or bypassed due to reservoir heterogeneities and/or because of unfavorable mobility ratio between injection fluids and the oil [50]. On the other hand, the residual oil is also trapped by the IFT between the injected fluid and the oil [58].

During the oil recovery, the overall oil displacement efficiency is determined by the combination of both macroscopic (volumetric sweep) and microscopic (pore-scale) displacement efficiency. Macroscopic displacement efficiency is a measure of the effectiveness of the injected fluids in contacting the oil zone volumetrically concerning the total reservoir volume. On the other hand, microscopic displacement efficiency is the efficiency related to the ability of the displacing fluids to mobilize oil trapped at the pore scale when it is in communication with the oil.

In general, any mechanism that can improve oil displacement efficiency at either the micro or macro-scale or both is a mean of EOR [20]. EOR processes are classified into four major types of operation, which are thermal recovery, gas injection, CEOR and other types of EOR. Each type has different functions and principles in recovering the residual oil. Among the EOR techniques, CEOR is identified as the most promising because of its higher efficiency, technical and economic feasibilities and reasonable capital investment [39,59]. Other EOR methods such as thermal EOR is found to be unsuitable with shallow depth reservoir and thin pay zone [60].

The well-known conventional CEOR consists of polymer, alkali, and surfactant flooding. Polymer flooding improves oil recovery by polymers injection with the waterflooding to increase the viscosity of the injection fluids, thus gives better control of mobility to avoid fingering and bypass oil toward producing well [61]. Alkali flooding is used as wettability alteration by injection alkaline solutions. Besides, Olajire et al. [20] reported that alkali application in chemical EOR has advantages in promoting crude oil emulsification, increasing the ionic strength of aqueous phase and reducing the IFT to ultralow values when a surfactant is present. On the other hand, surfactant flooding is significantly essential to mobilize the residual trapped by lowering the IFT between the oil and formation water [19,62]. The synergy of the combined conventional chemicals is recorded to achieve ultimate recovery potential. It includes a binary mix of alkali/surfactant (AS), surfactant/polymer (SP), alkaline/polymer (AP), and alkaline/surfactant/polymer (ASP) [8,63–66].

Even though CEOR shows excellent potential, it has its limitations. The primary challenge during CEOR flooding is surfactant losses due to adsorption on the rock surfaces [44]. Surfactant adsorption on rock pores results in loss and decrease in surfactant concentration, thereby reducing the amounts of surfactant molecules available for the IFT reduction of the oil-water interface.

This chapter aims to review the currently available research on application surfactants (surfactant flooding) in CEOR and put the adsorption into context. The surfactant flooding mechanism, the surfactant types, and their challenges are also

addressed. Realizing their potential, more studies on understanding the factor of surfactant adsorption in CEOR are being deployed and the new approach in designing more effective surfactant flooding is continuously under development.

2.2 Surfactant Flooding

The application of surfactants in CEOR is proven to mobilize the residual trapped oil in the reservoir [62]. A surfactant which is also known as the surface-active agent is the chemical substances that adsorb at the surface or fluid/fluid interface to alter the surface and interfacial properties, particularly lowering the surface tension or IFT [13]. The principal of surfactant flooding is illustrated in Figure 2.2.

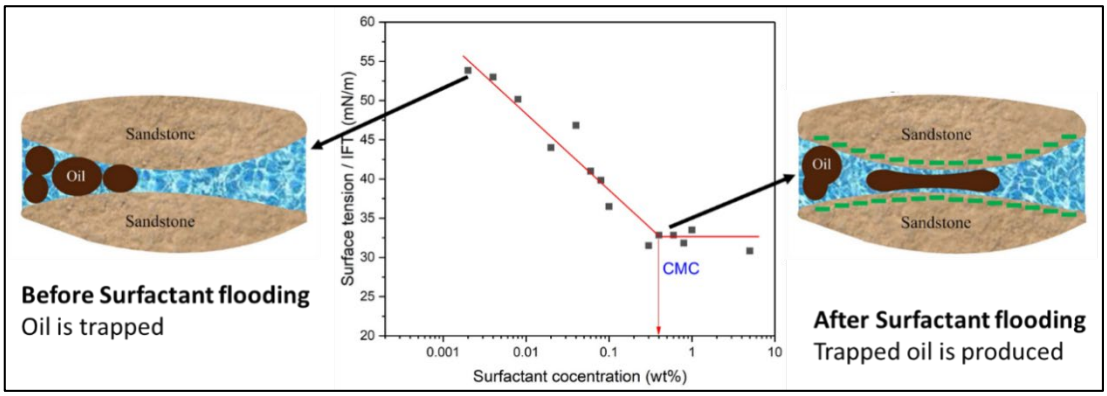

Figure 2.2 Principle of surfactant flooding, where residual oil is trapped in the reservoir. For the movement of oil through the narrow capillary pores, very low oil/water interfacial tension (IFT) is required; preferably ultra-low IFT at 0.001 mN/m is desirable [40,67].

The aim of surfactant injection into the reservoir for improving oil recovery factor is to alter the fluid/fluid interaction by reducing IFT between the oil and brine, and fluid/rock properties via wettability alteration of the porous medium. Various laboratory applications of surfactants have been reported in the literature, as summarized in Table 2.1.

Besides surfactants, co-surfactants are blended with the surfactant solution to improve the properties of the surfactant solution. The co-surfactant serves as a promoter or/and as an active agent in surfactant solution to provide optimum conditions concerning reservoir environments such as temperature, pH and salinity. It is well known that the stability of the surfactant system in the reservoir environment is also of great challenge such as surfactant losses due to adsorption. Surfactants are very sensitive to high temperature and high salinity and therefore, surfactants that can resist these conditions are most favorable [13]. In general, there are three types of implementation of surfactant flooding, as shown in Table 2.2.

Table 2.1 Various surfactants used in surfactant flooding.

Surfactant	**Surfactant concentration**	**Base fluid**	**Porous media**	**Recovery factor**	**References**
SDS	0.2 wt%	Deionized water	Quartz	4.68%	[68]
TX-100	0.1 wt%	Brine	Sandstone	8 %	[69]
CTAB	0.1 wt%	Brine	Micromodel	17.4%	[70]
SDS	1 wt%	Brine	Micromodel	5 %	[71]
Tween 20	0.74 wt%	Distilled water	Micromodel	18%	[72]
SDS	0.6 wt%	Deionized water	Sandstone	-	[73]
CTAB	0.4 wt%	Distilled water	Micromodel	-	[74]

The optimization criterion in surfactant flooding is meant to maximize the amount of oil recovered while minimizing the chemical cost. While it is necessary to reach low IFT for the surfactant system, minimizing only the IFT may not always coincide with optimal oil recovery, as low IFT is not the only essential condition to meet in order to get a successful and efficient oil recovery [12]. Understanding the reservoir environment and how it affects surfactant flooding is very crucial. Thus more study on this should be the focus as a way forward.

Table 2.2 Types of surfactant flooding.

Types of surfactant flooding	Technique	Description
Micelle/polymer flooding	A micelle slug usually of surfactant, co-surfactant, alcohol, brine and oil being injected into the reservoir.	Displacement efficiency close to 100% (measured in the laboratory)
Microemulsion flooding	Surfactants, co-surfactants, alcohol and brine are injected into the reservoir to form microemulsions to obtain ultra-low IFT.	It can be designed to perform well in, e.g. high temperature or salinity or low permeable areas where polymer and/or alkali cannot work.
Alkaline/surfactant/ polymer (ASP) flooding	The addition of alkaline chemicals reduces the IFT at significantly lower surfactant concentrations.	Lower concentration of surfactants is involved in this process, which reduces the cost of chemicals.

2.2.1 Surfactant Flooding Mechanism: IFT Reduction

The primary mechanism of surfactant flooding is minimizing the capillary forces by reducing the IFT between the formation of water and oil. During the end of water flooding, it is practically impossible for water to displace the oil because of the trapping of oil in the pore-scale by the capillary forces. The capillary forces are measured by the capillary numbers (N_c) [75].

$$N_C = \frac{\mu v}{\sigma \cos \theta} \tag{2.1}$$

Where,

$N_C = capillary\ number$

$\mu = displacing\ fluid\ viscosity$

$v = displacing\ Darcy\ velocity$

$\sigma = IFT\ between\ water\ and\ oil$

$\theta = contact\ angle$

N_c is defined as a ratio of viscous force to capillary force [76]. Residual oil can be recovered if the viscous force caused by injectant fluids exceeds the capillary retaining force. The recovery factor is found to be dependent of N_c. A higher N_c will result in a higher recovery factor, as shown in Figure 2.3. Typical N_c for water flooding is around 10^{-7} to 10^{-6}. Increasing the value of N_c to the value of 10^{-3} will reduce the residual oil to the barest minimum and will result in the increment in oil recovery. This can be achieved in three ways according to the above equation : (i) increasing the viscosity of displacing fluid; (ii) increasing the injectant fluid velocity and (iii) reducing the IFT between the formation fluid and oil.

Increasing the injection fluid velocity may cause the injection pressure to be higher than the fracture pressure of the reservoir resulting in the damage of the rock formation. Meanwhile, increasing the displacing fluid viscosity using polymer solutions increases the capillary number by less than 100 times [66,77]. To increase N_c by 1000 times, only the method of reducing IFT can be used. . Because of this, adding a surfactant will be a significant approach.

Surfactants have two main components in their structure, namely a hydrophilic head and a hydrophobic tail. When surfactants are injected into reservoirs, the hydrophilic head will react with water while the hydrophobic tail will adsorb and interact with the oil phase. Figure 2.4 illustrates the adsorbed film as a result of interaction between the oil and hydrophobic tail of surfactant, thus reducing the IFT at the oil/water interface. The reduction of IFT at the interface will reduce the capillary force that further causing the oil droplets to flow smoothly from the pore throat toward the producing well.

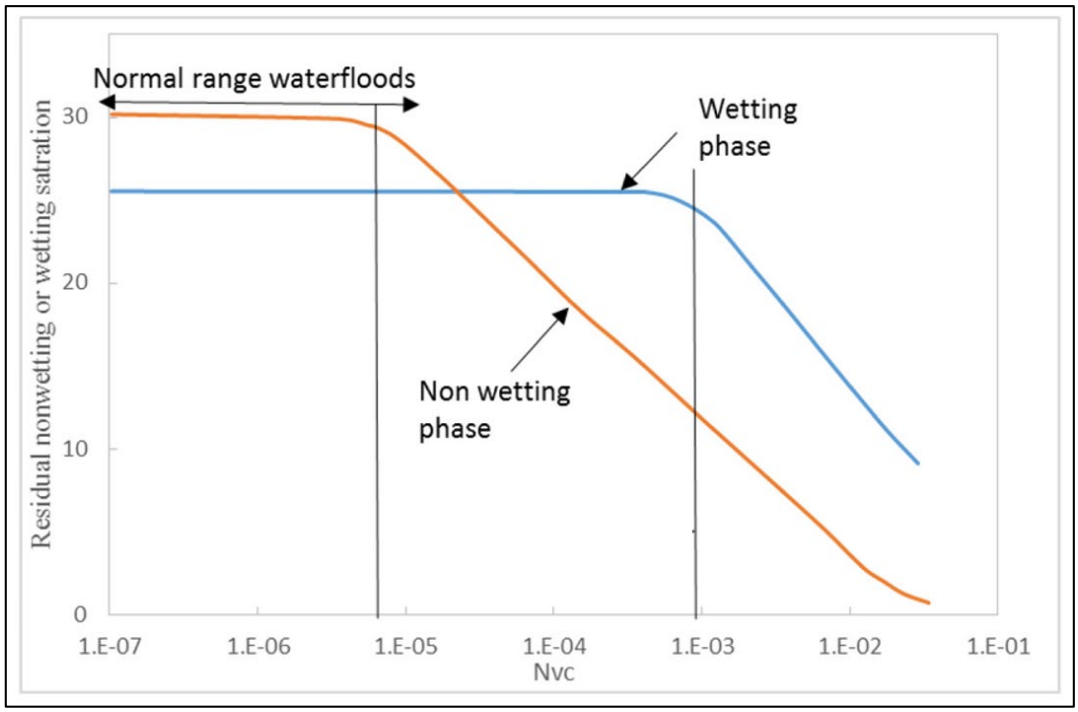

Figure 2.3 Schematic relationship between N_c and Residual oil. Modified from Guo et al. [10].

Choosing suitable surfactants for surfactant flooding is a crucial task. The surfactant tends to adsorb the rock surface due to charges property of the rock surfaces. Adsorption to be more significant when the charge of surfactant is opposite to the charge of rock surfaces. Therefore, understanding both charges properties of surfactants and the rock surface is key to successful implementation of surfactant flooding.

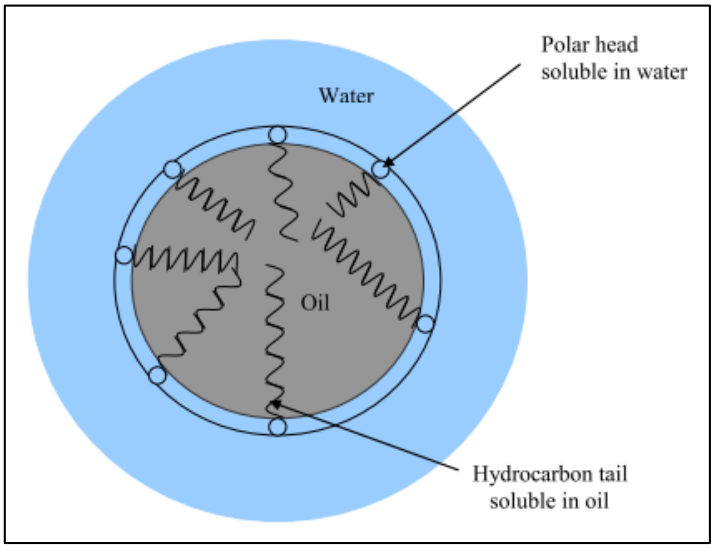

Figure 2.4 Principles of surfactants [20].

2.2.2 Surfactant Flooding Mechanism: Wettability Alteration

Wettability also plays a vital role in oil recovery. Wettability in a reservoir rock system refers to the tendency of oil to spread on a solid surface in the presence of other immiscible fluids such as water. It represents the interaction between the reservoir fluids and reservoir rock surface [78,79]. The wettability controls the location, fluid distribution and flows within the reservoir rock [80]. This property is significantly valuable because it influences the oil recovery, such as capillary pressure and relative fluid permeability. Figure 2.3 highlights the effects of wettability on N_c. The wetting phase needs higher N_c value to recover more residual oil as compared to the non-wetting phase.

The wettability of the oil reservoir is typically in water wet, oil-wet and mix wet state [81]. Surfaces with contact angle more than 90 degrees are called oil-wet, while contact angle less than 90 degrees is considered water wet. Altering wettability means to change the wettability of oil-wet to water wet or vice-versa. Wettability alteration involves the modification of the adhesive capillary force of the fluids [82]. Higher oil recovery is more favorable for the wet water system as compared to the oil wet system.

The application of surfactants in wettability modification have been studied for both conventional and unconventional reservoir [42,78,83]. Mirchi et al. [84] and Kathel et al. [82] have reported adding surfactants at appropriate concentrations into a fracturing fluid resulting in an improved performance of hydraulic fracture treatment via altering the wettability and thus enhance the fluid flow behavior. Similar, findings were recorded by Jarrahian et al. [85] and Salehi et al. [86,87] where adding surfactants helps increase oil recovery from conventional sandstone and carbonate reservoirs. The mechanism of wettability alteration of conventional rock pores by a surfactant is termed a cleaning mechanism whereby the surfactant desorbs the oil-wet layer. Desorption of the oil-wet layer by surfactant alters the wettability of the surface and changes it to a more water-wet state.

2.3 Surfactant Chemistry

Surfactants are molecules that exist preferentially at the interfaces. They are usually organic compounds that have an amphiphilic character composed of polar (hydrophilic) and non-polar (hydrophobic) components [88]. The hydrophobic group can generally be a long chain hydrocarbon, siloxane chain or a short polymer chain. The hydrophilic group consists of cationic, amphoteric or non-ionic. The amphiphilic character of surfactant makes the surfactants soluble in both organic solvent and water. The structures are shown in Figure 2.5**.**

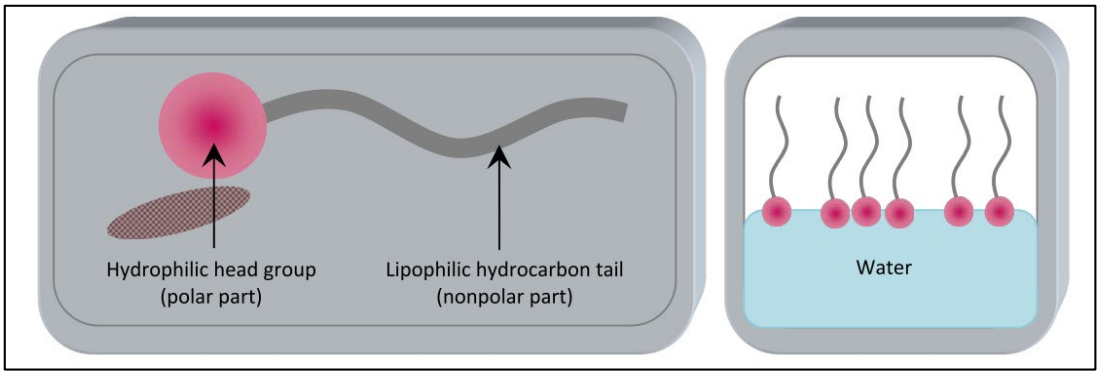

Figure 2.5 Structure of surfactants and their orientation in the water [13].

The surface-active of surfactant has the ability to adsorb at the interface of immiscible fluids. The driving force of this is to reduce the free energy of the fluid-fluids interface, which is known as interfacial tension. Interfacial tension or IFT is measured by force per unit length or energy per unit area. By this definition, the interfacial tension of immiscible oil-water is the amount of work required to expand the oil-water interface [55].

Surfactants exhibit different properties in solutions based on the hydrophobicity of their tail group (Figure 2.6). The first property is the formation of micelles by the aggregation on the solution. The second property is the adsorption at the interfaces. The mechanism of the surfactants orientation and structure at the interfaces is controlled by the nature of the interface; (i) at hydrophobic interfaces, they are attached to the hydrophobic chain facing the interface, either by monolayer

or as a hemic-micelles aggregate, (ii) at the hydrophilic interfaces, they are adsorbed either as bilayers or as separately aggregated structure.

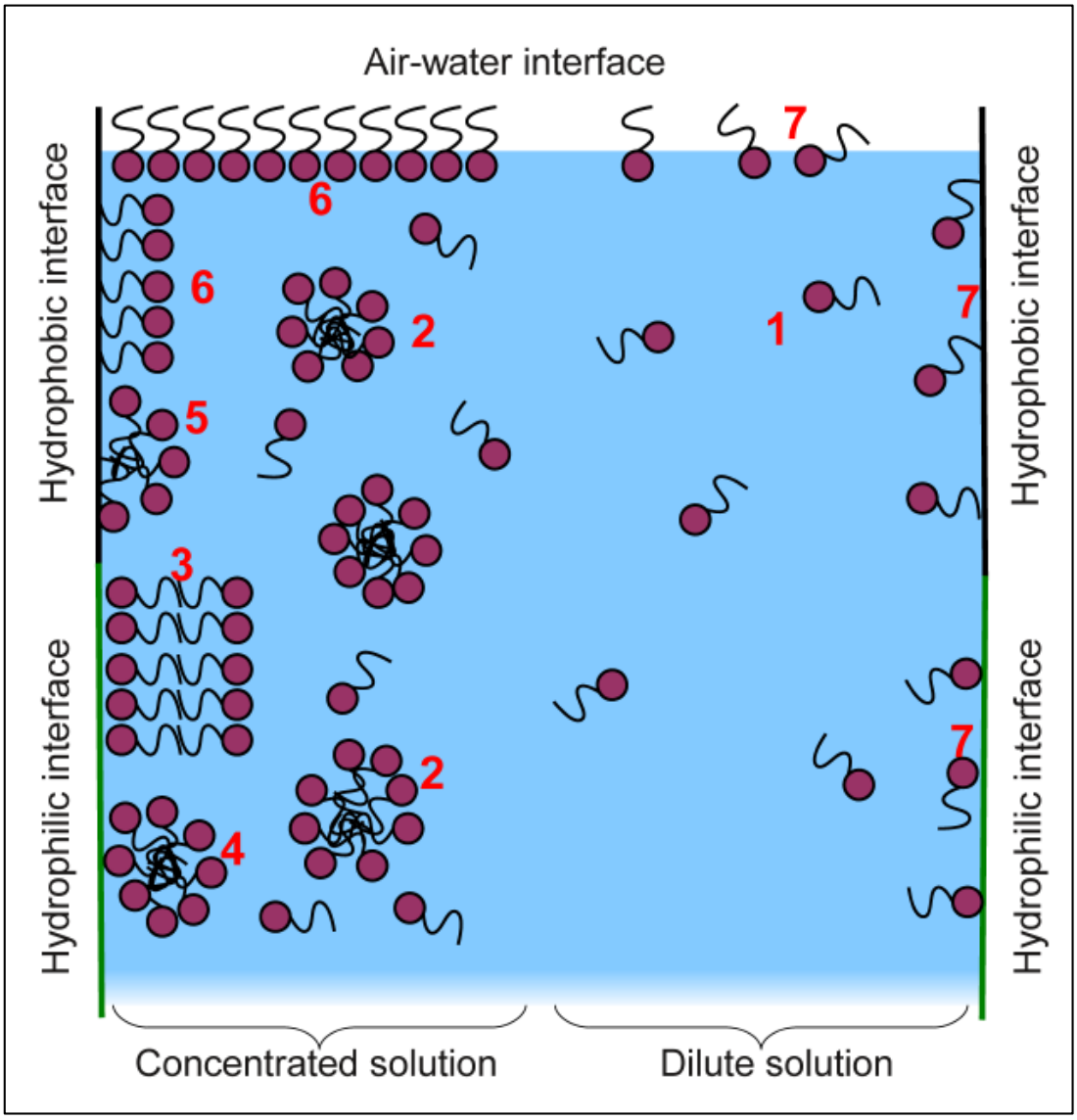

Figure 2.6 Behaviour of surfactants in solution and at interfaces. 1. Monomers in solution, 2. Micelles in solution, 3. Adsorbed bilayer, 4. Adsorbed admicelle, 5. Adsorbed hemi-micelle, 6. Adsorbed monolayer, and 7. Adsorbed monomers [89].

The main driving force that removes the tail group of surfactants in an aqueous solution is the hydrophobic effect. The removal happens when the hydrogen bonding structure in bulk water is disrupted by the non-polar tail [90]. To overcome the weakening of hydrogen bonding, the water molecule from structures surrounding the tail has to allow each of water molecule to remain tetrahedrally coordinated. However, this orientation comes at a substantial entropy cost, which is mainly

proportional to the surface area of the dissolved molecule [90]. The energetic contribution to dissolving the hydrophobic tails is small since there is little difference in the dispersion interactions of water-water, water-hydrocarbon, and hydrocarbon-hydrocarbon.

2.3.1 Surfactant Classification

Surfactants can be classified based on the nature of the head group, known as anionic, cationic, and zwitterionic [91]. Table 2.3 summarizes the examples of surfactants based on their types.

Table 2.3 Surfactant types.

Surfactant type	**Examples**
Anionic	Sodium dodecylbenzene sulfonate
	Sodium dodecyl sulphate (SDS)
	Sodium stearate
	N-Ethoxy sulfonate
	Alcohol propoxy sulphate (APS)
	Alpha-Olefin sulfonate (AOS)
	Branched alkyl benzene sulfonate
	Alkyl alcohol propoxylated sulphate
Nonionic	Polyoxyethylene alcohol
	Alkylphenol ethoxylate
	NEODOL
	NEODOL ethoxylate 91-8
	Synperonic PE/F68
	Triton X-100
Cationic	Cetyl trimethyl ammonium bromide (CTAB)
	Laurylamine hydrochloride
	Dodecyl trimethyl ammonium bromide (DTAB)
Zwitterionic	Dodecyl betaine
	Lauramidopropyl betaine
	Cocoamido-2-hydroxypropyl sulfo betaine

Anionic surfactants are most frequently used in chemical EOR. This is because they exhibit low surfactant adsorption on sandstone rock surfaces that have negative charges. The surface-active of anionic surfactant bears negative charges such as carboxylate (COO^-), sulphate (SO_4^{2-}) or sulphonate (SO_3^-). The sulphonate class of surfactants is found to be more stable at higher temperatures but susceptible to higher salinity and may be subject to precipitation in the presence of divalent cations [50]. The sulphate class group, however, has greater tolerance with salinity but decomposes at high temperatures [92].

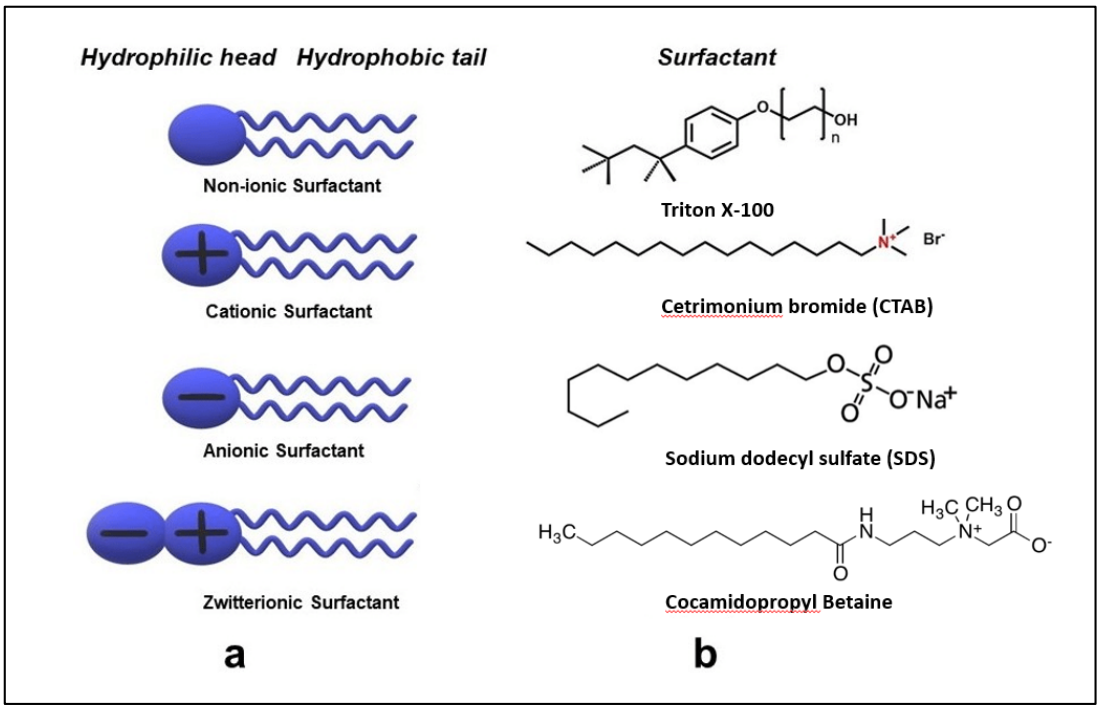

Figure 2.7 (a) A schematic of different types of surfactants and (b) Chemical structures of some typical surfactants that have been used in surfactant flooding [93].

Cationic surfactants are the surfactants that have an opposite charge to the ionic surfactants. They exhibit a positive charge and dissociate in water to form an amphiphilic cation and an anion. Cationic surfactants have a high tendency to attract the negative charge surfaces of clays. They are useful in altering the wettability of reservoir rock. However, they are more expensive compared to anionic surfactants due to high-pressure hydrogenation required in their synthesis process [94].

Non-ionic surfactants are relatively different from anionic and cationic surfactants. Non-ionic surfactant does not ionize in aqueous solutions. The

hydrophilic group consists of non-dissociable functional groups such as alcohol, phenol, ether, ester, or amide. Meanwhile, the lipophilic group consists of the alkyl or alkylbenzene group. Although the hydrophilic group lacks ionic charge, they are soluble in water because of their inherent polarity caused by the presence of hydrogen bond and van der Waals interaction. In comparison to ionic surfactants, non-ionic surfactants have a higher salinity tolerance, but a lower IFT reduction ability [36].

Zwitterionic surfactants are characterized by the presence of anionic and cationic surface charges on their hydrophilic head. They exhibit both anionic and cationic properties upon dissociation. They also possess a good tolerance to high salinity and temperature conditions. Typical examples of this class of surfactants are betaine and sulfobetaine [40].

2.3.2 Critical Micelle Concentration

The primary property of the surfactant is its critical micelle concentration (CMC). CMC is defined as the concentration of surfactant above which micelles are spontaneously formed [13]. The surfactant behaves differently at above and below CMC. Employing surfactant into the system reduces free energy by two approaches; (a) lowering the energy of the interface and (b) preventing/removing the hydrophobic parts of the surfactant from contact with water [91]. Whenever the surface coverage by the surfactant increases and the surface energy (surface/interfacial tension) decreases, the surfactant starts to aggregate into micelles, thus reducing the free energy by reducing the contact area of hydrophobic parts with water.

Upon reaching the CMC point, the addition of surfactant will increase the numbers of micelles, as shown in Figure 2.8. Before reaching CMC, the surface tension decreases sharply with the concentration of surfactant, while after reaching CMC, the surface tension stays constant [19].

The value of CMC of all surfactants depends on the chain length of the hydrophobic tail, temperature, and salinity [95,96]. Increasing the hydrophobic tails will strongly decrease the CMC value. The influence of temperature on CMC is in a lesser manner. The CMC reduced less than 20 percent at a temperature between 10 to 50 degrees Celsius. The effect of salinity is, however significant of ionic surfactants. The addition of salt will reduce the CMC due to the presence of extra ions in the system [97].

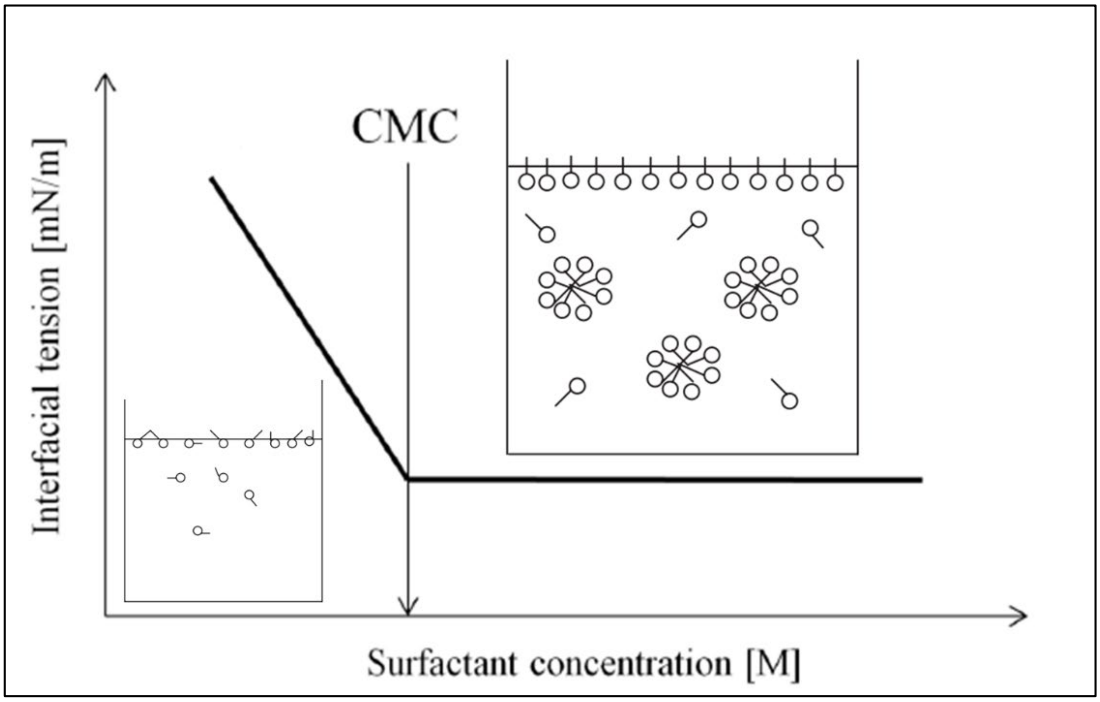

Figure 2.8 The CMC of the surfactant.

In surfactant flooding, CMC is an important criterion to be considered. The surfactant concentration used must be at higher than the CMC to obtain a lower oil-water IFT. In addition, the maximum adsorption of a surfactant on the reservoir rock surfaces occurs at the CMC. Adsorption at above CMC value does not show any significant increase.

2.3.3 Factors Affecting CMC

The CMC of the surfactant can be affected by many factors. The chemical structure of the surfactant is one of the parameters which determine the CMC. The structure includes the physical properties such as size and shape of the head of the surfactant as well as the tail. Following are the parameters that significantly control the CMC of the surfactant [98]:

i. The CMC of the surfactant will be substantially reduced by increasing the chain length of the tail.
ii. The CMC of ionic surfactant is relatively higher as compared to non-ionic surfactants.
iii. The headgroup of ionic surfactants does not influence the CMC drastically, but generally cationic has a higher CMC than anionic surfactants.
iv. The CMC of non-ionic increases as the head group becomes larger.
v. The CMC will be reduced, especially for organic counterion, by increasing the valency of the counterion.

2.3.4 Critical Packing Parameter

The critical packing parameter (CPC) is a tool to describe the micelle behavior in the solution. The surfactant structure tends to arrange their hydrophilic head directed toward the aqueous solutions and their hydrophobic tail stacked together to minimize exposure.

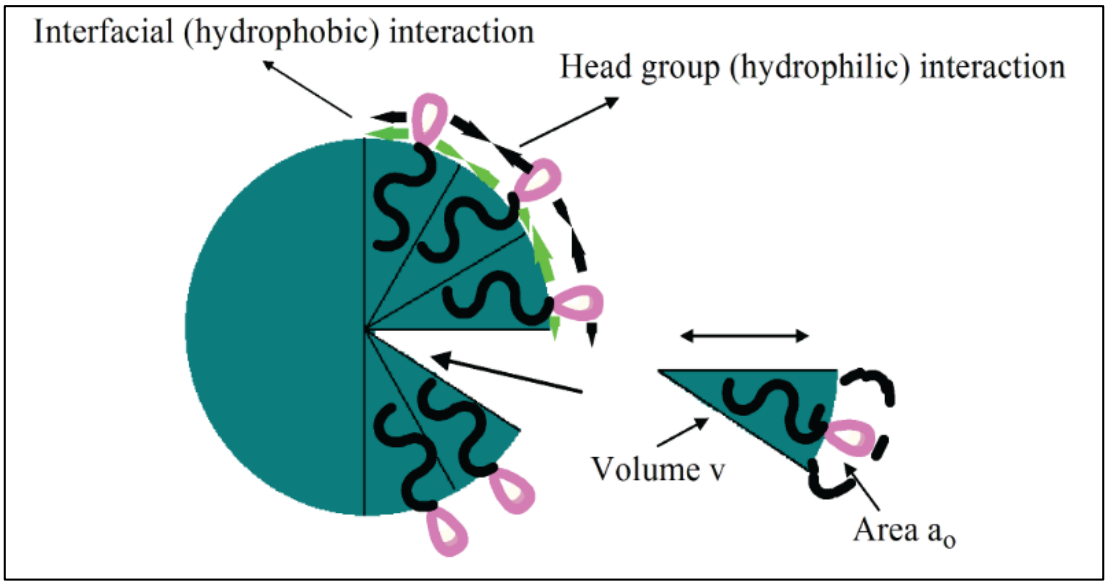

Figure 2.9 The CPC connects the head group area, the length and volume of the hydrocarbon chain into a dimensionless number [99].

The formation of the micelle and their aggregation can be expressed in the ratio between the volume of the micelle and the volume of single surfactant (Figure 2.9). This is illustrated by the following equation [100]:

$$N = \frac{V_{micelle}}{v} = \frac{\frac{4}{3}\pi R^3_{micelle}}{v} \tag{2.2}$$

Where,

$N = aggregation\ number$

$V_{micelle} = total\ volume\ of\ micelle$

$v = volume\ of\ one\ chain$

$R^3 = radius\ of\ micelle$

The aggregation numbers can be further simplified as the ratio between the micellar area and the area of one surfactant molecules as follows:

$$N = \frac{A_{micelle}}{a} = \frac{4\pi R^2_{micelle}}{a} \tag{2.3}$$

Where,

$A_{micelle} = area\ of\ micelle$

$$a = area\ of\ surfactant\ molecul$$

Merging these equations will result in:

$$\frac{v}{R_{micelle}a} = \frac{1}{3} \tag{2.4}$$

The final equation is known as the CPP for a spherical micelle. It is simplified as the ratio between the tail volume and the radius of the micelle multiplied by the area of the headgroup. Figure 2.10 illustrates the typical CPC of the surfactant and their geometrical shapes of micelles.

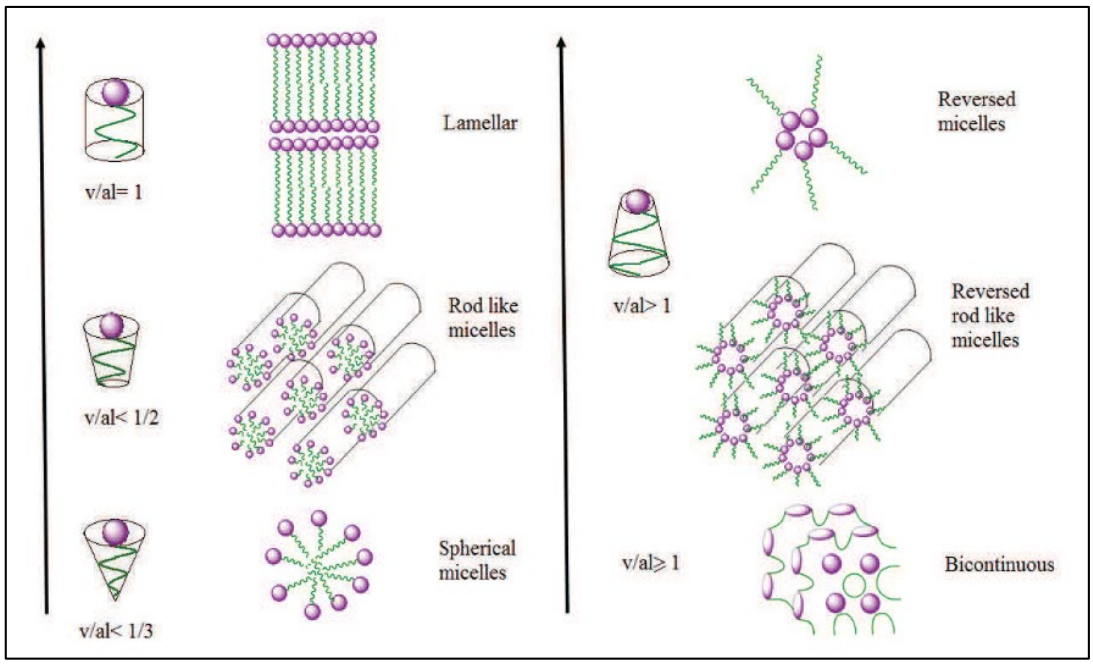

Figure 2.10 The surfactant aggregation structure base on CPP [99].

The CPP is also sensitive to the electrolyte. When the electrolyte is added into surfactant solutions, a few effects take place; the CMC will decrease and the surface tension or IFT above CMC will decrease. This indicates higher surfactant adsorption at the interfaces. The observation shows that the CPC becomes higher and the surfactant pack more tightly. This effect is a result of the repulsive of head group surfactants by the electrolyte addition [90].

2.4 Surfactant Adsorption

The success of the implementation of surfactant flooding is subjected to minimizing the surfactant losses in the porous reservoir rock. Surfactant losses involve several different mechanisms including adsorption, precipitation of surfactant when divalent ions present, surfactant degradation by temperature, as well as partitioning of surfactant into the oil phase [24]. Among these mechanisms, surfactant adsorption onto the rock surface has been the major contributor and controls the amount of surfactant loss [44].

Surfactant adsorption is governed by a number of forces including covalent bonding, electrostatic attraction, hydrogen bonding, and van der walls interaction between the surfactant and the rock surface [25,101]. The result of adsorption is involved in the commutative or all of the forces [41]. In the system where the ionic surfactant and the solid surface are charged, the electrostatic interactions play a vital role in the adsorption process [41]. Opposite charge of surfactant and the solid surface will cause severe adsorption due to attractive force. In addition, hydrogen bonding of surfactant and the solid surface containing hydroxyl, phenolic, carboxylic and amine groups on the surfactant may appear on the system [102]. For adsorption via hydrogen bonding to take place, the bonding between the surfactant functional group and the rock mineral surface must be stronger than that formed between the rock mineral and the interfacial water molecule [41].

Besides the forces, surfactant adsorption also depends on surfactant type and concentration, surfactant equivalent weight, ionic strength, pH, salinity and temperature [30–32,56]. According to Afeez et al. [50] and Rahul et al. [49], the rock mineralogy and rock surface charge also contribute a significant impact to the selection of surfactant and adsorption.

In this section, we will discuss details about the role of surfactant concentration, salinity, pH, temperature and surface charge in the surfactant adsorption. The performance of surfactant flooding can be improved, and a good recovery factor can only be achieved if the implementation is economically optimized by minimizing the surfactant adsorption [103].

2.4.1 Adsorption on Solid Surface

Surfactant adsorption from a solution into solid surfaces occurs most commonly in porous media, either on the walls of pores or throats or on fine particles in rock pores. This adsorption constitutes a loss of valuable surfactants; thus, this method is not efficient or economically feasible. Adsorption takes place when surfactants aggregate and micelles form on the surfaces, which means the concentration of the surfactant must exceed the CMC value. The adsorption isotherm is somewhat dependent on the type of surfactant and/or cosurfactant, the characteristics of the rock, and the type of electrolytes present in the system [104].

For hydrophobic surfaces, the adsorption is determined by the hydrophobicity of the surfactants, where the surfactants adsorb their hydrophobic tail towards the surface, and the hydrophilic head group is exposed to the solution. For very polar surfaces, the surfactants adsorb their head group towards the surface with their hydrophobic tail towards the solution. A monolayer begins to form, and when the equilibrium monolayer adsorption is reached, the system will form an additional layer. This is due to the hydrophobic tail exposure to the aqueous solution. Multilayer adsorption can cause significant surfactant losses in the reservoir. At still higher surfactant concentrations, aggregation of surfactants at the interface will form. This is the case when the hydrophobic attraction of the tail parts of the surfactants exceeds the strength of the interaction between the head group and the interface. A schematic illustration of different configurations of surfactant adsorption is shown in Figure 2.11.

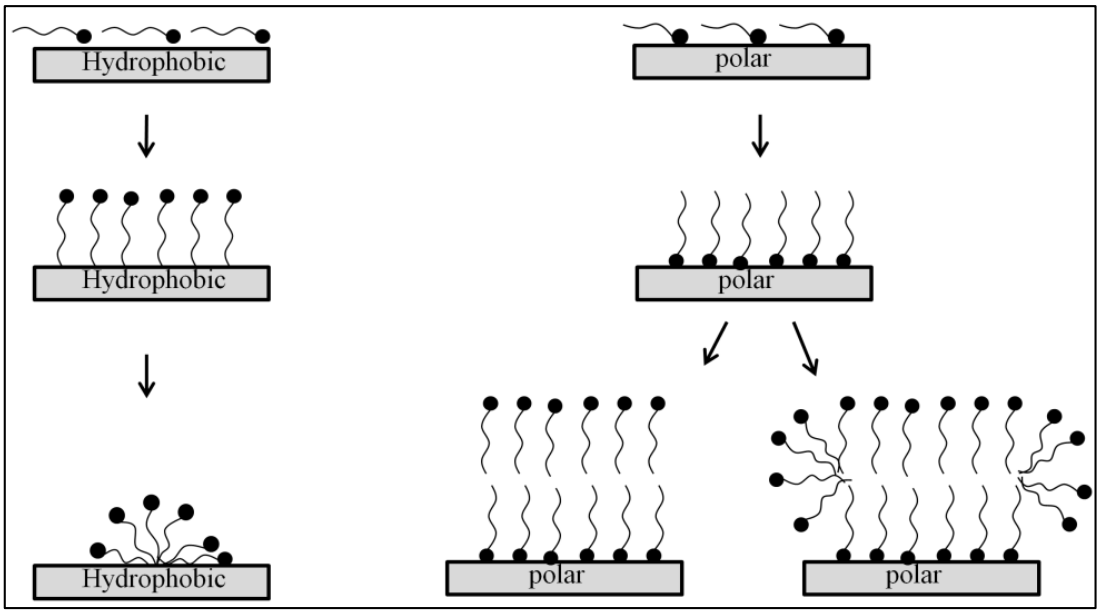

Figure 2.11 Schematic illustration of surfactants adsorbed to polar and hydrophobic surfaces [105]

2.4.2 Langmuir Adsorption Isotherm

The Langmuir isotherm is often used as a theoretical model for the analysis of adsorption on surfaces. For the application of the Langmuir equation, the following assumptions have been made [37,95]:

i. Adsorption does not proceed beyond monolayer coverage.
ii. All adsorption sites are equivalent, and the surface is entirely uniform.
iii. Adsorption to a given adsorption site is independent of the surface coverage (No lateral interactions between adsorbate molecules).
iv. No surface diffusion among localized adsorbate molecules.
v. Adsorption is completely reversible.

The Langmuir equation can be derived as follows [98]. The rate of adsorption can be defined as:

$$Rate\ of\ adsorption = k_a C(1 - \Theta) \quad (2.5)$$

where C is the surfactant concentration at equilibrium, $\boldsymbol{\Theta}$ is the fraction of surface covered with surfactants, and k_a is a rate of adsorption constant. Thus, the rate of desorption can be defined as:

$$Rate\ of\ desorption = k_d\Theta \tag{2.6}$$

where k_d is the rate of desorption constant. At equilibrium, the rate of adsorption will be equal to the rate of desorption, and the following equation is derived:

$$\Theta = \frac{KC}{1+KC} \tag{2.7}$$

where K is the newly defined equilibrium constant (k_a/k_d).

Surfactant adsorption can be presented as isotherms that are plots of the amount of surfactant adsorbed per gram of solid or per surface area of solid versus the equilibrium surfactant concentration at a constant temperature. These plots can be constructed using the log-log scale, as shown in Figure 2.12, which consists of a typical four-region isotherm [106]. It is important to note that the exact shape of the isotherm will depend on several factors, including the type of surfactant, the charge on the surface, and the presence and absence of additional compounds including electrolytes, co-surfactants, hydrotropes, or alcohol.

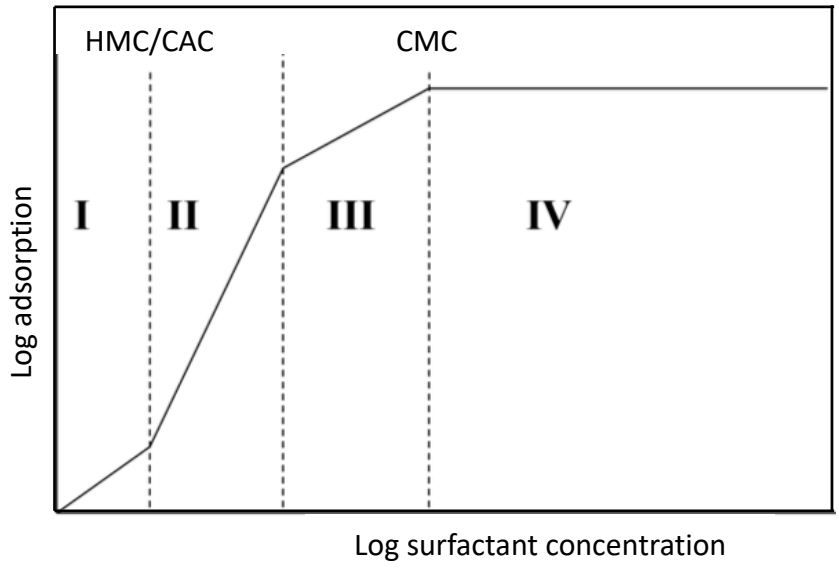

Figure 2.12 Typical four-region adsorption isotherm [106].

At low surfactant concentrations, labelled as region I, the adsorption behavior can usually be described by a simple Stern/Gouy double-layer model, where the surfactant is adsorbed as individual monomers with no interaction between the adsorbed molecules [107–109]. Surfactant adsorption may occur due to electrostatic interaction, van der Waals interaction, hydrogen bonding, and/or solvation and desolvation of adsorbate and adsorbent species. For non-ionic surfactants, the interactions involve hydrogen bonding between surface hydrogen and proton acceptors in the head groups and hydrophobic bonding between the hydrocarbon tails of surfactants and the surface. For ionic surfactants, there are electrostatic interactions between the head groups of the surfactants and charged sites on the surface. This electrostatic attraction is typically described in terms of the interaction of the charged surfactant ion with the EDL of the solid.

Adsorption in region II is due to the association of the adsorbed surfactants into patches at the solid/liquid interface. These associations were attributed to tail-tail interactions, which are the same hydrophobic interactions by which micelles form. The break between regions I and II corresponds to the concentration at which the first surfactant aggregates form at the surface. This concentration is referred to as the hemimicelle concentration (HMC) [32,110] or as the critical micelle concentration (CMC) [106]. The CAC varies with surfactant chain length and branching, in which increasing the chain length of the tail will strongly decrease the CAC. The same

effect will be shown if an electrolyte is added to a system that contains ionic surfactants.

In region III, a decrease in the slope relative to the slope in region II is seen. There have been several discussions proposed to explain this change. Somasundaran, *et al.,* [111] attributed this change in slope to the surfactant ions having filled all the surface sites by the end of region II with further adsorption due to association between first and second layer hydrocarbon chains in region III. The observed change in slope was also attributed to a reversal in surface charge due to the adsorbed surfactant ions. Scamehorn *et al.,* [112] proposed that bilayer formation begins in region II and continues into region III but at a different rate. This can also be viewed as adsorption taking place on the least energetic patches on the surface in region III.

Region IV or plateau adsorption generally begins at or near the CMC and is characterized by little or no increase in adsorption with increasing surfactant concentration. In this region, micelles exist in the bulk solution and act as a potential chemical sink for any additional surfactant added to the system. Most researchers agree that the surfactant aggregates have a bilayer structure when the solution concentration exceeds the CMC. However, the total adsorption above the CMC may still be substantially less than a complete bilayer and depend strongly on the surface charge and, therefore, the pH.

2.4.3 Effect of Surfactant Concentration

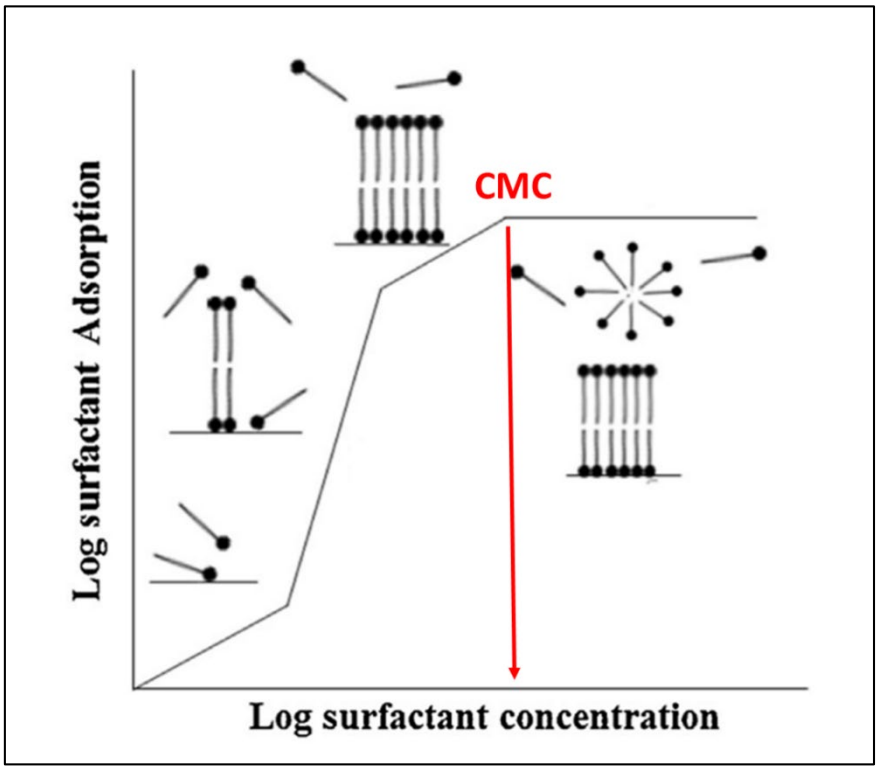

Figure 2.13 Surfactant adsorption isotherm (modified from Mahesh et al. [113])

Surfactant concentration has a significant effect on surfactant adsorption. The adsorbed surfactant typically increases when surfactant concentration in the solution increases. Numerous studies have discussed the effects of surfactant concentration for ionic and non-ionic surfactants. Adsorption of anionic surfactant increases as surfactant concentration increases. At the concentration below CMC, the adsorption is controlled by the charge in the electrical double layers due to electrostatic interactions that arise between the surfactant head group and net charge present on the rock surface [34]. Increasing the surfactant concentration results in lateral interaction that appears between the adsorbed surfactant molecule, which drives to surfactant aggregation such as monolayers, bilayers or mixture of both to take place. The formation of bilayers by the surfactant hydrophobic tail-tail interaction will slow down the surfactant adsorption due to the saturation of high energy patches at the surface until it reaches CMC [25,113]. However, when it reaches CMC, further addition of surfactant will not affect surfactant adsorption due to the monomer concentration of the surfactant not changing as more micelles added to the solutions [113].

At this stage, the adsorption remains constant and displays plateau behavior [114]; however, this is not desirable for the surfactant flooding process because the amount of surfactant required to form bilayers can exceed the economical limit.

Therefore, practically all surfactants have the same charge as the reservoir rock surfaces are used to minimize the surfactant bilayers formation. For example, the anionic surfactant is commonly applied for the negatively-charged sandstone reservoir and cationic surfactant is used for positively-charged carbonate reservoir. However, due to the complexities of the reservoir's system including rock mineralogy/composition, clay presence, salinity, multivalent ion, and pH, there is a possibility that adsorption could contribute to the surfactant loses.

2.4.4 Effect of Salinity and Divalent Ion

Tabary et al. [115] reported that the salinity and the presence of divalent ion have an impact on surfactant flooding design. Salinity directly affects the surfactant adsorption. According to Azam et al. [30] and Kamal et al. [25], increasing water salinity reduces the repulsive force arising between the ionic surfactant molecules to the rock surface. This is supported by Mannhandt et al. [116] which states an increase in salt concentration results in higher adsorption by decreasing the solvent power of the aqueous phase of surfactant, thus decreasing the electrostatic repulsion of the headgroup/headgroup at the adsorbed layers. Besides, an increase in electrolyte concentration will compress the electrical double layers, which will control the surfactant adsorption depending on the sign of the solid surface and surfactant [116].

Besides, Koopal et al. [88] have illustrated that ionic strength may also affect the surfactant adsorption. Ionic strength is subjected to both electrolyte concentration and the divalent ion presence. Divalent ion such as calcium has a substantial impact on the surfactant adsorption too. The surfactant adsorption increases with the presence of divalent ion (such as Ca^{2+}).

This result agrees with the findings from Mannhardt et al. [117], where the adsorption is more significant when divalent ions present compared to monovalent ions due to ionic strength effects. Surfactants containing ethylene oxide in the structure exhibit relatively high tolerance to divalent cations. Therefore, formation water salinities should be considered in the selection of optimum surfactant formulation.

2.4.5 Effect of pH and Surface Charge

The pH has a significant impact on the surfactant adsorption because it is associated with the rock surface charges. Rock surface charge varies with the pH. As the pH increases, the numbers of the hydroxyl group reduces, thus affecting the formation of hydrogen bonding [22]. This makes the hydrated mineral oxides on the solid surface become negatively charged. At lower pH, surfactant concentration leads the mineral hydroxyl to acquire a positive charge. This potentially increases the surfactant adsorption by attracting the negatively charged surfactant molecules onto the rock surface. As demonstrated by Azam et al. [30] who worked on Berea sandstone, increasing the pH from acidic condition to alkaline condition will boost the negative surface charge of the rock surfaces.

2.5 Development of Charges Surface in Porous Media

In general, when two phases of different chemical constituents are in contact, potential differences between them will be generated as a result of electric charges distributing themselves in a non-uniform way at the interface, such as electron and ionic groups. If one phase is a polar (ionic group) liquid, its dipolar molecules tend to be oriented selectively concerning the two phases. Due to this effect, the separation of charges marks the region between the two adjoining phases.

There are several possible mechanisms that can be used to describe the charge separation at the interface, which is addressed by Hunter [118]:

i. The differences in the affinity of the two phases for ions of one charge or another.
ii. The ionization of the surface group.
iii. The physical entrapment of the non-mobile charge in one phase.
iv. The differences in the affinity of the two phases for electrons.

These four mechanisms have their own significance. Mechanism (i) is important for describing the distribution of anions and cations between two immiscible phases and to differentiate adsorption of ions from a solution into a solid surface and the solution of one type of ion over another ion from a solid. Mechanisms 2 and 3 are significant for oxide surfaces, such as quartz, and for clay minerals, such as montmorillonite, respectively. The fourth mechanism is essential at the junction between a metal and semiconductor, where it is less relevant when dealing with solid-liquid or liquid-liquid interfaces [119].

2.5.1 Charge Development at the Quartz Surface

The mechanism of charge separation at an oxide surface in contact with brine is by ionization of the surface group. Oxide surfaces possess many amphoteric hydroxyl groups (M-OH where M is the metal ion) that can react either with H^+ or OH^- ions in the brine, depending on the pH of the solution. The equation is as follows:

$$MOH_2^+ \overset{H^+}{\longleftarrow} M-OH \overset{OH^-}{\longrightarrow} M(OH)_2^- \tag{2.8}$$

In this case, H^+ and OH^- ions are directly responsible for the development of the surface charge [27] and are widely considered potential determining ions [120]. The sign and density of the surface charge depend on the pH because this dictates the

relative proportions of H^+ and OH^- ions, which react with the surface. These potential determining ions completely leave the solution and enter tight chemical bonds with the solid, thus producing the charge density on the solid surface [121].

There are two types of surface groups present on the quartz surface: the singly coordinated group called silanol (SiOH) and the doubly coordinated group, siloxane (Si_2O). The siloxane group can be considered inert because its protonation is extremely low. However, the silanol group can react to produce either a positive or negative surface group [27]. At very low pH, where the density of H^+ is high, the reaction produces $Si(OH)_2^+$, while at high pH where the OH^- concentration is high, SiO^- will be produced. The pH at which there is no net charge on the solid surface is the PZC [118]. The PZC for silica has been recorded at a pH of 2-3 by Lykleme et al. [120]. If the brine is made of NaCl at a range of pH between 7 and 8, the typical pH for formation water , the reaction at the silanol surface sites can be written as follows [122]:

$$SiOH^0 \leftrightarrow SiO^- + H^+ \tag{2.9}$$

$$SiOH^0 + Na^+ \leftrightarrow SiONa + H^+ \tag{2.10}$$

The reaction releases H^+ ions into the solution, a process called deprotonation [27,123]. Therefore, in sandstone reservoirs, the mineral surfaces usually become negatively charged.

Ions that have the same charge as the mineral surface are called co-ions, and those that have the opposite charge are called counter-ions. Ions that are not part of the potential determining ions may also be classified as indifferent or specifically adsorbed if they do not interact chemically with the surface. Specifically, adsorbed ions contribute to the charge separation by differential adsorptions of ions from the solution into a solid surface. It is worth nothing that the exchange of OH^- and H^+ ions and the adsorption of Na^+ and/or Cl^- ions, means that both the pH and salinity of the brine may change as it equilibrates with the mineral surfaces.

2.5.2 Charge Separation at Clay Surfaces

In the case of clay minerals, a common charge separation involves an isomorphic substitution of ions [124]. Isomorphic substitution is described as phenomena in which an ion in the clay mineral lattice (such as Si^{4+} or Al^{3+}) is replaced by another ion of a similar size but generally of lower charge [106]. This occurs during the formation of clay crystals, which are different in structure compared to silica (quartz). Clay minerals exist as microscopic plate-like layers of silica tetrahedral and alumina octahedral sheets [125]. The basic building block of the silica tetrahedral sheets is the tetrahedron, which consists of one silicon atom surrounded by four oxygens **(**Figure 2.14**).**

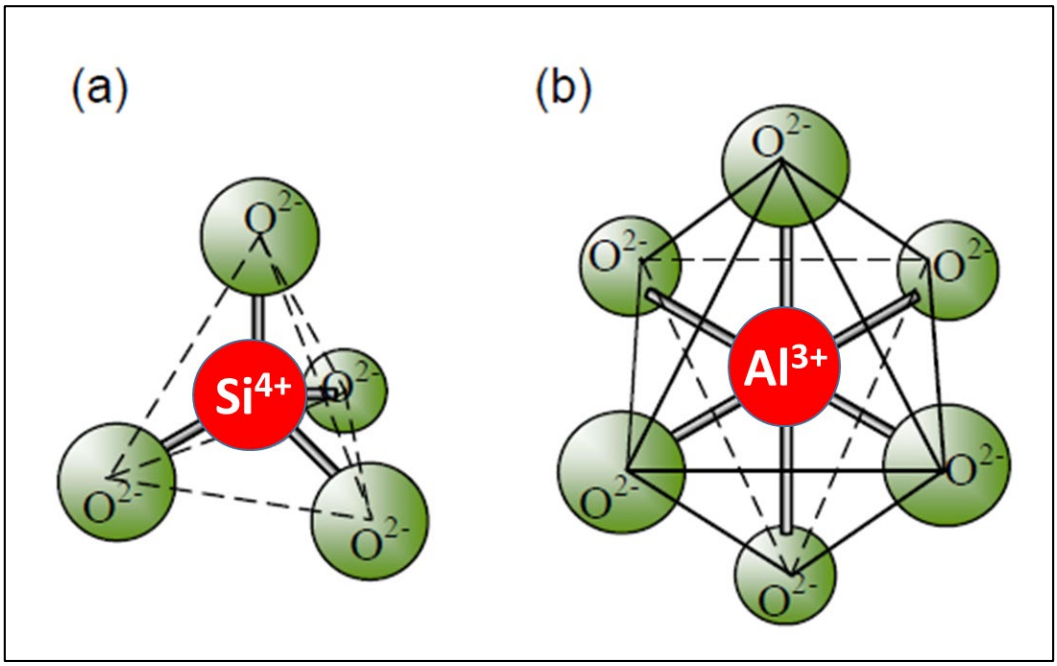

Figure 2.14 (a) Silica tetrahedron molecule of clay mineral structure. (b) Alumina octahedron molecule (modified from Jaafar [126]).

These tetrahedrons are linked horizontally and bound by the shared oxygen to form a tetrahedral sheet. Alumina octahedrons form alumina octahedral sheets (Figure 2.14). Each alumina octahedron consists of one aluminium that is linked covalently to six oxygen or hydroxyl ions. The octahedrons are arranged horizontally and are bound by the shared oxygen to form the octahedral sheet.

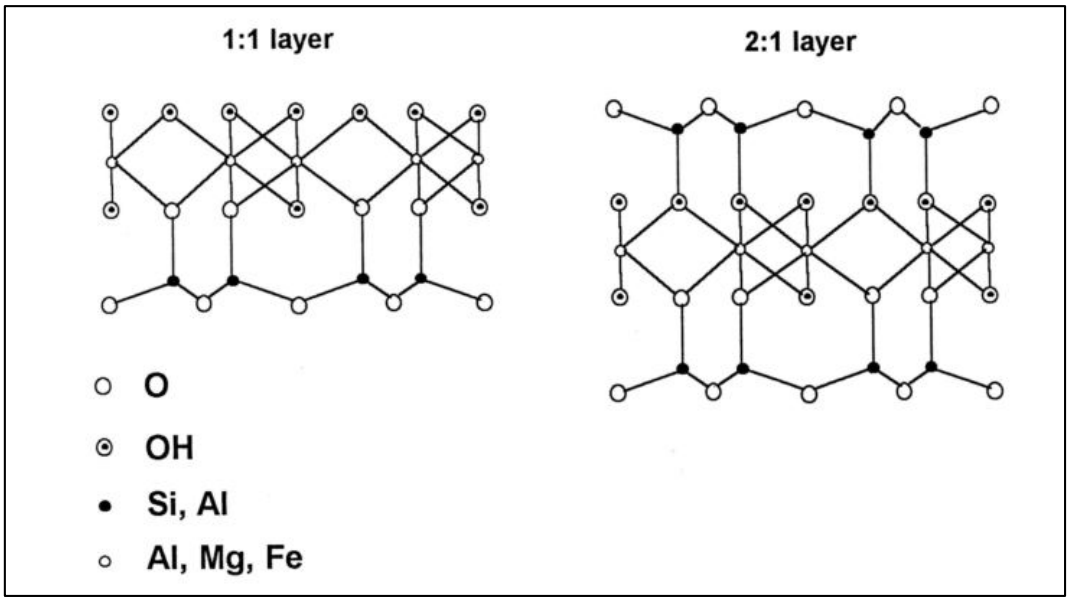

Figure 2.15 Tetrahedral sheet combines with an octahedral sheet to form 1:1 and 2:1 clay layers [126].

Clay layers can be built from one tetrahedral sheet linked to one octahedral sheet (Figure 2.15) in a 1:1 layer structure (such as kaolinite and serpentine) or one tetrahedral sheet between two tetrahedral sheets (Figure 2.15) in a 2:1 layer structure, such as montmorillonite, vermiculite, and mica (Bujdak and Rode, 1999). The silicon and aluminium layers are held together by shared chemical bonds. Kaolinite is a 1:1, non-expanding clay mineral, in which different layers are held together by hydrogen bonding. Kaolinite has a small net negative charge because the clay crystals have broken edges [127]. In some 2:1 clay minerals, such as montmorillonite, there is an ample space between the layers where water and other molecules or cations can gather (Figure 2.16).

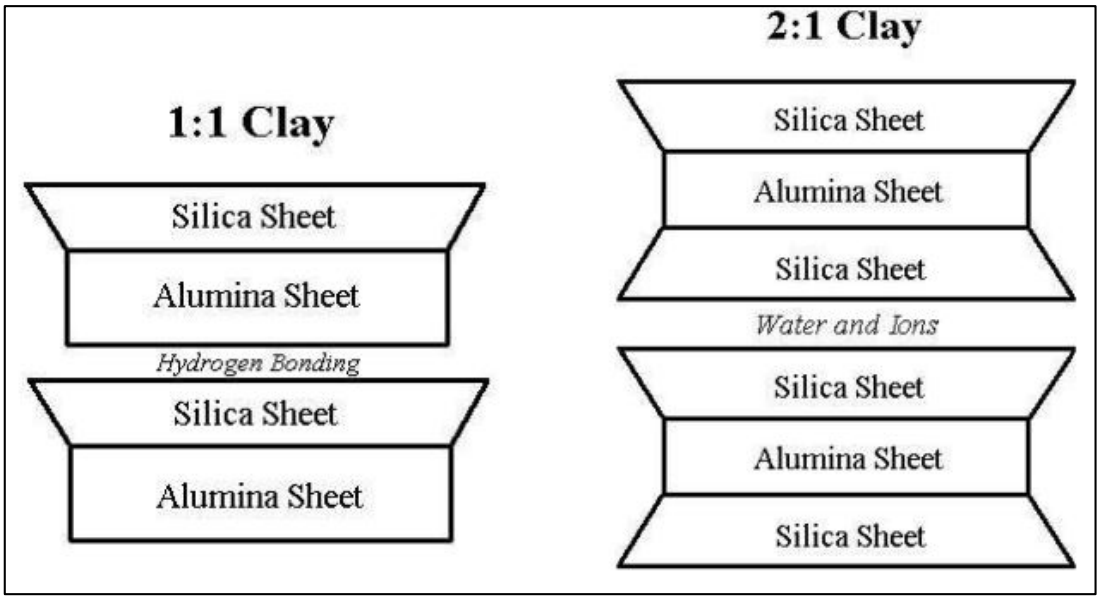

Figure 2.16 Arrangement of layers to form clay crystals. (a) 1:1 clay structure with hydrogen bonding between layers. (b) 2:1 clay structure with larger space between the layers which is occupied by water and ions [126].

Isomorphous substitution can take place in silica and tetrahedral and alumina octahedrons of the clay minerals. A replacement of one Si^{4+} by Al^{3+} in a silica tetrahedron or one Al^{3+} by Mg^{2+} in an alumina octahedron yields one negative and unbalanced charge in the crystal. This type of negative charge is independent of pH [127]. Through this isomorphous substitution, cations in the brine become entrapped within the clay mineral lattice. An access charge of opposite sign is formed in the pore fluid to counterbalance the charge deficiency of the clay minerals. This process involves the exchange of ions across the interface. The cation-exchange capacity (CEC) term is used to represent the excess surface charge per unit weight of the minerals [127]. It also indicates the extent of ions exchanged across the interface.

Isomorphous substitution is independent of pH, and the surface charge density cannot be reduced to zero [128]. However, altering the pH could promote the adsorption of H^+ and OH^- ions onto the silanol surface group at the edge of the crystal. The protonation and deprotonation of the surface group also contribute to the surface charge in clay minerals. Although the overall charge of the particle is negative in general, under acidic conditions, both negatively and positively charged parts of the surface of clay mineral particles could coexist simultaneously [129].

All the mechanisms of charge development in quartz and clay minerals involve the movement of ions across the interfaces. Electrical neutrality is maintained across the interfaces through the ion exchange. The charge in the liquid will balance the excess charge in the solid. The next question concerns how these excess charges are distributed in the solid phase and liquid phase. This question has led to the formation of the EDL model that will be discussed in the next section.

2.6 Electrical Double Layer

An electrical double layer (EDL) is a system describing the distribution of charges that contains excess surface charges opposing a layer with extra charges [130]. The double-layer model is developed to determine the charge distribution and the ionic environment on the surface charge. The concept plays a significant role in the field of electrochemistry, colloid surfaces, and surface chemistry in various applications, including in the petroleum industry [131].

Numerous theoretical models have been developed to explain the electrical double layer. The importance and the development of the electrical double layer are reviewed below.

2.6.1 Helmholtz's Model

The initial model of EDL was proposed by Helmholtz in 1985 when he conducted the study on the charge array at the interface between two dissimilar metals [132]. He developed a simple model consisting of two charge layers with thickness and distance apart are of the atomic dimension. The first layer is considered as adsorbed ions at the surface. This model guided Helmholtz to treat the double layers mathematically as simple as a capacitor. The interaction between the surface and the ions in the solutions is assumed to be electrostatic in nature. To maintain neutrality at the interface, the charge at the surface is balanced by the distribution of ions close to the surface (Figure 2.17). The distance between the

surface and the closer ions is assumed to be limited by the ionic radius. The potential drop is treated as a linear trend, and it is confined only to the region called a Helmholtz Plan.

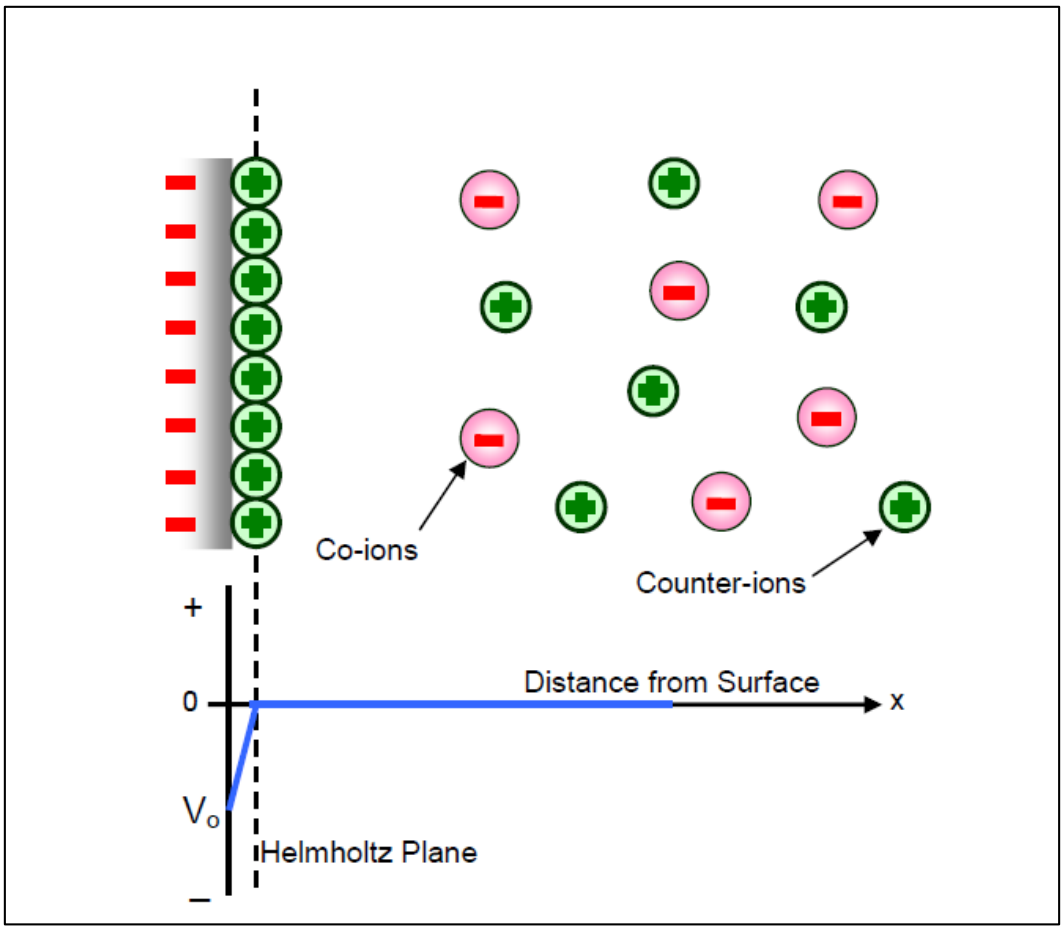

Figure 2.17 Helmholtz's model of Electrical Double Layer. Electric potential drops linearly analogous to a capacitor and only confined to the Helmholtz Plane [126].

The Helmholtz model successfully provides a basis for rationalizing the ionic behavior at the interface. However, it cannot explain many factors such as diffusion in the solution and the adsorption on the surface. Helmholtz model offers a reasonable representation of high concentration electrolytes [133] when the thin layer collapses but, it overestimates the density of counter-ions between solid and Helmholtz Plane. The hypothesis of rigid layers of opposite charges does not adequately account for many features.

2.6.2 Gouy-Chapman Model

Gouy and Chapman came later and proposed an improved EDL model by introducing a diffuse layer. This layer highlights an exponential potential decrease in the electrical (Figure 2.18) from the surface to the bulk of ions. The kinetic energy of the counter ions partially affected the thickness of the diffuse double layer.

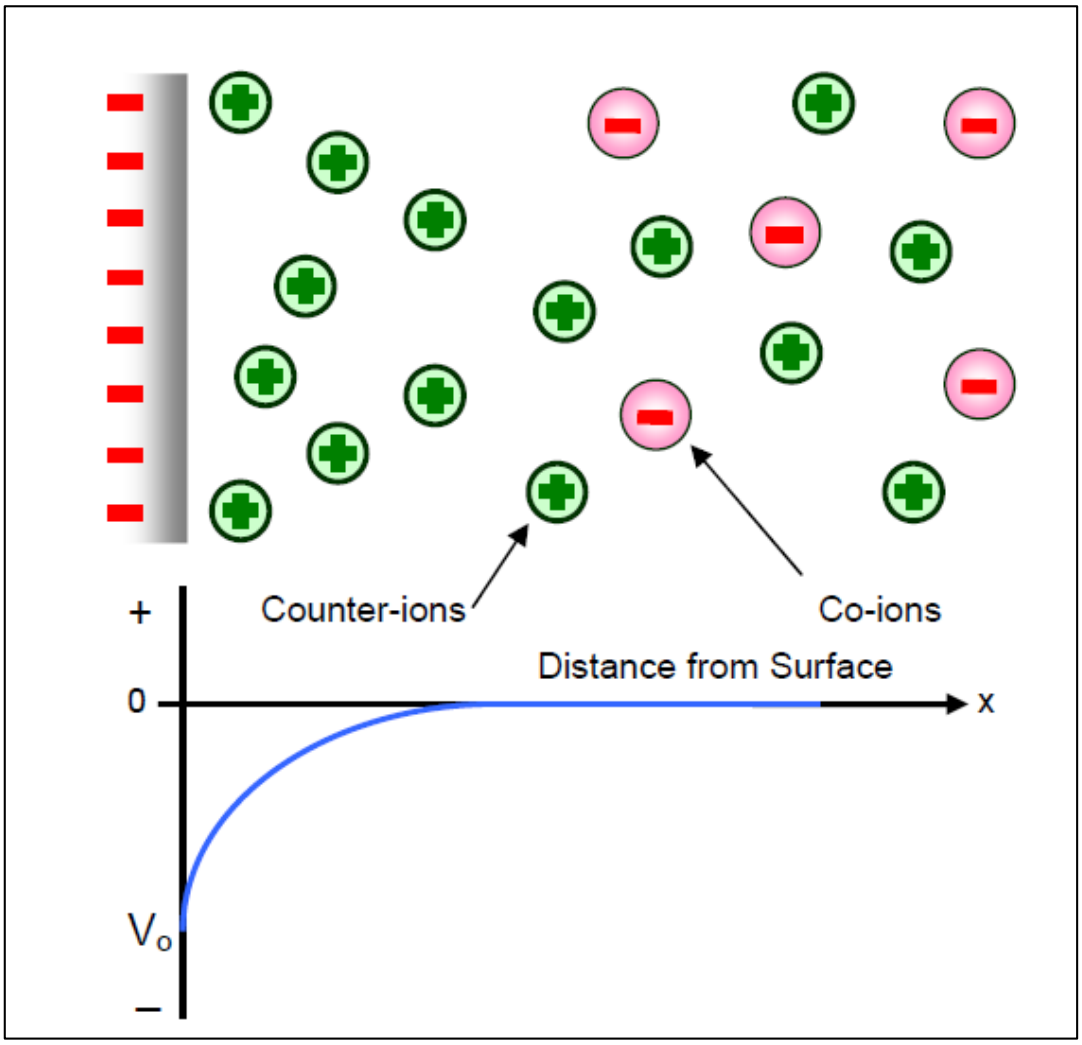

Figure 2.18 The Gouy-Chapman model of the diffuse layer. Electric potential drops exponentially away from the mineral surface [126]

Gouy [134] and Chapman [135] developed this diffuse layer theory in which the change in concentration of the counterions near a charged surface follows the Boltzmann distribution:

$$n_i = n_i^0 \exp(-\frac{eVz_i}{Tk_b}) \tag{2.11}$$

Where n_i is the local concentration in the double layer of ion of type i, n_i^0 is the ion concentration in the bulk fluid, z_i is the valency of the ion, e is the charge on a proton, V is the electric potential, k_b is the Boltzmann constant and T is the absolute temperature.

The relation of electrostatic potential and the electrical charge density (ρ) is given by Poison's equation by assuming constant permittivity (ε),

$$\nabla^2 V = -\frac{\rho}{\varepsilon} \tag{2.12}$$

The Volume charge density is given by

$$\rho = \sum_i n_i z_i e \tag{2.13}$$

Combining equation (2.11), (2.12) and (2.13) yields the complete Poisson-Boltzmann equation:

$$\nabla^2 V = \frac{d^2V}{dx^2} = -\frac{1}{\varepsilon} \sum_i n_i^0 z_i e \exp(-z_i \mathrm{eV} / Tk_b) \tag{2.14}$$

Equation 2.14 is solved by assuming V to be small everywhere in the double layer, thus $z_i eV \ll Tk_b$. This approach is known as the Debye-Huckel approximation [128]. The exponential term can be expanded using relation $e^{-x} = 1 - x$

$$\frac{d^2V}{dx^2} = -\frac{1}{\varepsilon}\left[\sum_i n_i^0 z_i e - \sum_i n_i^0 z_i^2 e^2 \mathrm{V} / Tk_b)\right] \tag{2.15}$$

Since the bulk solution is neutral, the first term in the parentless has to be zero, and equation 2.15 is reduced to

$$\frac{d^2V}{dx^2} = K^2V \tag{2.16}$$

Where

$$k = \left[\frac{e^2 \sum_i n_i^0 z_i^2}{\varepsilon T k_b}\right]^{\frac{1}{2}} \tag{2.17}$$

The solution for equation 2.17 is

$$V = V_o \exp(-kx) \tag{2.18}$$

Which is valid for $V_O < 25.7mV/Z$ at 25 °C.

Equation 2.14 can be simplified for a symmetrical electrolyte in which $n_{i+}^o \approx n_{i-}^o$ and the bulk concentration is $2n^0$. In this case, $z = z+ = -z$. Equation 2.13 can then be written as

$$\rho = \sum_i n_i \, z_i e = -2zen^o \sinh(\frac{zeV}{kT}) \tag{2.19}$$

Thus

$$\frac{d^2V}{dx^2} = \frac{2zen_o}{\varepsilon} sinh(zeV|Tk_b) \tag{2.20}$$

Equation 2.20 can be solved as follows

$$V = \frac{2kT}{ze} ln \left\{ \frac{1 + \exp(-kx) \tanh(zeV_O/4k_bT)}{1 - \exp(-kx) \tanh(zeV_O/4k_bT)} \right\} \quad (2.21)$$

Equation 2.21 gives the potential value at a distance x from the surface. The charge per unit area on the surface must be balanced to the adjacent fluid

$$q_o = -\int_o^\infty \rho dx \quad (2.22)$$

Which gives

$$q_o = -\varepsilon \left(\frac{dV}{dx}\right) = 2\sqrt{2k_bTn_o\varepsilon \sinh(zeV_O|2k_bT)} \quad (2.23)$$

Using the Debye-Huckel approximation

$$q_o = -\varepsilon \left(\frac{dV}{dx}\right) = \varepsilon k V_O \quad (2.24)$$

k has dimensions of reciprocal length. $1/k$ is known as Debye length that indicates the thickness of the double layer. With increasing electrolyte concentration, the width of the double layer $(1/k)$ will decrease.

Gouy-Chapman model has provided a better explanation of EDL as compared to Helmholtz's theory. However, the model does not fit for highly charged double layer. This is because the assumption made of ion can be neglected at high concentrations is not valid for high concentration [136]. This is also supported by Hunter [128] that at a near region of the surface, the ions cannot be regarded as point charges. Moreover, the high electrical fields approaching the surface will affect dipoles and alters the permittivity.

2.6.3 Stern and Grahame Modification of the Diffuse Layer

The improvement theory of EDL by Gouy-Chapman still has limited quantitative application. Stern, therefore, introduced the modified Gouy-Chapman where the layer is diffused by dividing the access charge in the electrolyte into two regions:

i. The Stern or inner layer very close to the surface where the charges and potential distribution are determined primarily by the geometrical restriction of ions and molecule size. Besides, it is also controlled by the interaction between ions, walls, and adjoining dipoles.
ii. The diffuse layer (Gouy-Chapman), which the Poisson-Boltzmann distribution represents the charges and potential distribution.

Stern theory suggests that ions do have finite sizes, and they cannot approach the surface closer than the physical ionic radius. Potential drops to be linear across the Stern layer as in the Helmholtz model and exponentially across the diffuse layer as predicted by the Gouy-Chapman model.

Grahame [137] in 1947 found the Stern model works well on presenting electrolytes such as Sodium Fluoride (NaF) which contains strongly hydrated ions. The firmly attached hydration layer prevents the ions from interacting chemically with the electrode surface. However, when other ions such as Cl^-, Br^- and I^- are in the solution, they may interact and become specifically adsorbed to the electrode. Grahame later suggested that the Stern layer be subdivided into the inner and outer layers. The plane of centers of the specifically adsorbed ions is termed the Inner Helmholtz Plane (IHP), and the plane of centers of the nearest hydrated counter-ions adsorbed to the surface is called the Outer Helmholtz Plane (OHP) [128].

The counter-ions in the Stern layer are firmly attached to the solid surface and are mostly immobile. In the diffuse layer, there is a shear plane close to the OHP. The counter-ions ahead of the shear plane are mobile. The potential at the shear plane is defined as zeta potential (Figure 2.19). The pH at which the zeta potential is zero is

called the iso-electric point (IEP). The specifically adsorbed ions can cause the IEP to be different from the PZC [138]. The excess concentration of ions is taken away from the surface until the fluid becomes electrically neutral. The neutral zone is called the free electrolyte [130].

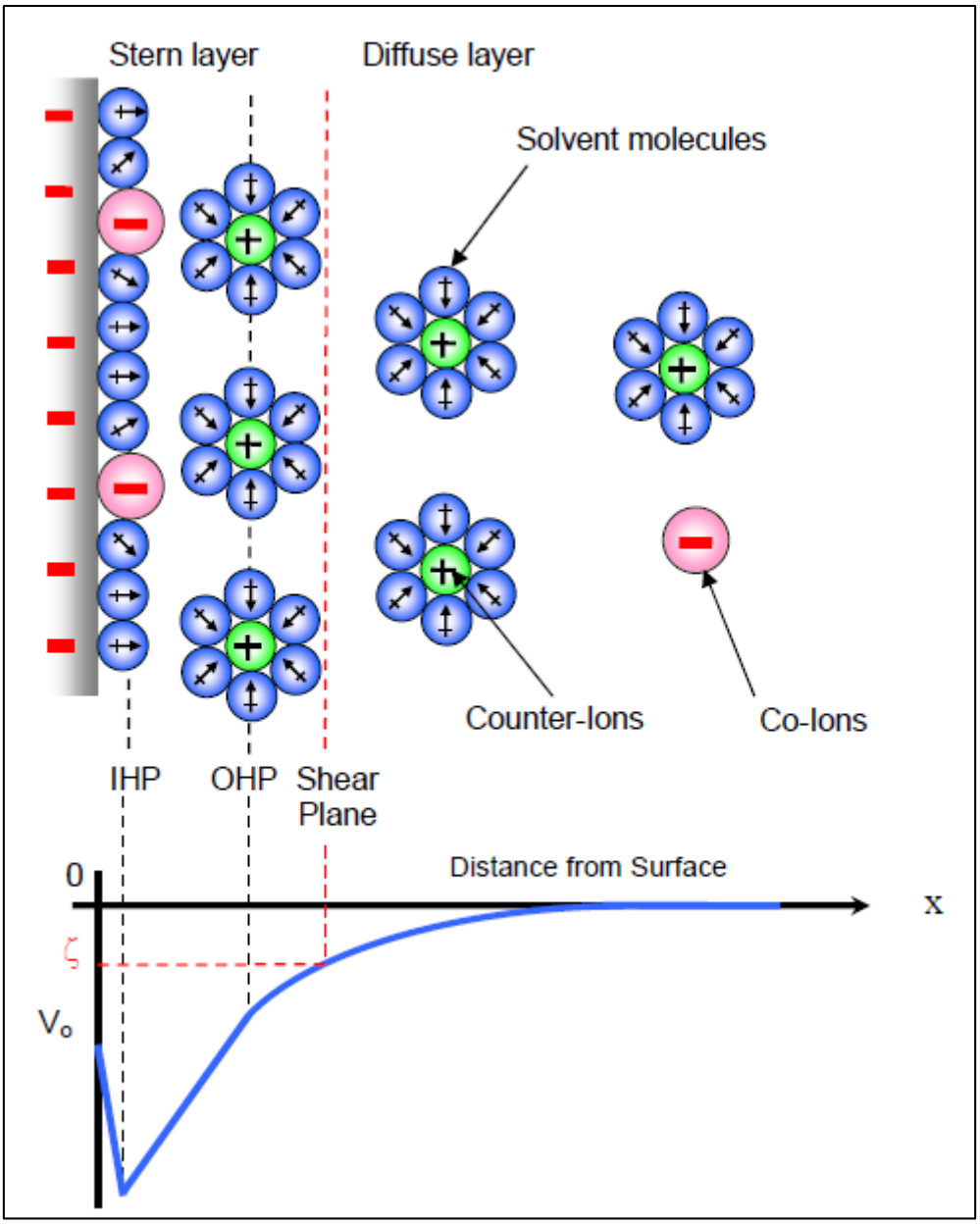

Figure 2.19 Modified double layer by Stern (1924) and Grahame (1947). Some ions can specifically be adsorbed to the mineral surface and affect the potential. Zeta potential is defined as the potential at the shear plane [126].

Despite having some limitations, the combined Gouy-Chapman-Stern-Grahame model is widely used. Their limitations have been discussed by Zhang [139] in 2007. He made the following assumptions to overcome the limitations;

i. Ions are treated as point charges in the diffuse layer.
ii. The only significant interaction in the diffuse layers is in coulombic nature.
iii. Dielectric permittivity is constant through the double layer.
iv. The viscosity of the fluid is constant above the shear plan.

2.6.4 Spherical Double Layers

The most practical problem involves the spherical surface (Figure 2.20 a) that occurs in connection with dispersion and emulsion.

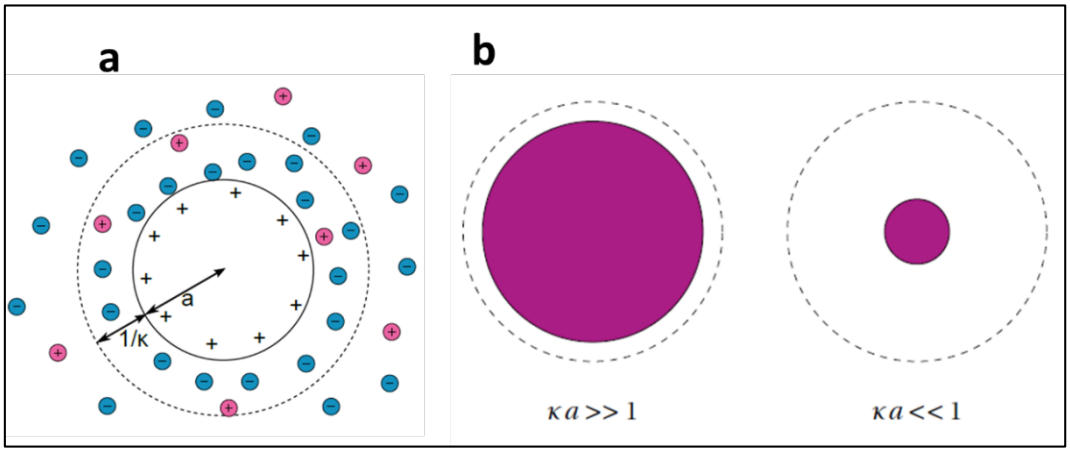

Figure 2.20 (a) Illustration of spherical Gouy-Chapman model of EDL, (b) the illustration of charged particles with a thin and thick double-layer [140].

When the spherical surface is considered, the Poisson equation (equation 2.12) can be rearranged as;

$$\nabla^2 V = -\frac{\rho}{\varepsilon} = \frac{1}{r^2}\frac{d}{dr}\left(\frac{r^2 dV}{dr}\right) = \frac{2zen_o}{\varepsilon} sinh\left(\frac{zeV}{kT}\right) \quad (2.25)$$

Where r is the distance from the center of the sphere of the shape and ρ has been substituted from equation 2.19. Using Debye-Huckel approximation ($zeV_O/2kT \ll 1$) for low potential, the equation can be solved explicitly. For particles of radius a, a double integration with boundary conditions $V = V_O$ for $r = a$ and $V = 0$ and $dV/dr = 0$ at $r = \infty$, the following expression is obtained;

$$V = V_O\left(\frac{a}{r}\right) exp[-k(r-a)] \quad (2.26)$$

The surface charge density (ρ) is determined by summing the charge in the spherical, diffused double layer (from $r = a$ to $r = \infty$) and divided by the surface area of the particle ($4\pi a^2$). Substituting the $\rho = f(r, V)$ from equation 2.25 and taking into account that $\varepsilon(dV/dr) = 0 \ and \ r = \infty$, the interaction gives,

$$\rho_o = -\frac{1}{4\pi a^2}\int_a^\infty \rho \, 4\pi r^2 dr = \frac{\varepsilon}{a^2}\int_a^\infty \frac{d}{dr}\left(r^2\frac{dV}{dr}\right) dr = -\varepsilon\left(\frac{dV}{dr}\right) \quad (2.27)$$

Substituting for $(dV/dr) = 0 \ and \ r = \infty$ obtained by derivation of equation 2.26, the expression gives;

$$\rho_o = \frac{\varepsilon V_O(1+ka)}{a} \quad (2.28)$$

Regarding equation 2.28, the surface potential at the surface becomes:

$$V_O = \frac{\rho_o a}{\varepsilon(1 + ka)} \tag{2.29}$$

If the $ka \gg 1$ ($1/k$ is in the nm range), Equation 2.29 becomes identical with the expression derived for flat double layers and low potentials. The following qualitative rules have been suggested [141];

i. When $|V_O| \ll 2kT/ze$, equation 2.29 should be used.
ii. If $|V_O| \gg 2kT/ze$ and $ka \ll 1$, equation 2.25 is more favourable.
iii. When condition $|V_O| \ll 2kT/ze$ is not fulfilled;
    a. If $ka \ll 1$, equation 2.29 is acceptable for the moderately high value of V_O, but it becomes worse if it exceeds 80-90 Mv.
    b. If $ka \gg 1$, the general equations for flat double layers should be used.

2.6.5 Surface Charge Density

According to Equation 2.29, the surface potential at the solid surface can be measured when the surface charge density is available. The surface charge density (ρ) is the number of charges per unit surface and usually is given as coulomb per m^2 (C/m^2) [141].

The primary method used to determine the surface charge density is the potentiometric titration of the suspension. It measures the charges which depend on the activities of the potential determining ions of H^+ and OH^- [142]. Titrations of suspension particles in aqueous electrolyte solutions can be in many ways such as acid-base titration, mass titration, and electrolyte titration, in which they are having different aims.

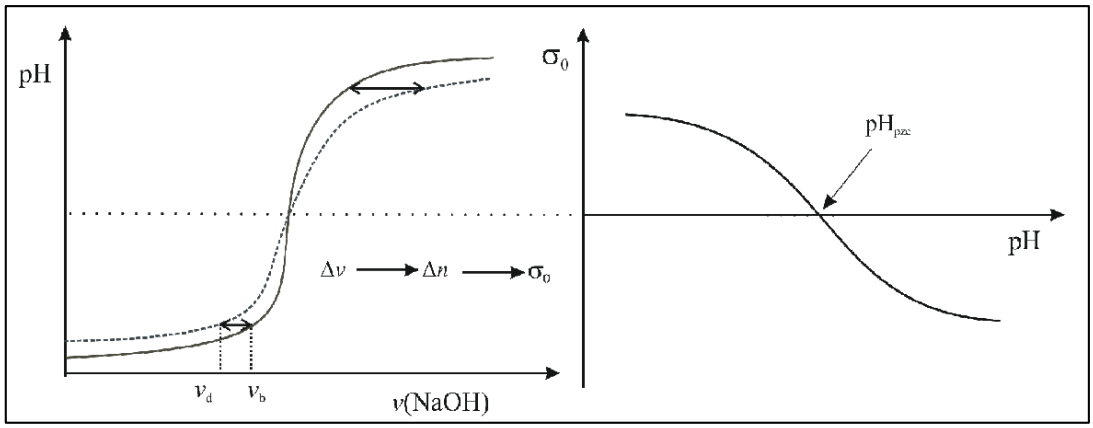

Figure 2.21 Schematic representation of the acid-base potentiometric titration of suspension. The dashed line is the solid suspension titration. The solid line is the blank titration without particles. The right graph is the resulting proton related to surface charge density as a function of pH [142].

In the case of acid-base titration (Figure 2.21), measurement is made on the dependency of pH equilibrium of protonation and deprotonation ions in the solutions. For the titration of an acidic suspension with base (NaOH), the relationship can be expressed as follows [127,142];

$$\Gamma_{H^+} - \Gamma_{OH^-} = \frac{C_{NaOH}(v_b - v_d)}{s\gamma V} \tag{2.30}$$

For titration of suspension with acid (HCl), the sign should be reversed;

$$\Gamma_{H^+} - \Gamma_{OH^-} = -\frac{C_{HCl}(v_b - v_d)}{s\gamma V} \tag{2.31}$$

Then, the surface charge density related to interactions of potential determining ions of H^+ and OH^- becomes;

$$\rho_o = F\,(\Gamma_{H^+} - \Gamma_{OH^-}) \tag{2.32}$$

Here Γ is the surface concentration of relevant species such as their amount (moles) divided by the surface area that related to the change of their concentration in the bulk solutions. To be noticed, the Γ_{H^+} *and* Γ_{OH^-} are positive in the case of

binding and negative in case of release ions from the solid surface. The difference $\Gamma_{H^+} - \Gamma_{OH^-}$ represents the net uptake of H^+ or release of OH^- ions. C_{HCl} and C_{NaOH} are the concentration of titrant. v_b is the volume added in the blank titration without solid suspension and would correspond to the volume v_d of titrant added in the solid dispersion to reach the same pH. s is represented as the specific surface area (surface area divided by the mass of solid), γ is the mass concentration of solid (mass of solid divided by the suspension volume) and F is the Faraday constant.

The plot of surface charge density against pH enables the determination of the PZC for the particles. The intersection of pH with the zero charge density is the PZC value. PZC value is essential for identifying the surface charge behavior of the particle.

2.6.6 Ionic Strength Effect on EDL

The zeta potential depends on the amount and valency of the ions present. The ionic strength enables the relationship to be treated mathematically by the following equation [140]:

$$I = \frac{1}{2}\sum_{i=1}^{n} C_i Z_i^2 \tag{2.33}$$

Where I is the ionic strength, C_i is the molar concentration of ions and Z_i is the charge number of ions. From the Gouy-Chapman theory, a correlation between the ionic strength and Debye length ($1/k$) can be derived:

$$k = \left(\frac{2000F^2}{\varepsilon_o \varepsilon_R RT}\right)^{1/2} \sqrt{I} \tag{2.34}$$

Here F is the Faraday constant, R is the gas constant per mole and T is the temperature of the system. From the equation, it can be observed that the Debye

length is inversely proportional to the square root of the ionic strength. This further illustrated that the double layer would be compressed by increasing the concentration or valency of counter-ions in the system [143].

2.7 Zeta Potential Measurement

Whenever the particles are exposed to electrical fields, they will be electrically charged and will exhibit certain effects called electrokinetic effects. The method of measuring zeta potential fundamentally derives by these electrokinetic effects. When a charged particle surrounded by an electric double layer is exposed to an electric field, the double layer is distorted and as a consequence creates its own electric field [144]. There are four different electrokinetic effects; electrophoresis, streaming potential, electroosmosis, and sedimentation potential.

2.7.1 Electrophoresis Method

The electrophoresis method involves the translation of solid particles with respect to the liquids under the action of external electrical fields. The parameter measured is the electrophoretic mobility (u_e), which is the velocity of particles moved by the electrical fields (E);

$$v_e = u_e E \tag{2.35}$$

The zeta potential is then calculated using the Helmholtz-Smoluchowski equation for electrophoresis;

$$u_e = \frac{\varepsilon_o \varepsilon_R \zeta}{\mu} \tag{2.36}$$

Where ε_R is the relative permittivity of the electrolyte solution, $\varepsilon_o$is the permittivity of vacuum, ζ is the zeta potential, and μ is the fluid viscosity. The range in which this method (details explained by Delgado et al in 2005 [145]) can be applied is determined by the value of ka, where a is the radius of curvature and k is the inverse value of Debye length in equation 2.34.

2.7.2 Streaming Potential Method

The methods of streaming potential involve the movement of electrolyte with respect to the stationary solid surface. The solid is typically in the form of a porous plug and confined in a pressurized vessel. The reading of streaming potential is taken at the boundaries of the plug [146]. The streaming current is directly detected by measuring the electric current between the upstream and downstream of the plug. This process can be achieved by means of nonpolarizable electrodes that are connected to an electrometer recorder of adequately low internal resistance.

The important issue when conducting the streaming potential measurement is the error happens due to the polarization electrode [147]. This occurs when the charges accumulate on the electrode surface, thus causing the formation of another double layer that strongly alters the ion distribution within the sample under investigation. Therefore, using nonpolarizable electrodes is the option to avoid this error.

2.7.3 Electro-Osmosis Method

The electro-osmosis method serves as an alternative to the streaming potential for measuring the zeta potentials [145]. The electro-osmosis flow is linked to zeta potential by the Smoluchowski equation as follows [148];

$$\zeta = \frac{\mu\sigma Q}{\varepsilon_o \varepsilon_R I} \tag{2.37}$$

Q and I are the macroscopic fluid flow rate for zero pressure gradient and the electrical current passing through the porous sample, respectively. The equation can be used when the $ka \gg 1$ and there is no surface conduction.

2.7.4 Electro-Acoustic Method

Electroacoustic methods used sound waves for measuring zeta potential. There are two phenomena to describe their mechanism. The first is if the sound wave passes through a colloidal suspension, the electrical current is created, which is known as colloid vibration current [149]. This arises due to the difference in density between the particles and the surrounding environment. The inertial forces induced by the vibration of the suspension as the wave travels, give rise to a motion of the charged particles relative to the liquid, generating an alternating electromotive force.

Secondly, the opposite effect occurs when an alternating electric field is applied to a colloidal suspension. It generates a sound wave called the electrokinetic sonic amplitude, as a result of the motion of the particles. For both cases, the applied field and the response occur at the same frequency. The electroacoustic technique offers an important advantage because it can be applied to concentrated dispersions [145].

2.7.5 Different Results between the Methods

Zeta potential is expected to be the same irrespective of different methods applied for measurement. Some experimental studies have shown good agreement between the methods [150]. However, the obtained zeta potential from different methods may vary due to the different positions of the shear plane [151].

In this study, the electrophoresis method is used to measure the zeta potential of particles suspension. From the measured electrophoretic mobility, the zeta potential is calculated using equation 2.36. This chapter continues with a review on application of zeta potential in describing the surfactant adsorption onto rock surfaces that are strictly related to the subject of the thesis.

2.8 Surfactant Adsorption study using Zeta Potential

There are various reasons for measuring the zeta potential in the laboratory. The most prominent application of zeta potential is in colloid science, where it is used as an indicator for colloid stability. A colloid system with a higher magnitude of zeta potential is expected to be more stable. This is because the potential energy of repulsion between the particles is higher [152]. The zeta potential is a microscopic manifestation of charged interfaces. In contact with porous media, zeta potential is an indication of the charging behavior of rock surfaces which can further extend to investigate the interaction between the surfactant and the rock surfaces. However, zeta potential is not only a rock property. It depends on many parameters including pore microstructure, fluid viscosity, flow rate, pH, salinity, ion valency, saturation, temperature, chemical composition and mineralogy of the rocks. This section provides a review of a previous laboratory study of the zeta potential. The section aims to identify research gaps in the area and the scope of this project.

The adsorption isotherm is widely used to explain the adsorption of surfactant onto the rock surfaces during surfactant flooding. By refering to adsorption isotherm, the amount of surfactant adsorbed (per unit mass or surface area) at a given temperature and the effectiveness of the surfactant adsorbed can be determined [153]. However, the orientation of surfactants at the interface and their adsorbed structure cannot be observed [154]. The first description of hemi-micelles structure adsorbed was published by Fuerstenau [155] in 1956, which is the first investigation on the surfactant adsorption mechanism by electrokinetic potential. Numerous published papers such as by Kosmulski [156], Fuerstenau [155], Rosen [153], and Karraker et al. [157] showed the possibility of this technique for such study. The

interaction of solid interface is determined by an EDL in which the adsorption is controlled by the charged process including ion-exchange, ion-pairing and acid-base interaction [153].

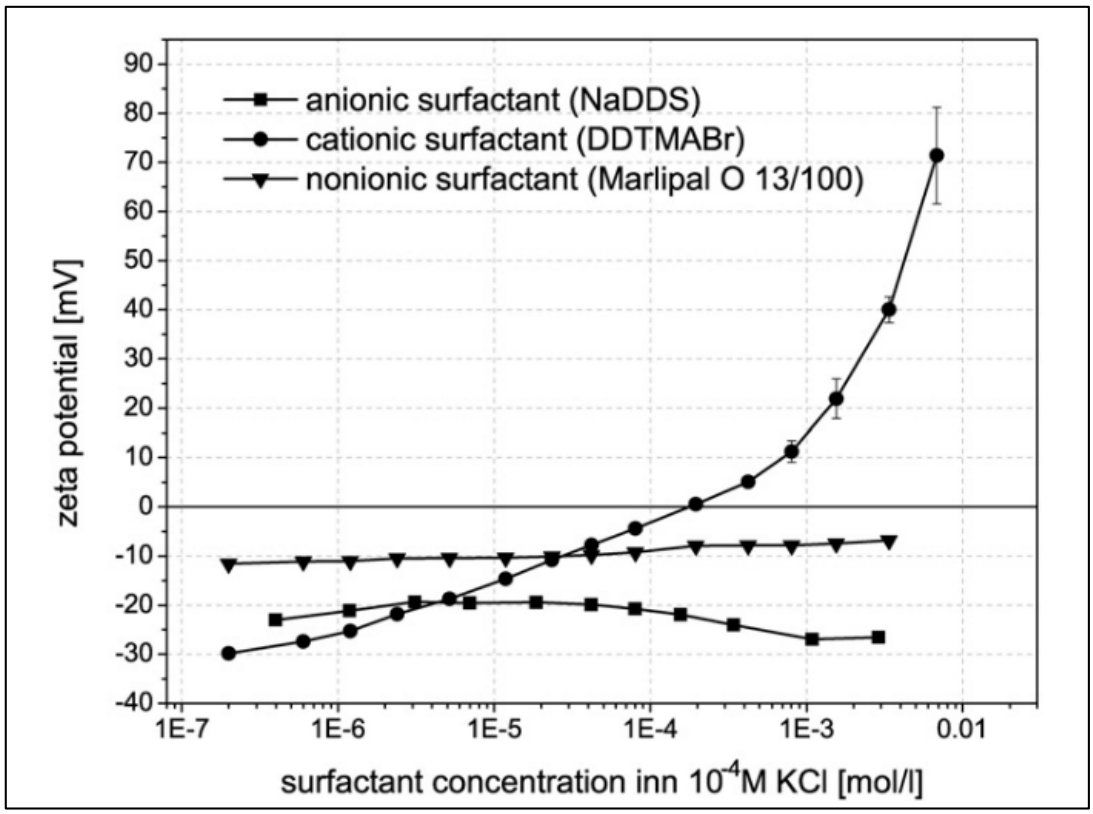

Figure 2.22 Surfactant adsorption on silica surface (wafer): (●) cationic surfactant (dodecyl trimethyl ammonium bromide), (▼) non-ionic surfactant, (■) anionic surfactant (sodium dodecyl sulfate) [154].

Figure 2.22 shows the different adsorption study based on the different head groups of surfactants onto the silica surface using zeta potential. In the case of an opposite charge of the surface, the surfactant and the driving force of the adsorption was controlled by the electrostatic nature. The surface charge changes with the adsorption as the progress can be observed and the IEP can be determined. For the case of both having the same charge, the repulsion force or hydrophobic bonding is possible for the adsorption mechanism. Hence, the surface charge only slightly increases during the first part of adsorption. However, the presented results do not indicates the effect of pH, electrolyte background and divalent ions in which these parameters have significant control over the surface charge and zeta potential behavior [158].

Alargova et al. [159] successfully interpreted the pH-dependent binding of various ions to the head group of adsorbed surfactants using adsorption isotherm combined with the theory of EDL which is enabled by zeta potential measurement. Their study was later extended by Bellmann et al. [154]. In the study, they determine the surfactant adsorption on the oppositely charged particle from the zeta potential measurement.

All the previous measurements of zeta potential show promising findings and explanations of the surfactant adsorption mechanism. However, there are limited studies reported for the combined effect of pH, electrolyte concentration and the effect of divalent ions (ionic strength) on the development of the surface charge.

2.9 Focus Area

For this project, experiments are designed to gather the zeta potential value across a wide range of brine salinity. Typical brine salinities for giant oil reservoir is 0.5 M (30 g/ L) for sandstone [160]. Besides, seawater salinity is commonly at about 0.6 M (35 g/L). Thus, there are three different concentrations used, which are 0.01M, 0.1M, and 1M. Using NaCl in the experiment is reasonable considering the relative proportion of sodium and chloride in the seawater composition. Table 2.4 shows a typical seawater composition.

Table 2.4 Typical seawater composition [161].

Component	Composition (mg/L)	Percentage (%)
Chloride	19375	55.33
Bromide	67	0.19
Sulfate	2712	7.75
Potassium	387	1.11
Sodium	10760	30.73
Magnesium	1294	3.70
Calcium	413	1.18
Strontium	8	0.02
Total	35016	100.00

Although NaCl is the main component in the seawater and oilfield brines, the effect of other ions should be determined to obtain more representative results. A typical element of oilfield water is detailed in Table 2.5. Therefore $CaCl_2$ is also used in the experiment to see the effect of divalent ion, the zeta potential, and the surface charge.

Table 2.5 Inorganic constituents of oilfield waters [161].

Cations	**Composition range (mg / L)**	**Anions**	**Composition range (mg / L)**
Sodium	10000	Chloride	10000 - 200000
Calcium	1000 - 30000	Bromide	50 - 6000
Magnesium	1000 - 30000	Iodide	10 - 1400
Aluminium, Ammonium, iron, lead, magnesium, zinc	> 10	Bicarbonate and sulfate	0-1000
		Arsenate, Borate, Carbonate, Flouride, hydroxide and phosphates	trace

Besides, to see the effect of surface charge on the surfactant adsorption, the zeta potential of different types of surfactants like anionic, non-ionic and zwitterionic are also measured.

CHAPTER 3

RESEARCH METHODOLOGY

3.1 Introduction

This chapter provides details of the experimental work undertaken in this study. Materials used and methods employed to gather the zeta potential and surface charge data to investigate the surfactant adsorption are specifically discussed.

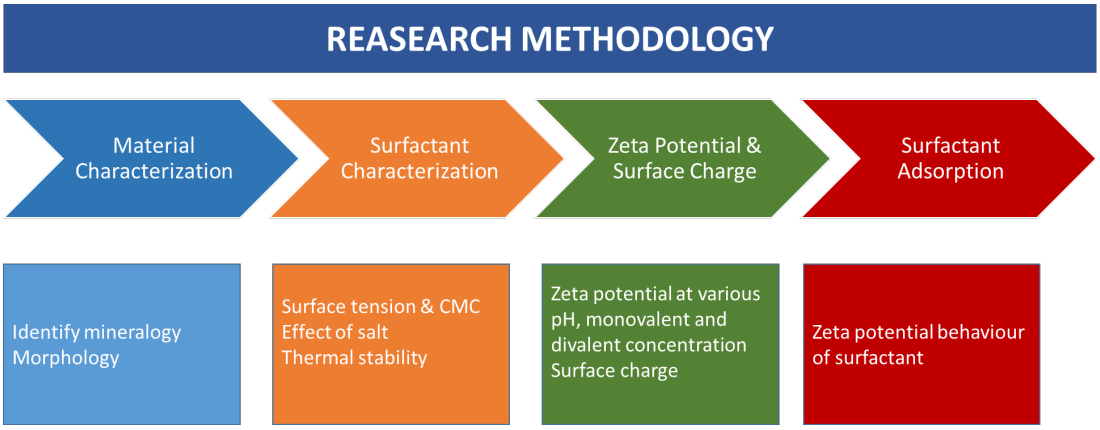

Figure 3.1 Research workflow.

The methodology of this study is divided into four main parts (Figure 3.1). The first part of this project was the material characterization to identify their mineralogy and physical morphology. The second part involved the surfactant characterization to investigate their surface tension and CMC. This part also included the study of the effect of salt on surface tension and the thermal stability of surfactants. The researcher continues to measure the zeta potential and surface charge under different conditions such as pH, and different concentrations of monovalent and divalent salts. The last part was the adsorption investigation by measuring the zeta potential with the presence of surfactant in the solutions.

3.2 Materials

3.2.1 Reservoir Minerals

Primary oil reservoir rocks are made of either sandstones or carbonates. Sandstone reservoir is encountered by about 60 percent of the world reserves [162]. Sandstone is a sedimentary rock composed of sand grain of different sizes combined. The formation of sandstone as reservoir rock is mainly from Quartz (silica) and/or feldspar because these are abundant minerals in the Earth's crust [163]. Apart from that, clay minerals such as kaolinite, montmorillonite, and illite are also present in the sandstone rock. Kaolinite minerals are the most commonly found clay minerals in the reservoir.

In this study, to be closely mimicking the sandstone reservoir rock, the materials used are silica and kaolinite. All the materials were purchased from Sigma-Aldrich, UK and without further purification. The description of the minerals is as shown in Table 3.1.

Table 3.1 Description of silica and kaolinite.

Minerals	**General chemical formula**	**Chemical structure**
Silica (powder)	SiO_2	SiO_4 tetrahedral, with each oxygen being shared between two tetrahedra, giving an overall formula SiO_2
Kaolinite (powder)	$Al_2Si_2O_5(OH)_4$	Silicate sheets (Si_2O_5) bonded to the aluminum oxide/hydroxide layers ($Al_2(OH)_4$) called gibbsite layers

The materials were analyzed by several characterization techniques to identify their chemical compound and physical properties. The data obtained were helpful in surfactant adsorption study which is the main aim of this project.

3.2.2 Brine Samples

The brine used in the experiments is a simple solution of NaCl and $CaCl_2$ in de-ionized water which represents monovalent and divalent respectively. Any other salt species are present at deficient concentrations. The NaCl and $CaCl_2$ salt were supplied by Merck and had a purity of 99.9 percent. Brine salinity varies from 0.01 M to 1 M. The number of salts required was calculated based on their molecular weight. For example, to prepare 1 M NaCl solution, 58.44 g of NaCl salt was dissolved in de-ionized water until they formed a 1 L of solution (details in Table 3.2). The pH of the brine was measured using a Metler Toledo pH meter.

Table 3.2 Brine concentration.

Parameter	**NaCl**	**$CaCl_2$**
Molecular weight	58.44 g / mol	110.98 g/mol
Concentration	**Amount required**	
0.01 M	0.5844 g/L	1.110 g/L
0.1 M	5.844 g/L	11.098 g/L
1 M	58.44 g /L	110.98 g/L

3.2.3 Surfactants

To address the comprehensive study of surfactant adsorption on the solid surface, three different surfactant types with different charges were used. The first was sodium dodecyl sulfate (SDS). SDS is an anionic surfactant that is most popularly used in chemical EOR studies. It belongs to an alkyl group. SDS has a negative charge of the head group.

Secondly, Trixon-X 100 which is a non-ionic surfactant was used. It has no charge at both of head group and the tail of its structure. The last surfactant was Coco-Betaine which represents a zwitterionic surfactant. All the surfactants used in this study were purchased from Sigma Aldrich. Table 3.3 shows a summary of the surfactant properties.

Table 3.3 Summary of the surfactants

Surfactant	Chemical formula	Molecular weight (g/mol)
SDS (anionic)	$NaC_{12}H_{25}SO_4$	288.4
Trixon X-100 (non-ionic)	$C14H_{22}O(C_2H_4)_n$	647.0
Coco-Betaine (zwiterrion)	$C_{19}H_{38}N_2O_3$	342.5

The surfactants were characterized by several characterization techniques such as surface tension and thermal stability before the surfactant flooding study.

3.2.4 Acid and Base

For the investigation of pH effects on zeta potential, hydrochloric acid (HCl) was used as the acid, and sodium hydroxide (NaOH) was used as the base, both were supplied by QRec Asia (New Zealand) as analytical grade reagent with an initial concentration of 1M. The dilution process was done to obtain 0.01M, and 0.1M concentration used to achieve the required pH.

3.3 Material Characterization

3.3.1 X-ray Fluorescence

The chemical composition of the silica and kaolinite was determined by the X-ray fluorescence (XRF) spectrometry (Rigaku brand). XRF is a method of elemental analysis that assesses the presence and concentration of various elements/ chemical composition in the powder sample by measuring the characteristic of secondary radiation emitted from a sample that has been excited by the X-ray source.

3.3.2 X-ray Diffraction

X-ray diffraction (XRD) is a technique that provides details about the atomic properties and structure of crystalline substances. In this study, XRD was used to identify the mineralogy of silica and kaolinite.

The silica and kaolinite powder was processed to identify different minerals phase using Rigaku (Japan) X-ray powder diffractometer in the range of $10° \leq 2\theta \leq 100°$ with Cu-Ka radiation at 45kV and 40 mAmps. The crystallite size (D) of the solid particles calculated using Debye-Scherer equation [164];

$$D = \frac{0.9\gamma}{\beta \cos\theta} \tag{3.1}$$

Where γ is the wavelength of X-ray beam (0.15 nm), β is the full width at half maximum (FWHM) of intense peak and θ is the Braggs angle.

3.3.3 Fourier Transform Infrared Spectroscopy

Fourier Transform Infrared Spectroscopy (FTIR) was used to identify the chemical bonding of a substance. The chemical bonding of silica and kaolinite were investigated using an attenuated total reflectance-FTIR (Perkin Elmer Inc, Spectrum 100, USA) spectroscopy. The samples were placed on the diamond plate (depth of penetration = 1.5-2.0 um), where the measurements were performed at the scanning range of 6500-400 cm-1. The FTIR spectra of silica and kaolinite were obtained and compared.

3.3.4 Brunauer-Emmett-Teller

The surface area of the silica and kaolinite were determined using Brunauer-Emmett-Teller (BET) by the monolayer of Nitrogen (N_2) gas on the particle surface. The samples are initially pre-treated in a particular container by applying heat and vacuum to remove the adsorbed contaminants from atmospheric exposure. The container containing the samples were then transferred to the analysis port and cooled to cryogenic temperature before being exposed to N_2 gas under precisely controlled pressures. With increasing pressure, the number of gas molecules adsorbed on the surface were recorded. The pressure at which the adsorption equilibrium achieved was measured and the universal gas law was applied to investigate the quantity of gas adsorbed, and subsequently, the surface area of samples.

3.3.5 Field Emission Scanning Electron Microscope

The morphological structure of silica and kaolinite were obtained from a field emission scanning electron microscope (FESEM, Zeiss Crossbeam 340) and a scanning electron microscope (SEM, HITACHI TM3000). Different FESEM with various magnifications were obtained from cross-section (Mag: x10k; EHT: 5kV; scale bar: 20µm) and surface (Mag: 50k; EHT: 4kV; scale bars: 200µm and 1µm). Meanwhile, SEM micrographs were observed for the cross-section of the support membrane (Mag: x5k; scale bar: 30µm and 20µm). For cross-section before analysis, the samples were submerged in liquid nitrogen to fracture the sample. Before imaging, the samples were kept overnight in a desiccator, and then samples were sputter-coated with a thin layer of gold (Au) and platinum (Pt), which improves the contrast and avoids charge accumulation.

3.3.6 Dynamic Light Scattering

Dynamic light scattering (DLS) was used to measure the dynamic particle size in the solution using Litesizer 500 by Anton Paar. While polydispersity index identifies the presence of particle uniformity and distribution in the suspension. The particle size is important for measuring the zeta potential using the electrophoretic method (electrophoretic light scattering). This method is applied for the particle size that is below 10 μm.

3.4 Surfactant Characterization

3.4.1 Surface Tension

The surfactant solutions were prepared in a standard 1000 ml volumetric flask. The surfactant was weighed and dissolved in deionized water. Various concentrations of surfactant were prepared ranging from 0.005 wt% to 10.0 wt%. The Sodium Chloride (NaCl) was used at a concentration of 0.01M, 0.1M, and 1M to investigate their effects on surface tension and the critical micellar concentration (CMC).

The surface tension of the surfactants was measured with Kruss tensiometer at a constant temperature of 25 °C. The Du Nouy principal was used in measuring the surface tension in which a platinum ring was suspended from the tension balance, and the force (Mn/m) that required to pull the ring off from the surface film was measured. The calibration and surface tension measurement were carried out according to the method described in ASTM Designation (D1331-89).

3.4.2 Critical Micellar Concentration

From the obtained surface tension data, the CMC of each surfactant was determined by the plot of surface tension versus surfactant concentration. The CMC matched the surfactant concentration where the surfactant first shows the lowest surface tension achieved and it remains relatively constant after this point.

3.4.3 Thermal Stability

The thermal stability of surfactants was determined by thermal gravity analysis (TGA) within the temperature range of 0 to 400 °C. The study was conducted with nitrogen gas which flowed at 40 ml/minutes at a heating rate of 10°C/minutes.

3.4.4 Zeta Potential

The electrophoretic mobility of silica and kaolinite in the solution was measured using Litesizer 500. The Litesizer instrument and software provided by Antoon Paar were used to monitor the experiment, and Smoluchowski's model (equation 2.36) was used by the software to calculate the zeta potential from the measured electrophoretic mobility. The temperature for the measurement was set to 25 °C. The refractive indexes used in the model were 1.459 and 1.553 for silica and kaolinite, respectively.

The solution was prepared with deionized water with 0.1 wt% mass of silica and kaolinite under different brine concentration of NaCl and $CaCl_2$. The solution was mixed and stirred using a magnetic stirrer. Ultrasonic sonicator was used to make the silica and kaolinite well suspended in the solution without any coagulation.

Following on, the initial pH was measured by pH meter from Mettler Toledo. The pH was adjusted by the addition of 0.01M hydrochloric acid (HCL) and 0.01M sodium hydroxide to achieved pH from 2 to 12. The pH meter was calibrated for each experiment to get a consistent reading. All the measurement was repeated three times, and 5 percent allowable error was considered to get the best results.

A 3 ml syringe was used to fill a clear, omega zeta cell cuvette with the suspension solution, and the cuvette was put into place in the Litesizer. The omega cuvette was cleaned with ethanol and deionized water between each parallel.

A plot of zeta potential against pH enabled determination of IEP for silica and kaolinite. Besides, the error was plotted to see the consistency of results.

3.4.5 Zeta Potential of Surfactants

Surfactant adsorption onto silica and kaolinite surface was determined by measuring the zeta potential of the surfactants. The same procedure in section 3.5 was used. The concentration for surfactants was varied based on CMC results obtained from section 3.4.2. The brine used was NaCl with different concentrations of 0.01M, 0.1M, and 1M. The pH for this experiment was between 5 to 6, the most common pH range for oil reservoir .

CHAPTER 4

MINERALOGY OF SILICA AND KAOLINITE

4.1 Introduction

This chapter discusses the mineralogy of silica and kaolinite from various characterization and analytical techniques.

4.2 Mineralogy

The adsorbent rock usually possesses a charge on its surface occurring due to the mineralogy and crystalline structure of the rock minerals. The presence of the surface charge affects the force between the rock surface and surfactant molecules. The source of surface charge can be initially determined by the chemical composition present in the minerals. The XRF, XRD and FTIR analysis were used for the identification of mineralogical constituents and chemical compositions of the silica and kaolinite.

4.2.1 XRF Analysis

The results of the XRF analysis of silica and kaolinite are shown in Table 4.1. The test was performed to understand their chemical compositions. The data obtained shows the SiO_2 as the primary chemical composition present in both silica and kaolinite. Silica is made of more than 99 percent of SiO_2.

Kaolinite is, however, had shown the presence of Al_2O_3 as a second significant chemical composition after SiO_2, which is approximately 58 percent and 37 percent respectively. Other compositions such as K_2O, P_2O_5, TiO_2, and CaO are the minor compositions traced in Kaolinite.

Table 4.1 XRF results for Silica and Kaolinite.

	Silica		**Kaolinite**	
Composition	**Concentration (ppm)**	**Mass (%)**	**Concentration (ppm)**	**Mass (%)**
SiO_2	997000	99.75	586000	58.65
Al_2O_3	2470	0.23	372000	37.23
Fe_2O_3	30.6	0.01	5500	0.55
MnO	17.6	0.01	134	0.01
K_2O	-	-	24500	2.45
P_2O_5	-	-	3740	0.37
TiO_2	-	-	6240	0.62
CaO	-	-	1110	0.11

4.2.2 XRD Analysis

The material was further tested by XRD study. The XRD pattern of Silica and Kaolinite are illustrated in Figure 4.1. The characteristic of Quartz in silica is obtained from an intense peak at two theta values of 21° and 26°. These patterns also correspond to the crystal structure of silica. The same pattern is also observed for kaolinite. The sharp peaks at the two theta values of 12° and 25° indicate the presence of kaolinite mineral [164]. Both materials have shown the same peak patterns indicating a crystal structure.

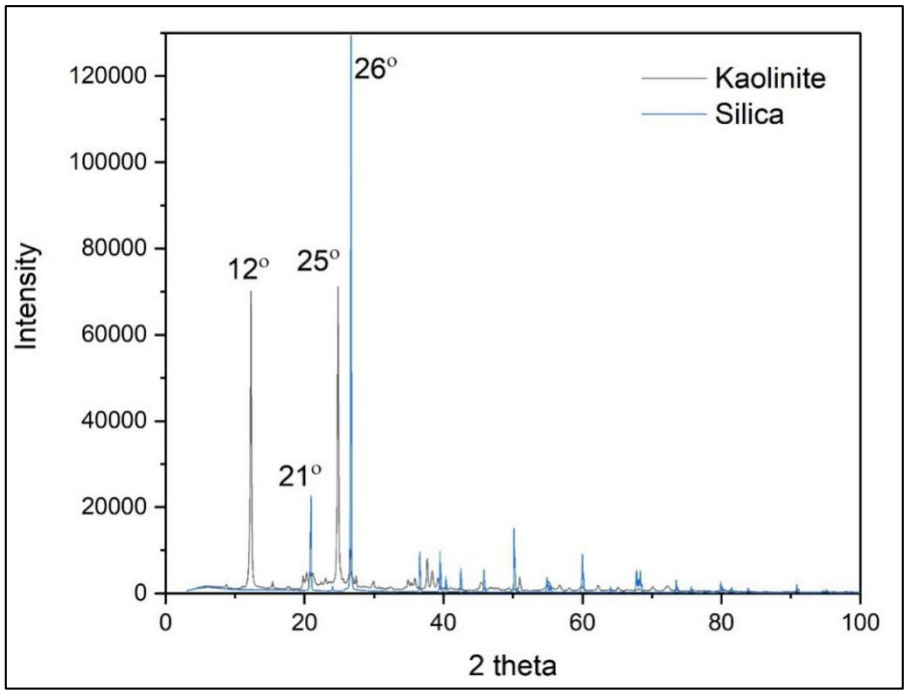

Figure 4.1 X-ray diffraction (XRD) pattern of Silica and Kaolinite.

The crystallite sizes (D) of the silica and kaolinite were measured using Debye-Scherer equation 3.1. The results are shown as shown in Table 4.2.

Table 4.2 Crystalline size of silica and kaolinite.

Minerals	Braggs angle	FWHM	Crystallite size, nm
Silica	21	0.1434	59.41
	26	0.1423	59.87
Kaolinite	12	0.2307	36.17
	25	0.2295	37.03

On the other hand, the particle diameters of the silica and kaolinite were measured through the DLS analysis. The results showed that the median diameter of silica and kaolinite was 0.1 µm and 7 µm respectively (Figure 4.2). The sizes measured were bigger as compared to the crystallite size. From a theoretical perspective, a particle diameter is always bigger than a crystallite size [165]. Besides that, the measured particle diameter was influenced by the existence of many agglomerations of particles on the samples which was detected by the DLS. In addition, DLS measurement is better for well-rounded particles and it measures

under dispersion condition. The existence of agglomeration and morphology of the sample can be seen in Figure 4.5.

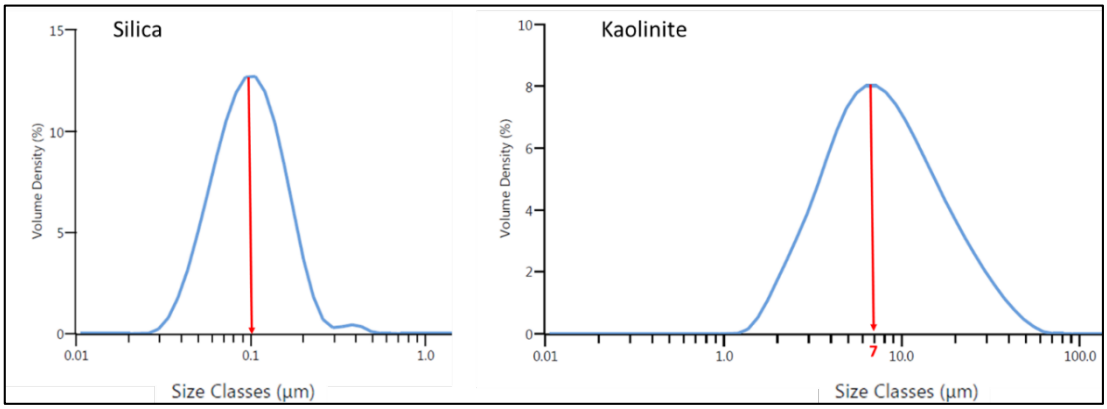

Figure 4.2 Hydrodynamic diameter of silica and kaolinite.

4.2.3 FTIR Analysis

The presence of the above minerals was further confirmed by FTIR analysis. The FTIR spectra of silica and kaolinite are shown in Figure 4.3. The complete assignment of the absorption bands in measured IR spectra is summarized in Table 4.3.

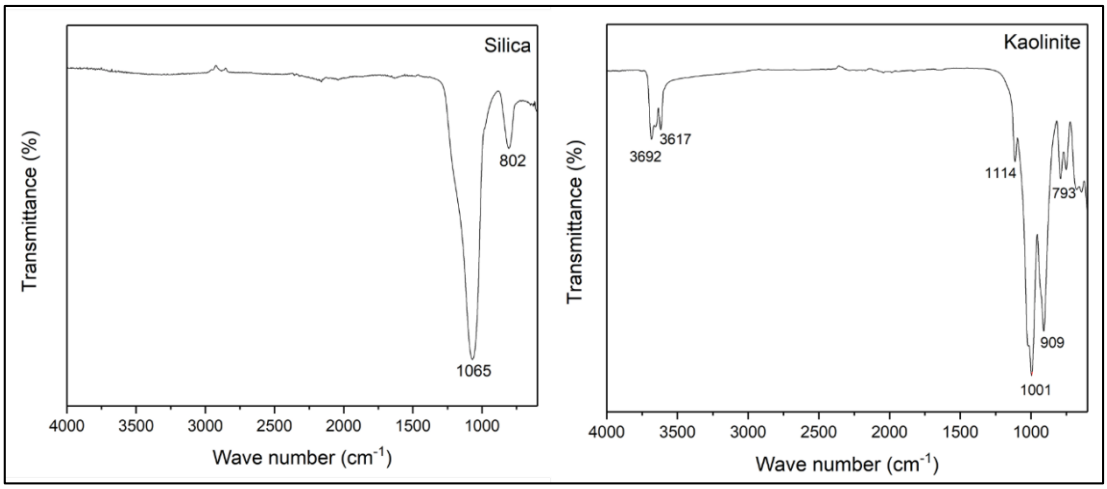

Figure 4.3 FTIR band of silica and kaolinite.

The Si-O stretching vibrations as observed at 802 and 993 for both silica and kaolinite show the presence of quartz. The strong band of 3692 and 3617 of kaolinite indicates the possibility of the hydroxyl linkage. Most of the bands such as 1114, 1001 and 909 show the presence of kaolinite minerals.

Table 4.3 Position and assignment of the various absorption bands in the FTIR spectra for silica and kaolinite.

Positions and assignment of the band (cm^{-1})	**Silica**	**Kaolinite**
OH stretching of inner surface hydroxyl	-	3692
Si-O stretching	-	1114
In-plane Si-O stretching	1065	1001
OH deformation of an inner hydroxyl group	-	909
Si-O	802	993

The presence of bands 1065 and 802 of silica can be attributed to Si-O bonding vibration [166] and asymmetric stretching vibration of the siloxane bonds (Si-O-Si) [167,168], respectively. The peak of 3692 of kaolinite indicates the existence of vibration OH which are bound to Al octahedral atoms on the surface or inter-layer silicate [165].

4.3 Morphology

4.3.1 BET

The amount of adsorption of an adsorbate on adsorbent can be related to the available surface area of the adsorbent. The BET analysis measures the dissolution rate, which is proportional to the surface area. Thus, the measured surface area helps to predict the availability of porous media for adsorption. The BET analysis of silica and kaolinite are recorded in the table 4.4.

The BET surface area and the pore volume were calculated by gas adsorption analyzer. It was assumed that for microporous adsorbent, the BET surface area, is an equivalent area rather than the actual area. As shown in the Table 4.4, the BET area was observed for silica at a maximum level and kaolinite at a minimum level. This can be translate that silica potentially to have adsorption capacity higher than kaolinite.

Table 4.4 BET analysis for silica and kaolinite

Reservoir mineral	**Surface area**	**Pore volume**	**Pore size**
	m^2/g	cm^3/g	Å (1 Å = 0.1 nm)
Silica	172.4	0.44	101.6
Kaolinite	7.1	0.03	171.7

The adsorption and desorption curve were plotted based on Barret-Jayner-Halenda (BJH) model. Figure 4.4 shows the Langmuir plot of the silica and kaolinite. Both are classified under type II(H3) isotherm [166] and confirmed with the existence of a slit-shaped pore with a mix of mesoporous and macroporous.

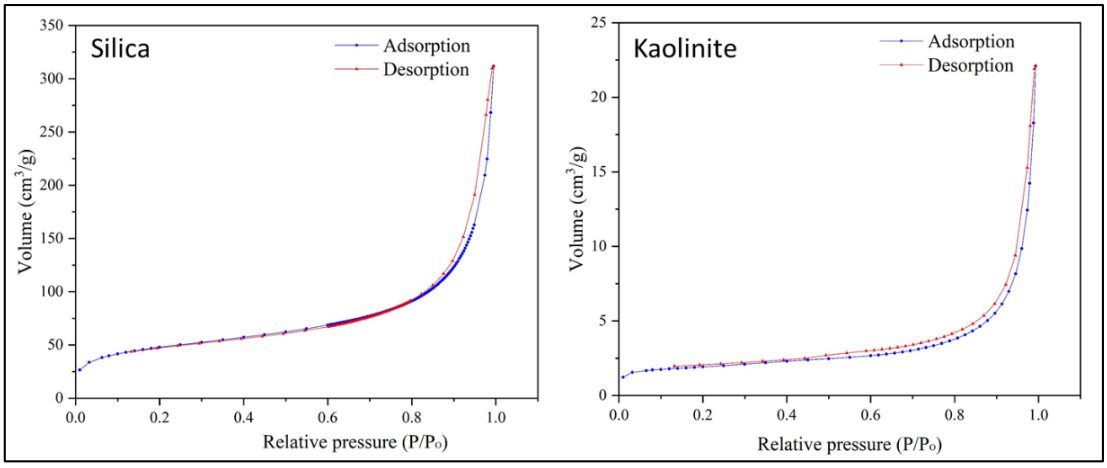

Figure 4.4 Adsorption and desorption of silica and kaolinite from BET.

4.3.2 FESEM and EDX

FESEM analysis helps to study the surface characterization of silica and kaolinite such as morphology, textures, and roughness. These characteristics may affect the adsorption capacity of the rock surface. Figure 4.5 shows the captured microphotographs and surface of silica and kaolinite from FESEM. Both images highlight the fact that silica and kaolinite had porous structures with different shapes. The morphology of silica samples shows micro-flake and irregular rounded shape with agglomeration.

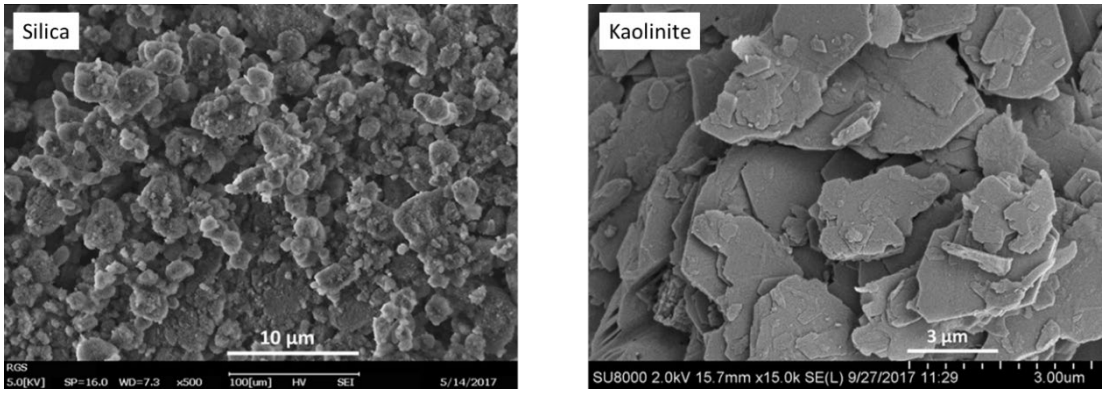

Figure 4.5 The FESEM/SEM image of silica and kaolinite.

On the other hand, the kaolinite morphology is clearly seen in the form of heterogeneous layered sheets with heterogeneous sizes. According to Murray [169], kaolinite structure can be measured at between 1 and 10 µm with the numbers of sheets per layer of about 10-50 pieces.

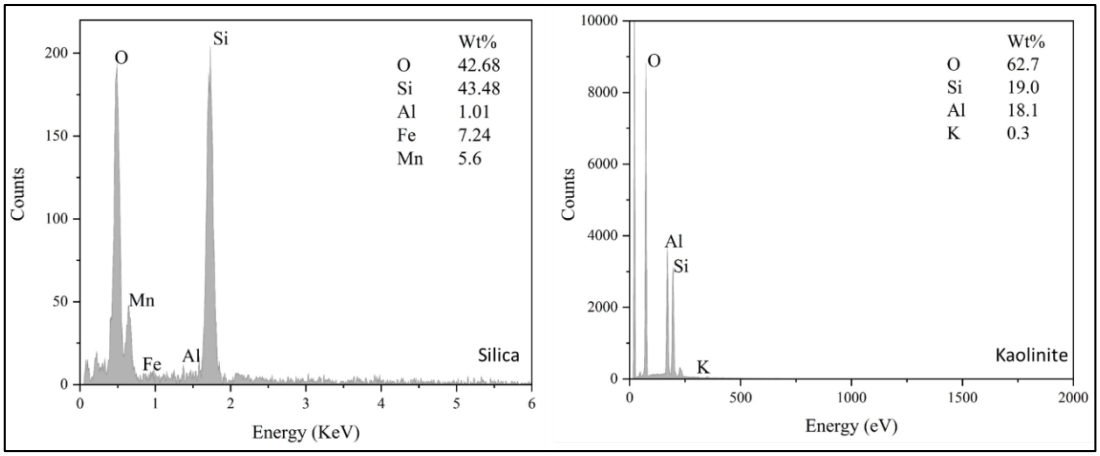

Figure 4.6 The results of EDX measurement of silica and kaolinite.

The elemental analysis by EDX that was performed together with FESEM is shown in Figure 4.6. The presence of oxygen in the EDX results indicates the formation of silica as silicon dioxide, while the presence of Alumina (Al) is confirmed in kaolinite mineral.

CHAPTER 5

SURFACE CHARGE

5.1 Introduction

This chapter discusses the surface charge of silica and kaolinite from electrophoretic measurement at various monovalent NaCl and divalent $CaCl_2$ concentration with different pH values that range from 2 to 12.

5.2 Silica

5.2.1 Zeta Potential

The distribution of zeta potential with various pH values from 2 to 12 is compared with different concentration of monovalent NaCl, as shown in Figure 5.1. The IEP was observed for silica. The IEP value varied with NaCl concentration - 2.4, 2.9 and 4.4 for 0.01M, 0.1M and 1M respectively. The IEP increased with increasing NaCl concentration. The presence of IEP demonstrates the negatively charged of silica change to positive at below IEP value. With increasing pH value, the magnitude of zeta potential increased. The magnitude of zeta potential was smaller, with increasing NaCl concentration as a trend. The same finding was obtained by Motoyoshi et al. [170].

The increasing zeta potential with increasing pH value is expected due to silica surface charge density, as shown in Figure 5.2 by Pengxiang et al. [171]. They presented that the increase of magnitude surface charge density with the rise in pH and NaCl concentration was due to the existence of silonal groups (Si-OH) and dehydration [172].

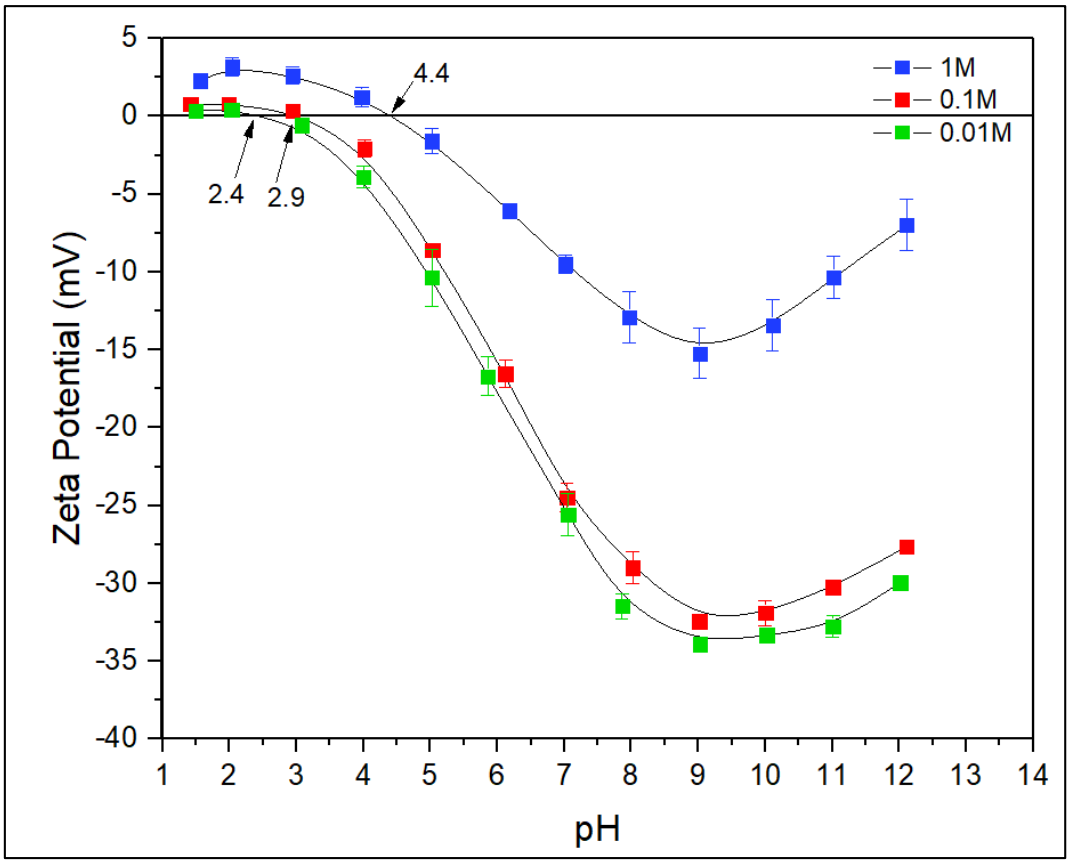

Figure 5.1 Zeta potential of silica and different pH and NaCl salinity.

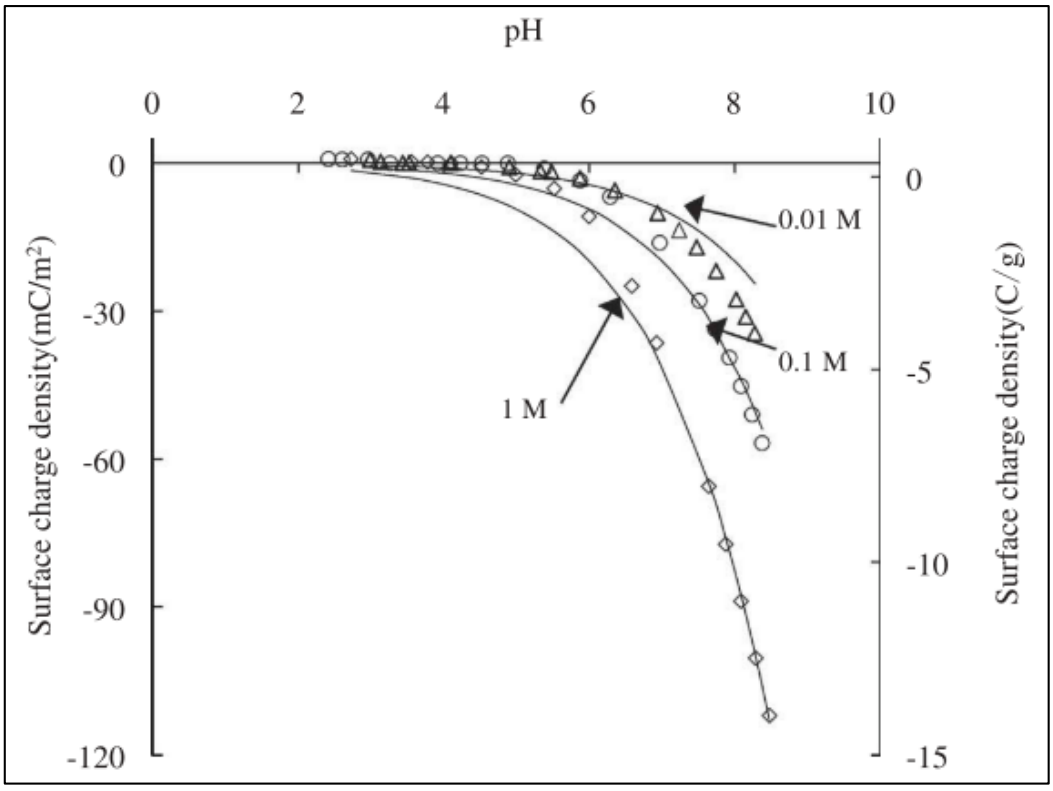

Figure 5.2 Surface charge density of silica [171].

5.2.2 Effect of Divalent Ions

The effect of adding divalent ion of $CaCl_2$ on zeta potential of silica is shown in Figure 5.3. The IEP was observed at pH 2.3 for 1M and 8.7 for 0.1M. There is no IEP observed for 0.01M concentration however, it can be assumed the IEP is less than 2.

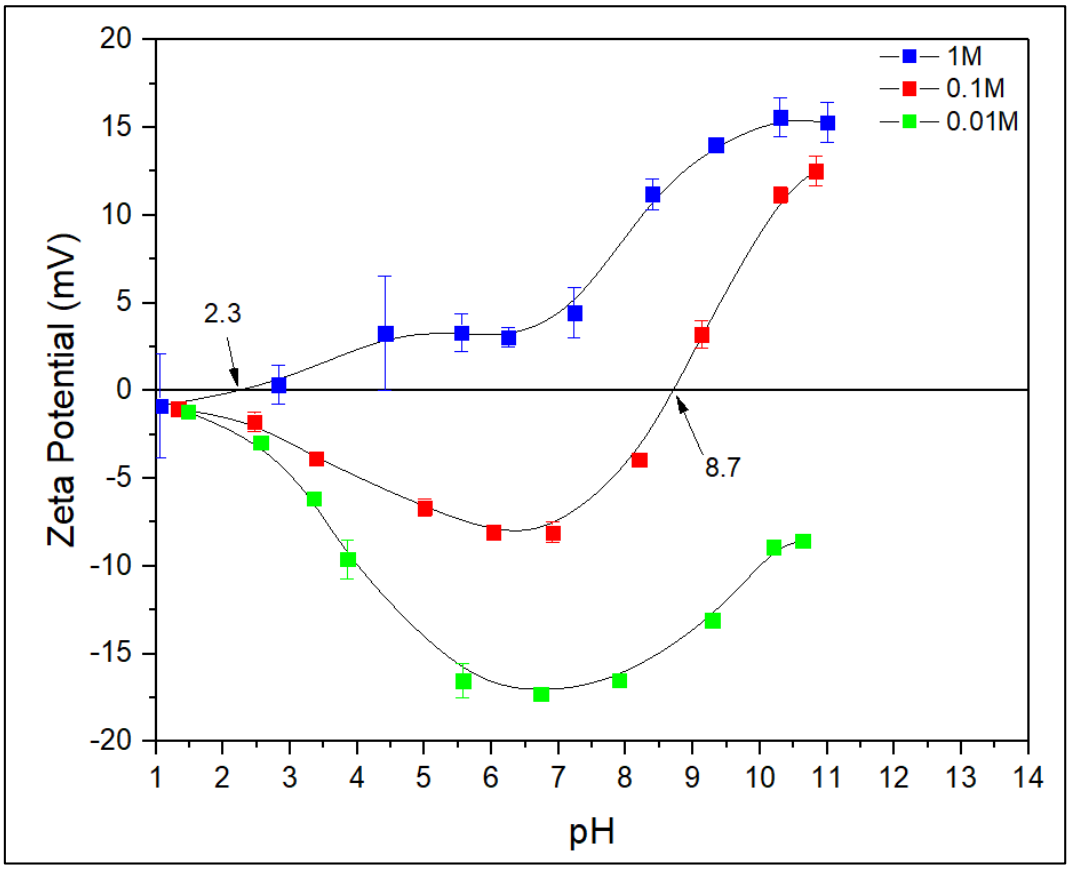

Figure 5.3 Zeta potential of silica and different pH and $CaCl_2$ salinity.

When comparing the magnitude of zeta potential for NaCl and $CaCl_2$ electrolyte concentration, it can be observed that the addition of $CaCl_2$ affects the lower zeta potential which is between -20mV to 20 mV. It may seem as though the belief that the effect of Cl^- ions is adsorbed to the surface more strongly than Na^+ is negligible compared to the neutralising effect of Ca^{2+} ions. Calcium ions also have a low degree of hydration in aqueous solution, making them even more prone to adsorb the negatively charged species than those of high degree of hydration [171].

5.3 Kaolinite

5.3.1 Zeta Potential

The zeta potential of kaolinite (measured by electrophoresis) as a function of pH and NaCl concentration is shown in Figure 5.4. As depicted in the figure, the IEP of kaolinite particles is less than 2. Similar results for the IEP for kaolinite at less than pH 3 were reported by several researchers [173–175]. Smith et al [174] determined that IEP of kaolinite was at pH 2.2 by micro-electrophoresis. Yuan et al [176] also reported that the IEP of kaolinite was between pH 1.5 and 3.5 for commercially produced kaolinite.

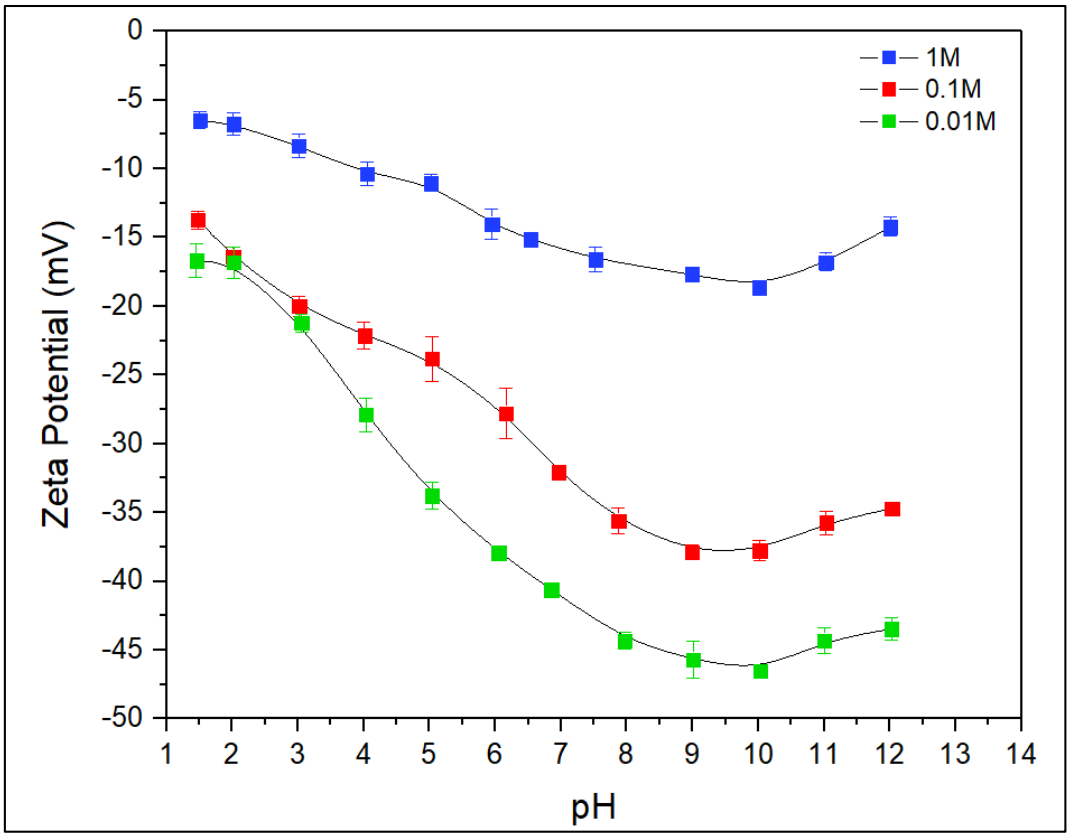

Figure 5.4 Zeta potential of kaolinite and different pH and NaCl salinity.

The measured IEP from electrophoresis is quite intriguing. As expected, the kaolinite should show IEP at pH between 5 and 8, considering the average of silica IEP of pH 2.2 and pH 9.2 of Alumina (gibbsite) [177] since the composition of silica to alumina is almost 1:1. However, the measured IEP of kaolinite was always less

than pH 3 which is close to silica. This happens because the alumina hydroxide octahedral layer does not contribute to the surface charge properties of kaolinite particles.

The investigation of zeta potential of kaolinite by the electrophoretic mobility using Smoluchowski equation has been criticized. It is because of the heterogeneous nature of the kaolinite surface charge, and the hexagonal platy shape of its structure[178]. In addition, the calculation of zeta potential for nonspherical kaolinite particle by assuming equivalent to the sphere led to a misleading value. The measured zeta potential from such mobility does not reflect the potential at the shear plane because the screening effect of charges and charges on the edges relative to those negative charges at the surface resulted in lower negative mobility [127]. Therefore another method such as potentiometric titration should be considered to understand its electrokinetic properties better.

5.3.2 Potentiometric Titration

Figure 5.5 demonstrates the surface charge densities of kaolinite by acid-base potentiometric titration. The titration curve was corrected by the blank titration without kaolinite suspension. The PZC was found between pH 6 and 8. These results show a good agreement with the PZC reported by Brady et al. [179] and Morari et al. [127].

The disagreement between experimental data from electrophoresis and the potentiometric titration is due to the structure of kaolinite itself as shown in **Figure 5.6**. The silica basal plane shows expected results (Figure 5.4), assuming it has similar IEP with the silica (Figure 5.1). This arises from the isomorphic substitution within the particles and not dependent on the proton concentration. The kaolinite edge surfaces may expose hydroxyl groups to the solution, which may take up or release protons depending on the pH of solutions that are determined by the potentiometric titration. The specific pH at which the zero net charge on such surfaces is defined as PZC.

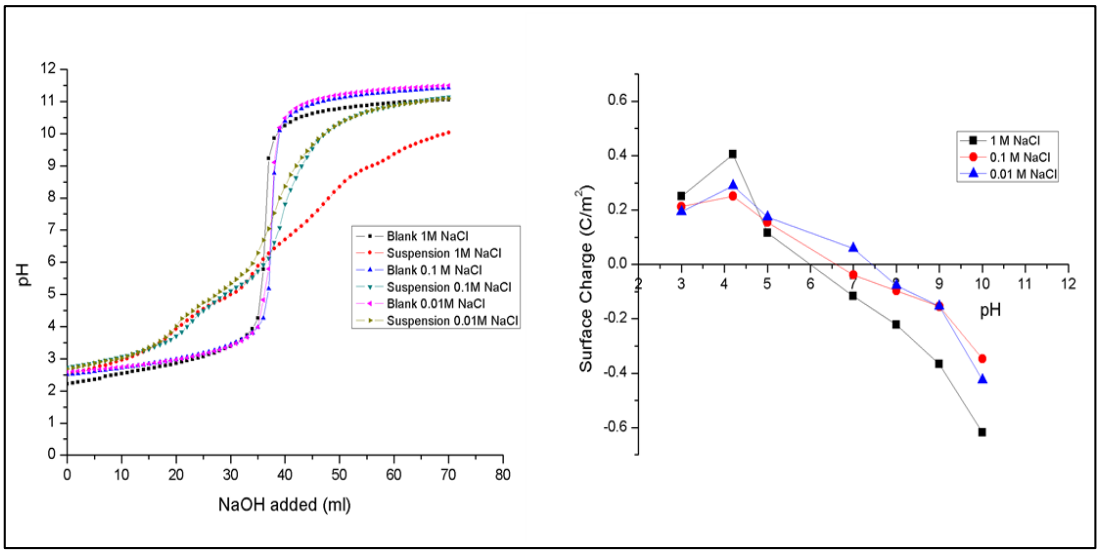

Figure 5.5 Surface charge densities of kaolinite particles as determined by acid-base potentiometric titration.

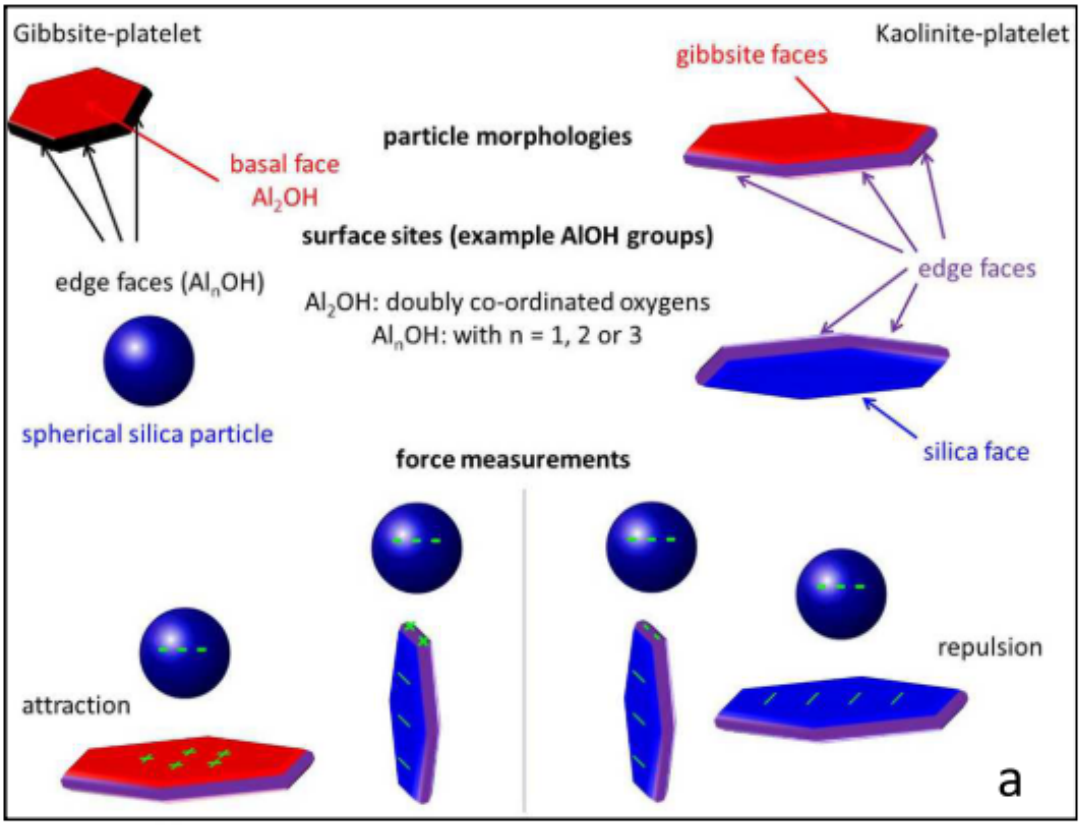

Figure 5.6 Faces on kaolinite and their relations to oxide minerals [127].

5.3.3 Effect of Divalent Ions

The effect of $CaCl_2$ on kaolinite particle is shown in Figure 5.7. A similar finding was observed on the same effect to silica. This is entirely an expected finding as explained before. The electrophoretic for kaolinite articles will be more bias towards silica face of kaolinite. From the graph, it can be seen that, the magnitude of zeta potential was reduced to a range of between -20 mV and 20 mV. The IEP was observed at pH 4.4, 10.1 and 10.8 for the concentration of 1M, 0.1M and 0.01M.

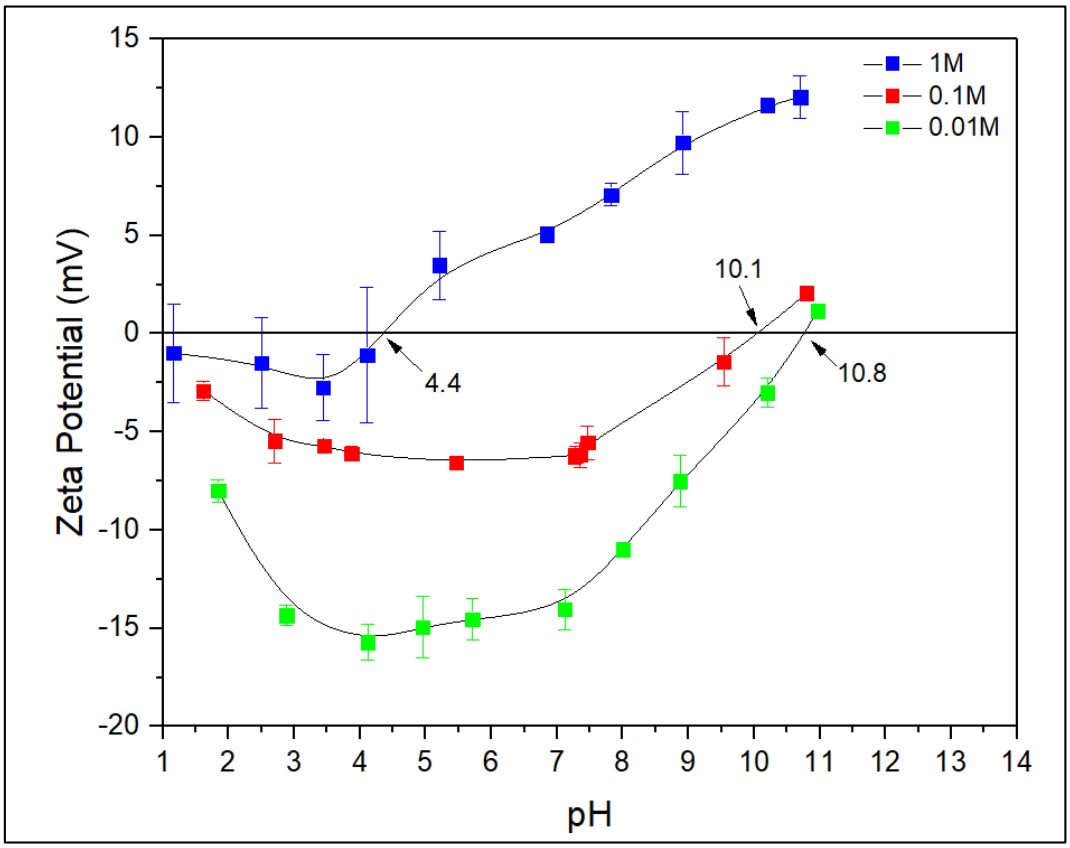

Figure 5.7 Zeta potential of kaolinite at different pH and $CaCl_2$ salinity.

5.4 Discussion

The electrokinetic behaviors of silica and kaolinite show many similar features. Figure 5.8 and Figure 5.9 show the zeta potential of both silica and kaolinite at typical reservoir fluid pH which, according to Shi et al. [180] and Thyne et al. [181] is between 4 and 8.

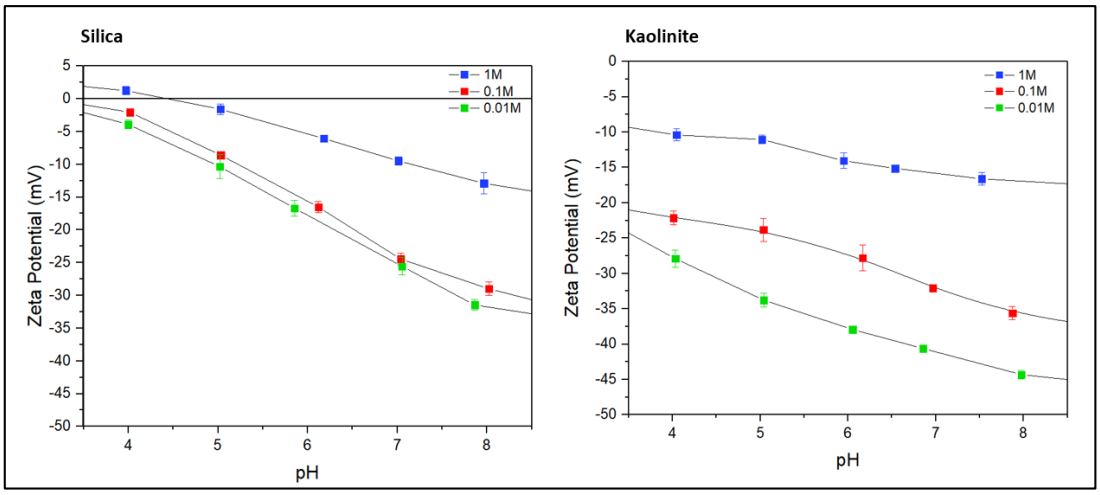

Figure 5.8 Zeta potential of silica and kaolinite with typical reservoir fluid pH range at different NaCl concentration.

Irrespective of the type of electrolyte used, the overall zeta potential gradually increased to a more negative value with increasing pH. More significantly, the zeta potential becomes less negative on increasing electrolyte concentration for both NaCl and $CaCl_2$, indicating a decrease in the electrostatic repulsion between the solid surface at high concentrations [182].

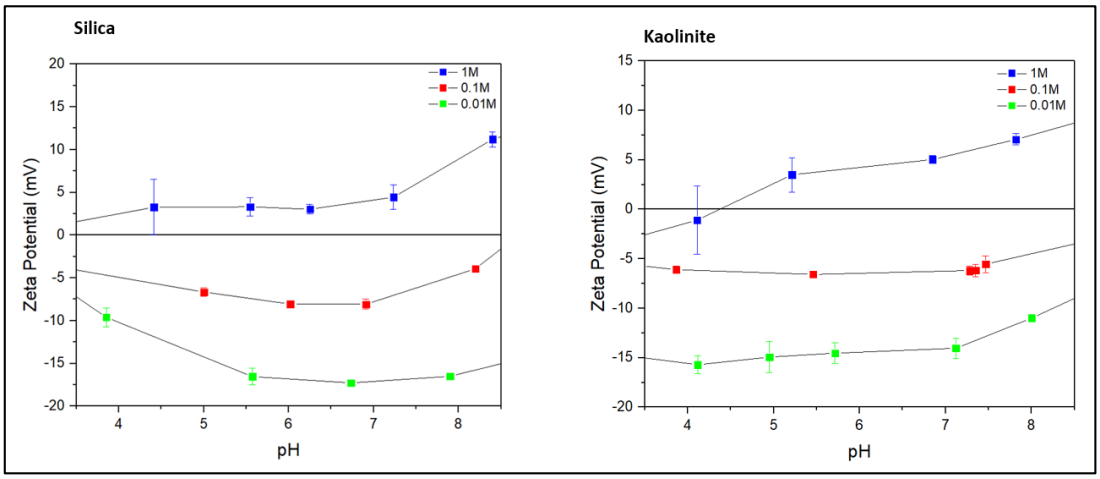

Figure 5.9 Zeta potential of silica and kaolinite with typical oil reservoir pH range at different $CaCl_2$ concentrations.

Besides, it can be clearly observed that the decreasing negatively zeta potential with electrolyte concentration is more rapid for $CaCl_2$ as compared to NaCl. This can be explained by the theory of Gouy-Chapman, which describes the behaviour of EDL of the suspension particle given by equation 2.34. Figure 5.10

shows the evident from equation 2.34 that an increasing electrolyte concentration and cations valency (increasing ionic strength) result in a corresponding reduction in EDL (represented as debye length) thickness. The compression in EDL thickness is increasing with the growing of valency as indicated by $CaCl_2$ in this study.

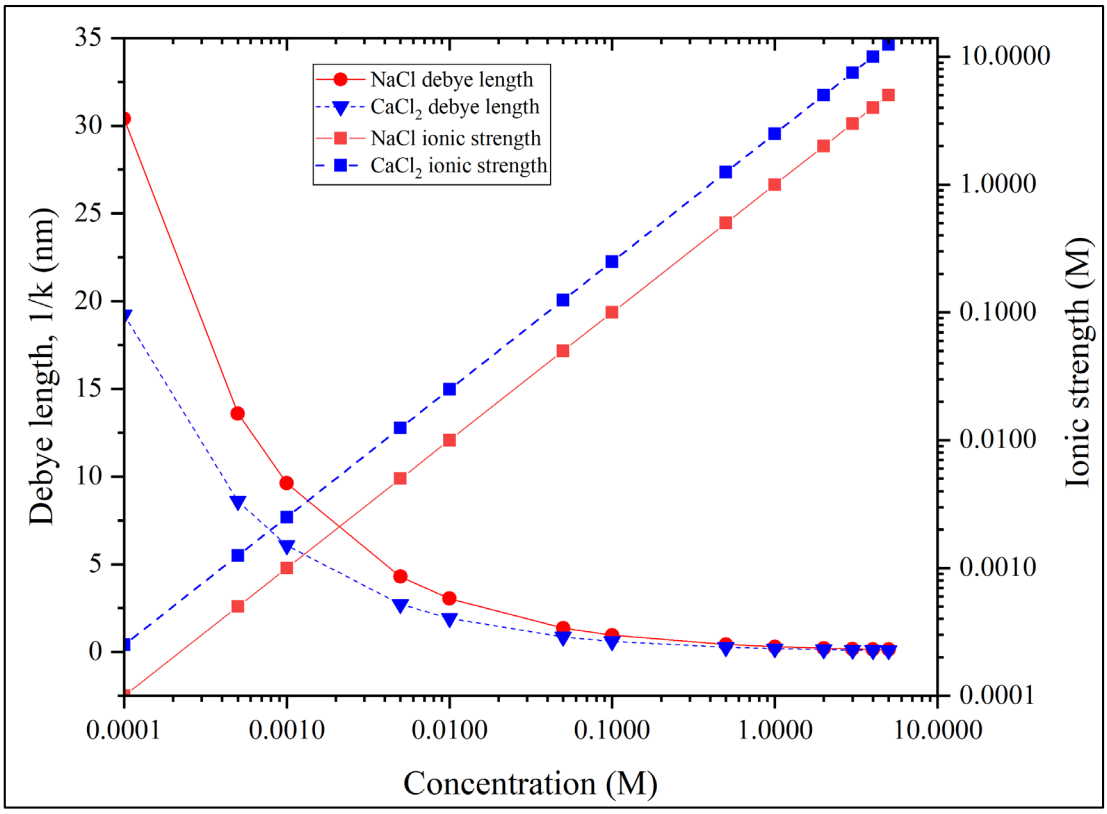

Figure 5.10 The ionic strength and the debye length with change in electrolyte concentration.

Besides, the reduction in the negative value of zeta potential also indicates a more flocculated behaviour of the particles [183]. The zeta potential of between -20 and 20 mV shows that the particles suspension was not stable, which tend to aggregate [184]. Within this range, the attractive force was dominant as compared to the repulsive force. This is clearly observed for both silica and kaolinite particles in $CaCl_2$ suspension solution in Figure 5.9. The values outside between-20 and 20 mV indicated stable condition which means particles are well dispersed and did not aggregate. This stable dispersion was observed on silica and kaolinite in NaCl suspension (Figure 5.8).

Figure 5.11 shows the comparison of zeta potential at pH 5.5 for silica and kaolinite at different NaCl concentration. As discussed in section 2.9, a typical oil reservoir fluid is less than sea water salinity at 0.6M. Based on the figure, both silica and kaolinite have stable zeta potential at below sea water salinity that indicates a dominant repulsive force .

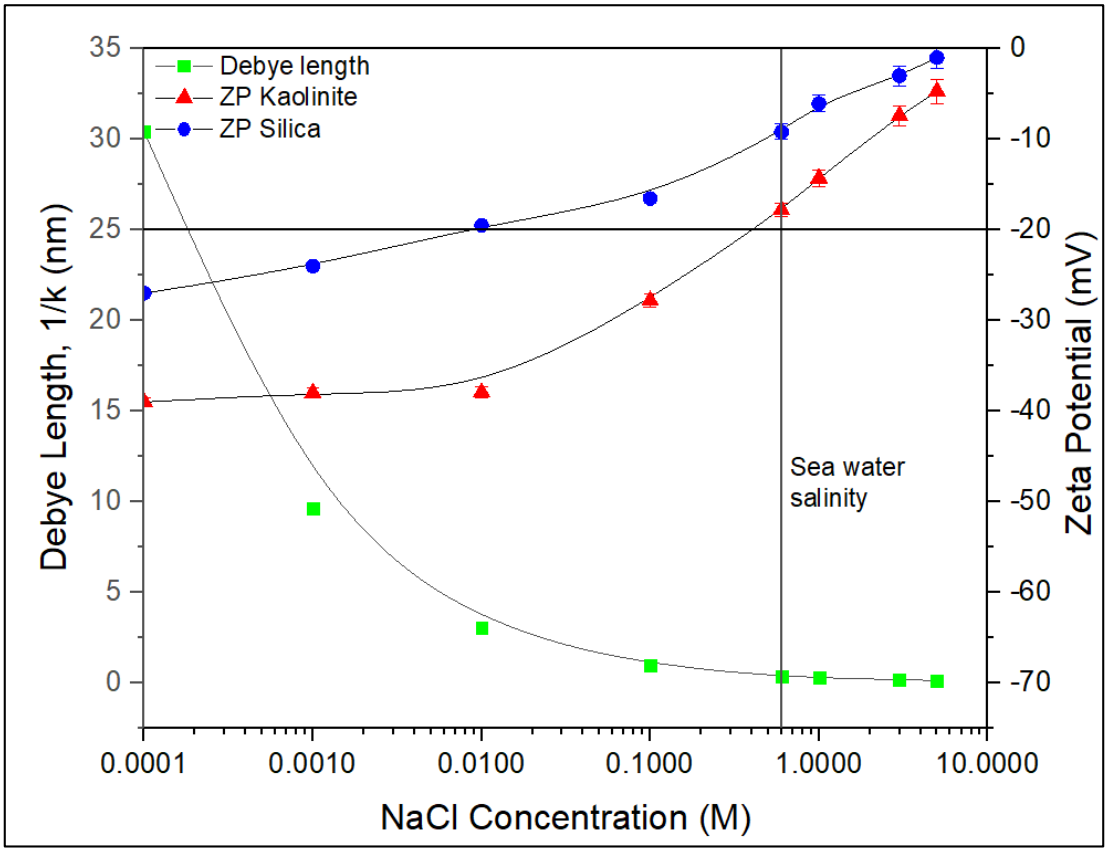

Figure 5.11 Comparison of zeta potential of silica and kaolinite at pH 5.5 (±0.5).

CHAPTER 6

SURFACTANT ADSORPTION

6.1 Introduction

6.2 Surfactant Characterization

The primary selection of surfactant for surfactant flooding is determined by the charged nature of the reservoir rock. As discussed in section 4.2, it is confirmed that the silica and kaolinite have anionic nature. From this, the evaluation of cationic surfactant is not considered due to the opposite charge nature, which obviously will result in higher surfactant adsorption. This section presents the primary properties of a surfactant such as their surface tension, CMC, salt tolerance and also thermal stability.

6.2.1 Surface Tension

As shown in Figure 6.1**,** it was observed that the zwitterionic coco betaine surfactant has greater potential in reducing surface tension/ IFT reduction and closely followed by Trixon X-100. The dissimilarity between the air and water molecules at the interface was reduced when the surfactant was adsorbed at the interfaces, which result in surface tension reduction [185].

The significant reduction of surface tension by the Coco Betaine is due to chemical structure. Based on Table 3.3, Coco Betaine has a long structure as compared to SDS and Trixon X-100. According to Holmberg et al. [95], increasing alkyl chain length of the surfactant will decrease surface tension. Another reason

could be due to temperature. However, the effect of temperature can be eliminated because the study was conducted at room temperature.

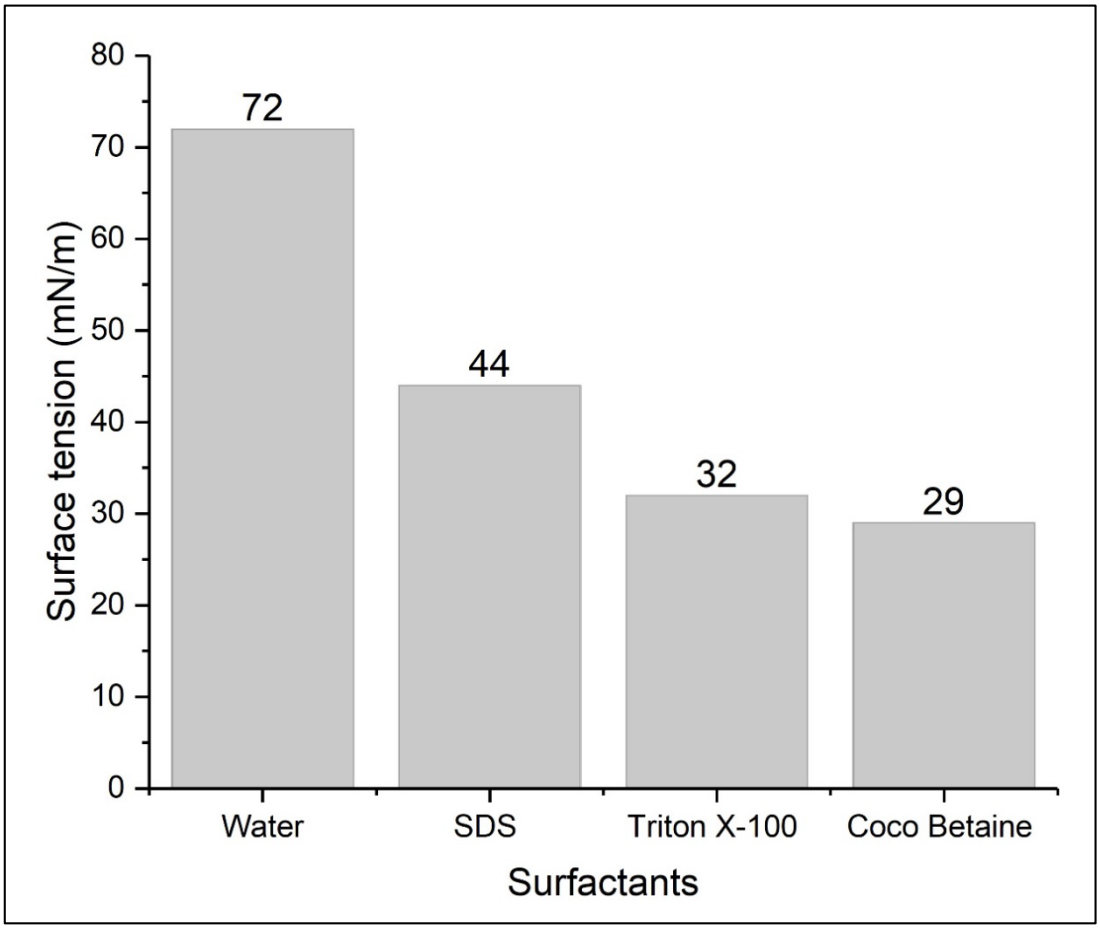

Figure 6.1 Surface tension of SDS, Triton X-100, and Coco Betaine.

6.2.2 Effect of Brine Salinity of Surface Tension

The synthetic brine water by NaCl contributes to a variety of surface tension/IFT with different salinity. The equilibrium surface tension of the surfactants is depicted in Figure 6.2. It can be seen that when salt was introduced in the solution, the surface tension reduced significantly for the SDS surfactant. The surface tension reduction was not significant and fairly constant for Trixon X-100 and Coco Betaine. Thus, they have more salt tolerance as compared to SDS.

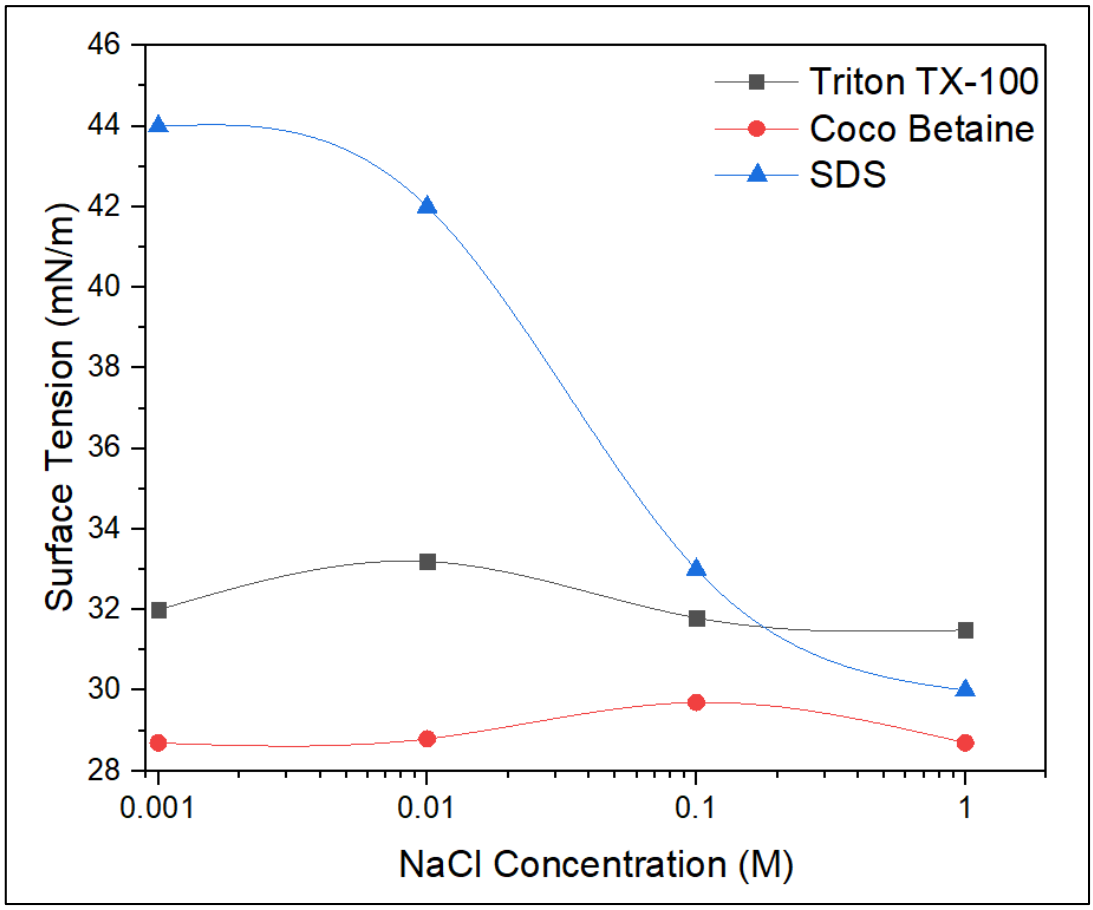

Figure 6.2 Effect of NaCl concentration on the surface tension of surfactants.

6.2.3 Effect of Brine Salinity on CMC Surfactants

The addition of NaCl with various concentration effectively influenced the micellazation behaviour and the aggregation state of the surfactant in an aqeous solution. For anionic surfactant, the addition of salt can compress the thickness of the ionic surrounding the ionic head group, which decreases the electrostactic repulsion between the ionic head group. This leads to the formation of micelles and the reduction of the CMC of the surfactant, as can be seen in Figure 6.3. The CMC of SDS is found to decrease significantly with the increasing of NaCl concentration.

When salt is added to non-ionic and zwiterrionic surfactant, CMC decreases because of the salting-in or salting-out effect. The effect is presented in Figure 6.4 for zwiterionic of coco-betaine and Figure 6.5 for non-ionic of Trixon X-100. With the increasing of NaCl concentration, the CMC value of coco betaine surfactant was

slightly lower or nearly constant. This can be due to the owing of the zero charge of headgroup within the isoelectric point. The change of the CMC by addition of salt is mainly attributed to the effect of salting-in or slating-out of the hydrophobic group instead of the electrostatic effect.

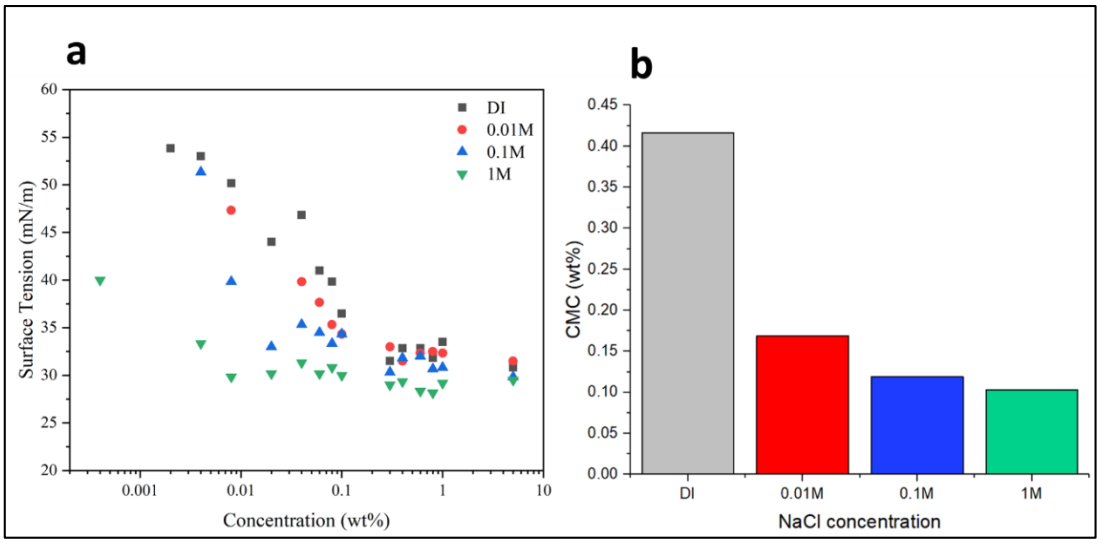

Figure 6.3 The effect of NaCl on SDS (a) Surface tension (b) CMC.

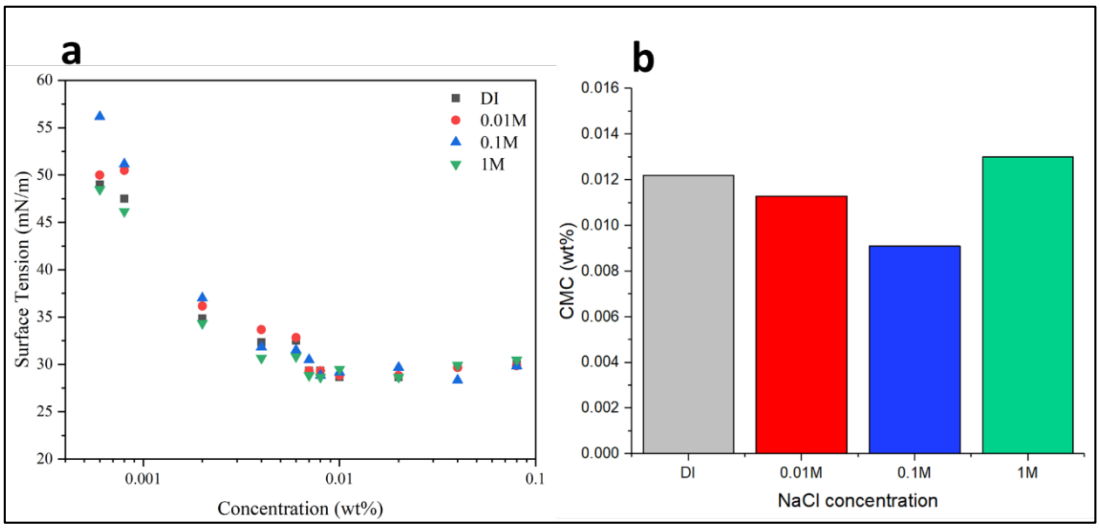

Figure 6.4 The effect of NaCl on Coco Betaine (a) Surface tension (b) CMC.

Besides, the addition of salt in surfactant solution may reduce the solubility of the surfactant in the aqueous solution. The contribution of salt to the process of micellazation may be less than its real value when the salt concentration is high.

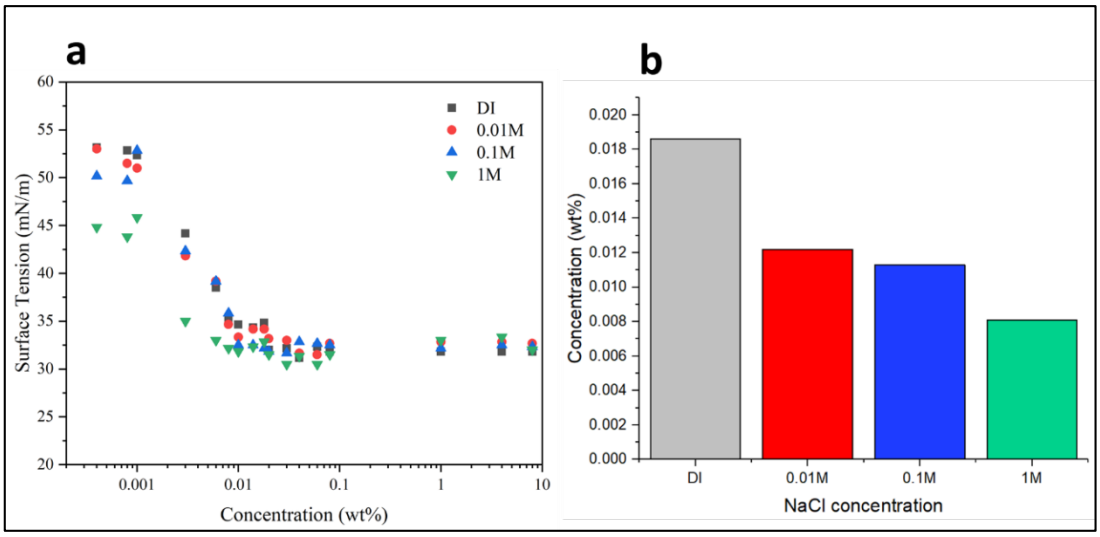

Figure 6.5 The effect of NaCl on Triton X-100 (a) Surface tension (b) CMC.

The decrease of the presented CMC is also caused by the hydration of ions. This means that the original hydrated structure of the hydrophobic group on the surfactant may be destroyed. This will enhance the hydrophobic ability of the hydrophobic group and promote the formation of micelles. The higher the salt concentration is, the stronger the hydrophobic interaction between the hydrophobic group, thus causing more favourableness of micellazation, which results in lower CMC [186].

6.3 Thermal Stability

The stability of surfactants was evaluated using TGA. Figure 6.6 illustrates the variation of weight loss with the temperature from 0 to 500 ºC. The temperature of which degradation starts to occur can be determined. From the TGA graph, it can be observed that SDS and Trixon-X100 are thermally stable at up to 200 ºC and 275 ºC, respectively. On the other hand, Coco Betaine shows quick degradation from the beginning and loses more than 50 percent of its weight at the temperature of 150 ºC.

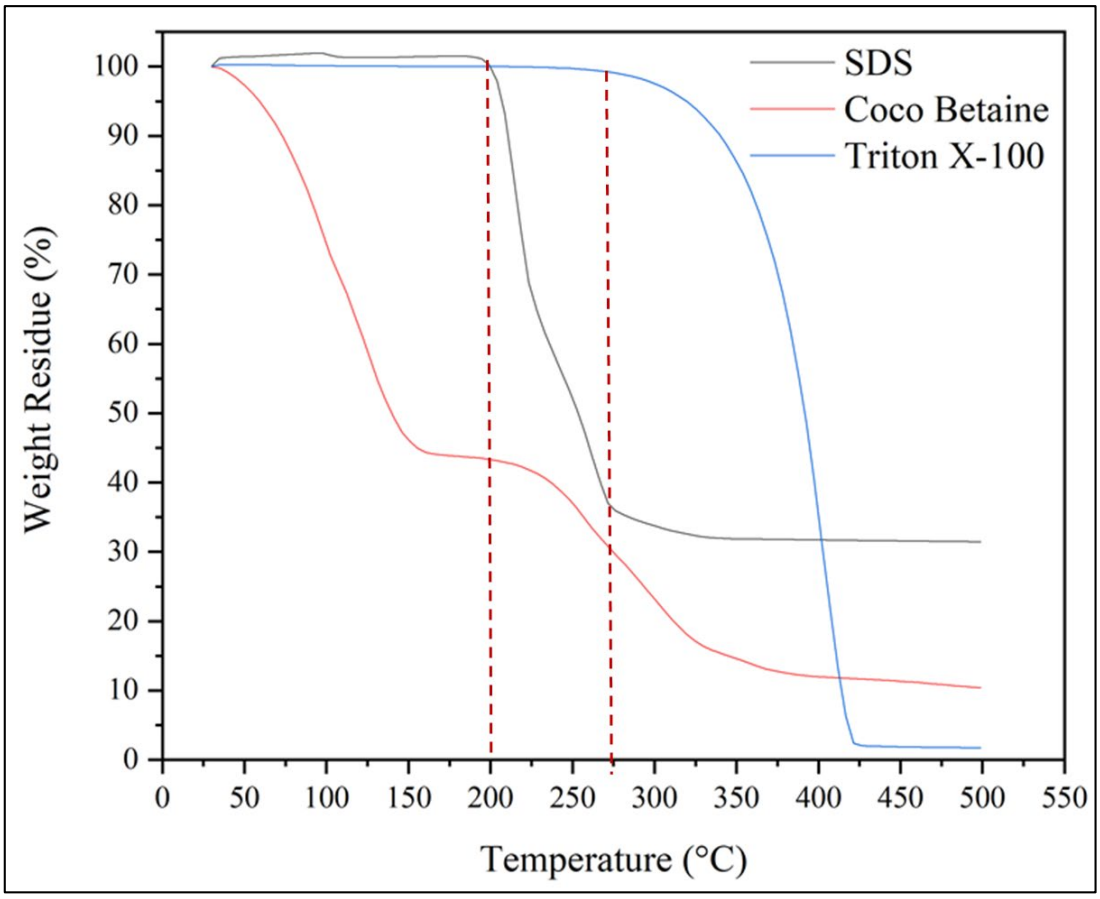

Figure 6.6 The degradation (weight loss) by TGA analysis.

Reservoir temperature is typically varied from 70 to 90 ºC [49]. From this perspective, SDS and Trixon X-100 are more favorable because they are thermally stable without any weight loss.

6.4 Surfactant Adsorption

The adsorption of SDS, Coco Betaine and Trixon X-100 on silica and kaolinite surface was studied to provide a better understanding of surfactant adsorption phenomena based on their surface charge. In order to achieve this, the adsorption experiment was conducted according to the findings in Chapter 5. As previously discussed, both silica and kaolinite are negatively charged at pH between 4 and 8 which is the common pH at reservoir condition. In addition, there is no IEP observed in this pH range for both under 0.1M and 0.01M of NaCl. However, the IEP of pH 4.4 is observed at high concentrataion of 1M NaCl. In order to make sure

the silica and kaolinite surface are negatively charged, this adsorption study was conducted at pH 5.5 (±0.5) for all NaCl concentration. The effect of $CaCl_2$ was excluded because their zeta potential values were within -20 and 20 mV (see chapter 5) for all pH range which indicates silica and kaolinite are within unstable suspension which is dominated by the attractive force. When the attractive was dominant, the adsorption was expected to be more favourable. In addition, the surfactant concentration used in this study was above CMC value obtained in section 6.3. These similar phenomena also was observed for silica as in Figure 6.7 and kaolinite in Figure 6.8.

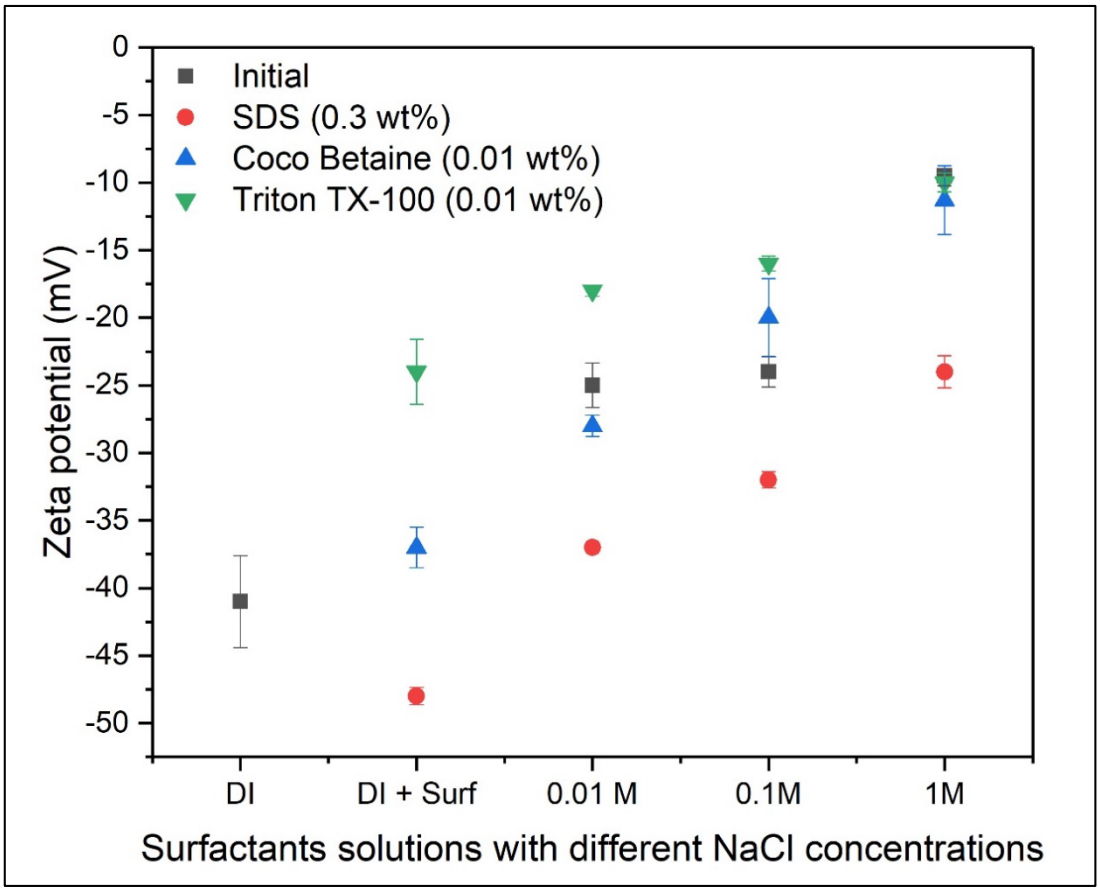

Figure 6.7 Surfactant adsorption onto silica surface.

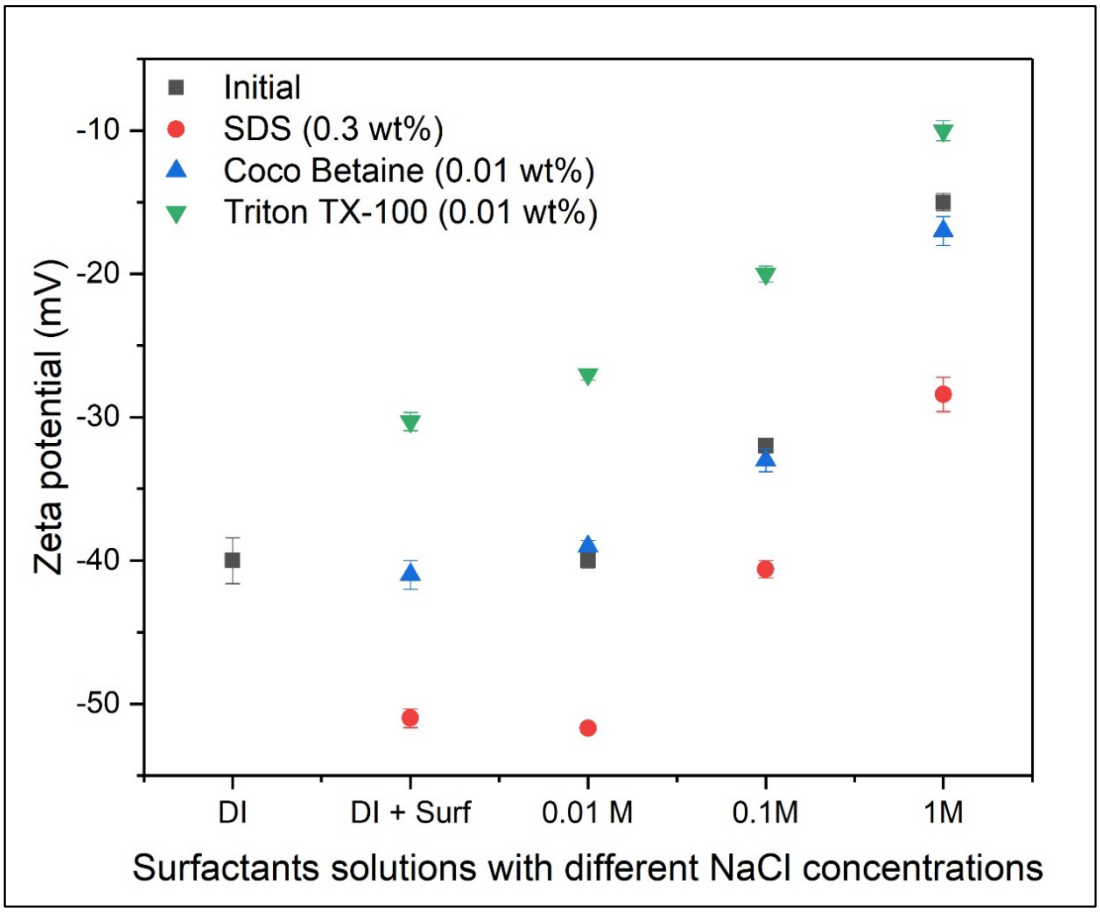

Figure 6.8 Surfactant adsorption onto kaolinite surface.

CHAPTER 7

CONCLUSION AND RECOMMENDATIONS

7.1 Conclusion

A direct method of electrophoresis has been successfully used in investigating the surface charge development of silica and kaolinite at different pH, brine salinities and divalent ions. The surfactant adsorption onto silica and kaolinite minerals by the surface charge and the zeta potential also are successfully presented. The main conclusions which can be drawn from the results are;

7.1.1 Mineralogy

i. The chemical compound of silica consists of 99 percent SiO_2 while kaolinite is composed of 58 percent SiO_2 and 37 percent Al_2O_3. These indicate that SiO_2 was the main component in charge development.
ii. Morphological study shows that both silica and kaolinite have porous structures with different particle size. The surface area of silica is bigger than kaolinite. This indicates the tendency to have high degree of surfactant adsorption.

7.1.2 Surfactant characterization

i. Coco Betaine gives lowest surface tension as compared to SDS and Trixon X-100. In the presence of brine concentration, SDS shows significant reduction in surface tension.

ii. Thermal degradation analysis shows coco betaine degrade significantly as compared to SDS and Trixon X-100. With the typical reservoir temperature of between 70 and 90 degrees Celcius, the Coco Betaine became less favourable.

7.1.3 Surface Charge

Surface charge of silica and kaolinite were significantly influence by the present of different pH, salinities and divalent ions (ionic strength). Silica shows negative surface charge over pH 4 at all different salinities of NaCl while the positive surface charge was observed at present of $CaCl_2$ especially at concentration of 1M. The same were observed for kaolinite where positive surface charge shows at 1M over pH 4.4 at $CaCl_2$ concentration. This can be concluded that increasing salinities and ionic strength will result both silica and kaolinite toward more negative surface charge.

7.1.4 Surfactant Adsorption

Surfactant adsorption of SDS, Coco Betaine and Triton X-100 were show similar trend for both silica and kaolinite. The non ionic surfactant of Trixon X-100 indicates compare to SDS and Coco Betaine. The SDS surfactant which having similar charge with silica and kaolinite surface charge show less surfactant adsorption with greater zeta potential magnitude.

7.2 Remaining Uncertainties

While this work managed to resolve some uncertainties in determining the zeta potential and surface charge for silica and kaolinite, there are still significant uncertainties to be resolved before the measurements can be interpreted with confidence.

i. The study was conducted with individual determination of zeta potential and surface charge. However, the mixed solid particles and their surface charge behaviour are not specified.
ii. The solid samples used in this study are water-wet. The zeta potential and surface charge in an oil- wet or mixed-wet system has not been studied. It is not conclusive whether there is an EDL between the oil and mineral surface, and between the oil phase and the water phase.

7.3 Recommendations for Future Work

7.3.1 Rock types and brine formulation

i. This study used a simple NaCl brine formulation. Ideally, the brine used in the experiment should be able to replicate the formation of water that also contains other ions as listed in Table 2.4 (Chapter 2).
ii. Future studies should measure the zeta potential in a broader range of real rocks samples. Samples with a higher clay content or different minerals composition might result in different surface charge behaviour, especially if they contain multivalent ions, which could specifically be adsorbed onto the mineral surface, and change the zeta potential. Carbonate rocks might also behave differently because of their higher point of zero charges.

7.3.2 Effect of other parameters

i. This study was conducted at room temperature, which is around 23ºC. Future work should investigate the effect of temperature on the measurement.
ii. Zeta potential in multiphase flow is another critical area which needs to be explored. Understanding the behaviour of the zeta potential in an oil-water system is essential for applications in petroleum engineering. Future study should also look at oil-wet and mixed-wet rocks to investigate the effect of wettability on the surface charge.

7.3.3 Application of Zeta Potential

i. Low salinity water flooding

   Zeta potential used to identify the surface potential phenomena at rock/brine and oil/brine interfaces. Charge on rock/brine and oil/brine interfaces are the govern stability of aqueous water film on the rock surfaces and the wettability. Reducing the zeta potential can alter the interface stability and thus can help increasing oil production during waterflooding.

ii. Fine migration control

   Formation damage is outstanding challenging during oil and gas production which more severe in near wellbore area. Fine migration is the major problems especially in sandstone reservoir. Increasing in fluid salinity and pH value is the main factor that initiate fine migration because increase strength the electrical double layer forces between the fine particles and pore surface. The zeta potential is a way to control the electrical double layer buy reducing its value thus by manipulation of fluid salinity and the Ph.

REFERENCES

1. The Quran (55,19).
2. Waals JD van der. Thermodynamische Theorie der Kapillarität unter Voraussetzung stetiger Dichteänderung. *Zeitschrift Für Phys Chemie* 2017;13U. doi:10.1515/zpch-1894-1338.
3. v. Smoluchowski M. Molekular-kinetische Theorie der Opaleszenz von Gasen im kritischen Zustande, sowie einiger verwandter Erscheinungen. *Ann Phys* 1908;330:205–26. doi:10.1002/andp.19083300203.
4. Saxena N, Kumar A, Mandal A. Adsorption analysis of natural anionic surfactant for enhanced oil recovery: The role of mineralogy, salinity, alkalinity and nanoparticles. *J Pet Sci Eng* 2019. doi:10.1016/j.petrol.2018.11.002.
5. Xu X, Saeedi A, Liu K. An experimental study of combined foam/surfactant polymer (SP) flooding for carbone dioxide-enhanced oil recovery (CO2-EOR). *J Pet Sci Eng* 2017;149:603–11. doi:10.1016/j.petrol.2016.11.022.
6. Farouq Ali SM, Thomas S. The promise and problems of enhanced oil recovery methods. *J Can Pet Technol* 1996;35:57–63. doi:10.2118/96-07-07.
7. Guo H, Dou M, Hanqing W, Wang F, Yuanyuan G, Yu Z, et al. Proper Use of Capillary Number in Chemical Flooding. *J Chem* 2017;2017. doi:10.1155/2017/4307368.
8. Nwidee LN, Theophilus S, Barifcani A, Sarmadivaleh M, Iglauer S. EOR Processes, Opportunities and Technological Advancements. Chem Enhanc Oil Recover - a Pract Overv 2016. doi:10.5772/64828.
9. Guo H, Dou M, Hanqing W, Wang F, Yuanyuan G, Yu Z, et al. Review of Capillary Number in Chemical Enhanced Oil Recovery. SPE Kuwait Oil Gas Show Conf., *Society of Petroleum Engineers*; 2015. doi:10.2118/175172-MS.
10. Guo H, Dou M, Hanqing W, Wang F, Yuanyuan G, Yu Z, et al. Review of capillary number in chemical enhanced oil recovery. Soc Pet Eng - SPE Kuwait Oil Gas Show Conf 2015. doi:10.2118/175172-MS.
11. O'Brien BM. Enhanced oil recovery chemical needs. J Am Oil Chem Soc 1982;59:839A-852A. doi:10.1007/BF02634451.

12. Fathi Z, Ramirez WF. Optimal injection policies for enhanced oil recovery: part 2 - surfactant flooding. Soc Pet Eng J 1984;24:333–41. doi:10.2118/12814-PA.
13. Don W. Green. Enhanced_Oil_Recovery_Willhite_(tupeg.ir).pdf. Soc Pet Eng 1998.
14. Porse PB. Enhanced Oil Recovery - Surfactant Flooding 2014:115.
15. Sheng JJ. Surfactant-Polymer Flooding. Enhanc Oil Recover F Case Stud 2013:117–42. doi:10.1016/B978-0-12-386545-8.00005-1.
16. Gale W. Surfactant Flooding : Petroleum 1973.
17. Hirasaki G, Miller C, Puerto M. Recent Advances in Surfactant EOR. SPE J 2011;16:3–5. doi:10.2118/115386-PA.
18. Glover CJ, Puerto MC, Maerker JM, Sandvik EL. Surfactant Phase Behavior and Retention in Porous Media. Soc Pet Eng AIME J 1979;19:183–93.
19. Sandersen SB. Enhanced Oil Recovery with Surfactant Flooding. Thesis 2012:1–162.
20. Olajire AA. Review of ASP EOR (alkaline surfactant polymer enhanced oil recovery) technology in the petroleum industry: *Prospects and challenges*. Energy 2014;77:963–82. doi:10.1016/j.energy.2014.09.005.
21. Gao C, Shi J, Zhao F. Successful polymer flooding and surfactant-polymer flooding projects at Shengli Oilfield from 1992 to 2012. J *Pet Explor Prod Technol* 2014;4:1–8. doi:10.1007/s13202-013-0069-7.
22. Belhaj AF, Elraies KA, Mahmood SM, Zulkifli NN, Akbari S, Hussien OSE. The effect of surfactant concentration, salinity, temperature, and pH on surfactant adsorption for chemical enhanced oil recovery: a review. *J Pet Explor Prod Technol* 2019. doi:10.1007/s13202-019-0685-y.
23. ShamsiJazeyi H, Verduzco R, Hirasaki GJ. Reducing adsorption of anionic surfactant for enhanced oil recovery: Part II. Applied aspects. Colloids Surfaces A Physicochem Eng Asp 2014;453:168–75. doi:10.1016/j.colsurfa.2014.02.021.
24. E.C. Donaldson G.V. Chilingarian T.F. Yen. Enhanced Oil Recovery, II, Volume 17B. Elsevier Science; 1989.
25. Kamal MS, Hussein IA, Sultan AS. Review on Surfactant Flooding: Phase Behavior, Retention, IFT, and Field Applications. Energy and Fuels 2017;31:7701–20. doi:10.1021/acs.energyfuels.7b00353.

26. Gogoi SB. Adsorption-Desorption of Surfactant for Enhanced Oil Recovery. *Transp Porous Media* 2011;90:589–604. doi:10.1007/s11242-011-9805-y.
27. Revil A, Pezard PA, Glover PWJ. Streaming potential in porous media: 1. Theory of the zeta potential. *J Geophys Res Solid Earth* 1999;104:20021–31. doi:10.1029/1999jb900089.
28. Idahosa PEG, Oluyemi GF, Oyeneyin MB, Prabhu R. Rate-dependent polymer adsorption in porous media. *J Pet Sci Eng* 2016;143:65–71. doi:10.1016/j.petrol.2016.02.020.
29. Amirianshoja T, Junin R, Kamal Idris A, Rahmani O. A comparative study of surfactant adsorption by clay minerals. *J Pet Sci En*g 2013;101:21–7. doi:10.1016/j.petrol.2012.10.002.
30. Azam MR, Tan IM, Ismail L, Mushtaq M, Nadeem M, Sagir M. Static adsorption of anionic surfactant onto crushed Berea sandstone. J Pet Explor Prod Technol 2013;3:195–201. doi:10.1007/s13202-013-0057-y.
31. Paria S, Khilar KC. A review on experimental studies of surfactant adsorption at the hydrophilic solid-water interface. *Adv Colloid Interface Sci* 2004;110:75–95. doi:10.1016/j.cis.2004.03.001.
32. Somasundaran P, Hanna HS. Adsorption of Sulfonates on Reservoir Rocks. Soc Pet Eng J 1979;19. doi:10.2118/7059-PA.
33. Wang C, Cao XL, Guo LL, Xu ZC, Zhang L, Gong QT, et al. Effect of adsorption of catanionic surfactant mixtures on wettability of quartz surface. Colloids Surfaces *A Physicochem Eng Asp* 2016;509:564–73. doi:10.1016/j.colsurfa.2016.09.057.
34. Bera A, Kumar T, Ojha K, Mandal A. Adsorption of surfactants on sand surface in enhanced oil recovery: Isotherms, kinetics and thermodynamic studies. *Appl Surf Sci* 2013;284:87–99. doi:10.1016/j.apsusc.2013.07.029.
35. ShamsiJazeyi H, Verduzco R, Hirasaki GJ. Reducing adsorption of anionic surfactant for enhanced oil recovery: Part I. Competitive adsorption mechanism. Colloids Surfaces *A Physicochem Eng Asp* 2014;453:162–7. doi:10.1016/j.colsurfa.2013.10.042.
36. Ahmadi MA, Zendehboudi S, Shafiei A, James L. Nonionic surfactant for enhanced oil recovery from carbonates: Adsorption kinetics and equilibrium. Ind Eng Chem Res 2012;51:9894–905. doi:10.1021/ie300269c.

37. Ahmed Muherei M, Radzuan J. Equilibrium Adsorption Isotherms of Anionic , Nonionic Surfactants and Their Mixtures to Shale and Sandstone. *Mod Appl Sci* 2009;3:158–67.
38. Ahmadi MA, Shadizadeh SR. Adsorption of a nonionic surfactant onto a silica surface. Energy Sources, Part A Recover Util Environ Eff 2016;38:1455–60. doi:10.1080/15567036.2011.652761.
39. Levitz PE. Adsorption of non ionic surfactants at the solid/water interface. Colloids Surfaces A Physicochem *Eng Asp* 2002;205:31–8. doi:10.1016/S0927-7757(01)01139-6.
40. Kumar A, Mandal A. Synthesis and physiochemical characterization of zwitterionic surfactant for application in enhanced oil recovery. *J Mol Liq* 2017;243:61–71. doi:10.1016/j.molliq.2017.08.032.
41. Zhang R, Somasundaran P. Advances in adsorption of surfactants and their mixtures at solid/solution interfaces. *Adv Colloid Interface Sci* 2006;123–126:213–29. doi:10.1016/j.cis.2006.07.004.
42. Durán-Álvarez A, Maldonado-Domínguez M, González-Antonio O, Durán-Valencia C, Romero-Ávila M, Barragán-Aroche F, et al. Experimental-Theoretical Approach to the Adsorption Mechanisms for Anionic, Cationic, and Zwitterionic Surfactants at the Calcite-Water Interface. Langmuir 2016;32:2608–16. doi:10.1021/acs.langmuir.5b04151.
43. Curbelo FDS, Santanna VC, Neto ELB, Dutra TV, Dantas TNC, Neto AAD, et al. Adsorption of nonionic surfactants in sandstones. Colloids Surfaces A *Physicochem Eng Asp* 2007;293:1–4. doi:10.1016/j.colsurfa.2006.06.038.
44. Dang CTQ, Chen Z, Nguyen NTB, Bae W, Phung TH. Development of isotherm polymer/surfactant adsorption models in chemical flooding. Soc Pet Eng - SPE Asia Pacific Oil Gas Conf Exhib 2011 2011;2:1562–71.
45. Alyoshina NA, Agafonov A V, Parfenyuk E V. Comparative study of adsorption capacity of mesoporous silica materials for molsidomine : Effects of functionalizing and solution pH. *Mater Sci Eng C* 2014;40:164–71. doi:10.1016/j.msec.2014.03.052.
46. Ahmadi MA, Shadizadeh S. Experimental and Theoretical Study of a New Plant Derived Surfactant Adsorption on Quartz Surface: Kinetic and Isotherm Methods. *J Dispers Sci Technol* 2015;36:441–52. doi:10.1080/01932691.2013.860035.

47. Ahmadi MA, Shadizadeh SR. Experimental investigation of a natural surfactant adsorption on shale-sandstone reservoir rocks: Static and dynamic conditions. Fuel 2015;159:15–26. doi:10.1016/j.fuel.2015.06.035.
48. Salari Z, Ahmadi MA. Experimental studies of ionic surfactant adsorption onto carbonate rocks. *Energy Sources, Part A Recover Util Environ Eff* 2016;38:549–54. doi:10.1080/15567036.2011.647245.
49. Saha R, Uppaluri RVS, Tiwari P. Effect of mineralogy on the adsorption characteristics of surfactant—Reservoir rock system. Colloids Surfaces A *Physicochem Eng Asp* 2017;531:121–32. doi:10.1016/j.colsurfa.2017.07.039.
50. Gbadamosi AO, Junin R, Manan MA, Agi A, Yusuff AS. An overview of chemical enhanced oil recovery: recent advances and prospects. vol. 9. Springer Berlin Heidelberg; 2019. doi:10.1007/s40089-019-0272-8.
51. Dimov NK, Kolev VL, Kralchevsky PA, Lyutov LG, Broze G, Mehreteab A. Adsorption of ionic surfactants on solid particles determined by zeta-potential measurements: Competitive binding of counterions. *J Colloid Interface Sc*i 2002;256:23–32. doi:10.1006/jcis.2001.7821.
52. Al Mahrouqi D, Vinogradov J, Jackson MD. Zeta potential of artificial and natural calcite in aqueous solution. *Adv Colloid Interface Sci* 2017;240:60–76. doi:10.1016/j.cis.2016.12.006.
53. Kosmulski M. The pH-dependent surface charging and the points of zero charge. *J Colloid Interface Sci* 2002. doi:10.1006/jcis.2002.8490.
54. Kosmulski M, Rosenholm JB. High ionic strength electrokinetics. Adv Colloid Interface Sci 2004;112:93–107. doi:10.1016/j.cis.2004.09.005.
55. Green D, Willhite P. Enhanced Oil Recovery 1988:Chapter 7, 239-289, ISBN 1-55563-077-4.
56. Bavière M, Bazin B, Miléo JC. Physicochemical properties of sulfonated fatty acid esters for oil recovery by surfactant flooding. *Colloids and Surfaces* 1991. doi:10.1016/0166-6622(91)80023-H.
57. Muggeridge A, Cockin A, Webb K, Frampton H, Collins I, Moulds T, et al. Recovery rates, enhanced oil recovery and technological limits. *Philos Trans A Math Phys Eng Sci* 2014;372:20120320. doi:10.1098/rsta.2012.0320.
58. Sheng JJ. Status of surfactant EOR technology. Petroleum 2015;1:97–105. doi:10.1016/j.petlm.2015.07.003.

59. Levitt D, Pope GA. Selection and Screening of Polymers for Enhanced-Oil Recovery. SPE Symp. Improv. O*il Recover., Society of Petroleum Engineers*; 2008. doi:10.2118/113845-MS.
60. Thomas S. Enhanced oil recovery - An overview. Oil Gas Sci. Technol. - Rev. IFP, 2008, p. 9–19. doi:10.2516/ogst:2007060.
61. Raffa P, Broekhuis AA, Picchioni F. Polymeric surfactants for enhanced oil recovery: A review. *J Pet Sci Eng* 2016;145:723–33. doi:10.1016/j.petrol.2016.07.007.
62. Abbas AH, Sulaiman WRW, Jaafar MZ, Gbadamosi AO, Ebrahimi SS, Elrufai A. Numerical study for continuous surfactant flooding considering adsorption in heterogeneous reservoir. *J King Saud Univ - Eng Sci* 2018. doi:10.1016/j.jksues.2018.06.001.
63. Sheng JJ. Modern Chemical Enhanced Oil Recovery. 2011. doi:10.1016/B978-1-85617-745-0.00001-2.
64. Liu S, Li RF, Miller CA, Hirasaki GJ. ASP Process: Wide Range of Conditions for Good Recovery. *SPE Symp Improv Oil Recover* 2008:1–18. doi:10.2118/113936-MS.
65. Liu Q, Dong M, Ma S, Tu Y. Surfactant enhanced alkaline flooding for Western Canadian heavy oil recovery. *Colloids Surfaces A Physicochem Eng Asp* 2007;293:63–71. doi:10.1016/j.colsurfa.2006.07.013.
66. Romero-Zern L. Advances in Enhanced Oil Recovery Processes. Introd to Enhanc Oil Recover Process Bioremediation Oil-Contaminated Sites 2012. doi:10.5772/45947.
67. Rosen MJ, Wang H, Shen P, Zhu Y. Ultralow interfacial tension for enhanced oil recovery at very low surfactant concentrations. Langmuir 2005;21:3749–56. doi:10.1021/la0400959.
68. Wu Y, Chen W, Dai C, Huang Y, Li H, Zhao M, et al. Reducing surfactant adsorption on rock by silica nanoparticles for enhanced oil recovery. J Pet Sci Eng 2017;153:283–7. doi:10.1016/j.petrol.2017.04.015.
69. Zhao M, Lv W, Li Y, Dai C, Wang X, Zhou H, et al. Study on the synergy between silica nanoparticles and surfactants for enhanced oil recovery during spontaneous imbibition. *J Mol Liq* 2018;261:373–8. doi:10.1016/j.molliq.2018.04.034.

70. Pei H, Zhang G, Ge J, Zhang J, Zhang Q. Investigation of synergy between nanoparticle and surfactant in stabilizing oil-in-water emulsions for improved heavy oil recovery. Colloids Surfaces A Physicochem Eng Asp 2015;484:478–84. doi:10.1016/j.colsurfa.2015.08.025.
71. Mobaraki S, Zakavi M, Mahmoodi O, Omidvar Sorkhabadi M, Khalilinezhad SS, Shiri Torkmani R. An experimental study on the mechanisms of enhancing oil recovery by nanoparticles-assisted surfactant flood. *Geosystem Eng* 2018. doi:10.1080/12269328.2018.1515670.
72. Bazazi P, Gates ID, Sanati Nezhad A, Hejazi SH. Silica-Based Nanofluid Heavy Oil Recovery A Microfluidic Approach. SPE Canada Heavy Oil Tech. Conf., *Society of Petroleum Engineers*; 2017. doi:10.2118/185008-MS.
73. Zargartalebi M, Barati N, Kharrat R. Influences of hydrophilic and hydrophobic silica nanoparticles on anionic surfactant properties: Interfacial and adsorption behaviors. *J Pet Sci Eng* 2014;119:36–43. doi:10.1016/j.petrol.2014.04.010.
74. Ahmadi MA, Shadizadeh SR. Induced effect of adding nano silica on adsorption of a natural surfactant onto sandstone rock: Experimental and theoretical study. *J Pet Sci Eng* 2013;112:239–47. doi:10.1016/j.petrol.2013.11.010.
75. Johannesen EB, Graue A. Mobilization of remaining oil - Emphasis on capillary number and wnttability. Soc Pet Eng - 2nd Int Oil Conf Exhib Mex 2007 2007:470–5.
76. Fulcher RA, Ertekin T, Stahl CD. Effect of Capillary Number and Its Constituents on Two-Phase Relative Permeability Curves. *JPT, J Pet Technol* 1985;37:249–60. doi:10.2118/12170-PA.
77. Wei B, Romero-Zerón L, Rodrigue D. Oil displacement mechanisms of viscoelastic polymers in enhanced oil recovery (EOR): a review. *J Pet Explor* Prod Technol 2014;4:113–21. doi:10.1007/s13202-013-0087-5.
78. Mohammed M, Babadagli T. Wettability alteration: A comprehensive review of materials/methods and testing the selected ones on heavy-oil containing oil-wet systems. *Adv Colloid Interface Sci* 2015;220:54–77. doi:10.1016/j.cis.2015.02.006.

79. Alhammadi AM, Alratrout A, Singh K, Bijeljic B, Blunt MJ. In situ characterization of mixed-wettability in a reservoir rock at subsurface conditions. Sci Rep 2017;7. doi:10.1038/s41598-017-10992-w.
80. Christensen M, Tanino Y. Waterflood Oil Recovery from Mixed-Wet Limestone: Dependence upon the Contact Angle. Energy and Fuels 2017;31:1529–35. doi:10.1021/acs.energyfuels.6b03249.
81. Alvarez JO, Schechter DS. Wettability alteration and spontaneous imbibition in unconventional liquid reservoirs by surfactant additives. SPE Reserv. Eval. Eng., vol. 20, *Society of Petroleum Engineers*; 2017, p. 107–17. doi:10.2118/177057-PA.
82. Kathel P, Mohanty KK. Wettability alteration in a tight oil reservoir. Energy and Fuels 2013;27:6460–8. doi:10.1021/ef4012752.
83. Negin C, Ali S, Xie Q. Most common surfactants employed in chemical enhanced oil recovery. Petroleum 2017;3:197–211. doi:10.1016/j.petlm.2016.11.007.
84. Mirchi V, Saraji S, Goual L, Piri M. Dynamic interfacial tension and wettability of shale in the presence of surfactants at reservoir conditions. Fuel 2015;148:127–38. doi:10.1016/j.fuel.2015.01.077.
85. Jarrahian K, Seiedi O, Sheykhan M, Sefti MV, Ayatollahi S. Wettability alteration of carbonate rocks by surfactants: A mechanistic study. Colloids Surfaces *A Physicochem Eng Asp* 2012;410:1–10. doi:10.1016/j.colsurfa.2012.06.007.
86. Mohammad Salehi M, Omidvar P, Naeimi F. Salinity of injection water and its impact on oil recovery absolute permeability, residual oil saturation, interfacial tension and capillary pressure. *Egypt J Pet* 2017;26:301–12. doi:10.1016/j.ejpe.2016.05.003.
87. Salehi M, Johnson SJ, Liang JT. Enhanced wettability alteration by surfactants with multiple hydrophilic moieties. J Surfactants Deterg 2010;13:243–6. doi:10.1007/s11743-010-1193-8.
88. Ishiguro M, Koopal LK. Surfactant adsorption to soil components and soils. Adv Colloid Interface Sci 2016;231:59–102. doi:10.1016/j.cis.2016.01.006.
89. Woods DA. Dynamics of Surfactant Adsorption at Solid – Liquid Interfaces 2011.

90. Israelachvili J. Intermolecular and Surface Forces. Elsevier Inc.; 2011. doi:10.1016/C2009-0-21560-1.
91. Sheng JJ. Surfactant Flooding. 2011. doi:10.1016/b978-1-85617-745-0.00007-3.
92. Pal S, Mushtaq M, Banat F, Al Sumaiti AM. Review of surfactant-assisted chemical enhanced oil recovery for carbonate reservoirs: challenges and future perspectives. *Pet Sci* 2018;15:77–102. doi:10.1007/s12182-017-0198-6.
93. Mohammad Soleimani Zohr Shiri WH and MRM. Microemulsion-Based Synthesis Methodologies Used for Preparing Nanoparticle Systems of The Noble. Materials (Basel) 2019;12:1–8.
94. Kumar S, Panigrahi P, Saw RK, Mandal A. Interfacial Interaction of Cationic Surfactants and Its Effect on Wettability Alteration of Oil-Wet Carbonate Rock. Energy and Fuels 2016;30:2846–57. doi:10.1021/acs.energyfuels.6b00152.
95. Holmberg K. Surfactants and polymers in aqueous solution. John Wiley & Sons; 2003.
96. Nagy R, Kothencz R. Surfactants and their Investigation for Petroleum Industrial Applications. Int J Pet Petrochemical Eng 2015;1:11–21.
97. Surfactants and Polymers in Aqueous Solution, 2nd Edition | Wiley n.d. https://www.wiley.com/en-us/Surfactants+and+Polymers+in+Aqueous+Solution%2C+2nd+Edition-p-9780471498834 (accessed October 30, 2019).
98. Holmberg K, Bo J, Kronberg B. Solutions and Polymers in Aqueous Solutions. 2002.
99. Mehta SK, Kaur G. Microemulsions: Thermodynamic and Dynamic Properties. Thermodynamics 2011. doi:10.5772/12954.
100. Bijsterbosch BH. Characterization of silica surfaces by adsorption from solution. Investigations into the mechanism of adsorption of cationic surfactants. *J Colloid Interface Sci* 1974;47:186–98. doi:10.1016/0021-9797(74)90092-7.

101. Advances in interfacial phenomena of particulate/solution/gas systems : applications to flotation research / P. Somasundaran and R. B. Grieves, editors. - Version details - Trove n.d. https://trove.nla.gov.au/work/21435513?selectedversion=NBD237062 (accessed October 30, 2019).
102. Zhang L, Somasundaran P, Mielczarski J, Mielczarski E. Adsorption mechanism of n-dodecyl-β-D-maltoside on alumina. J Colloid Interface Sci 2002;256:16–22. doi:10.1006/jcis.2001.7858.
103. Park S, Lee ES, Sulaiman WRW. Adsorption behaviors of surfactants for chemical flooding in enhanced oil recovery. *J Ind Eng Chem* 2015;21:1239–45. doi:10.1016/j.jiec.2014.05.040.
104. Curbelo FDS, Garnica AIC, Neto ELB. Enhanced oil recovery and adsorption of ionic surfactant. *Pet Sci Technol* 2013;31:663–71. doi:10.1080/10916466.2010.523750.
105. Behrens EJ. Investigation of loss of surfactants during enhanced oil recovery applications - adsorption of surfactants onto clay materials. Master Sci Ind Chem Biotechnol Nor Univ Sci Technol 2013:101.
106. Wesson LL, Harwell JH. Surfactant Adsorption in Porous Media. 2010. doi:10.1017/cbo9780511524844.005.
107. Be´rube´ YG, de Bruyn PL. Adsorption at the rutile-solution interface. J Colloid Interface Sci 1968;28:92–105. doi:10.1016/0021-9797(68)90211-7.
108. Zhongyun L, Jia J, Qingjun L, Zhang P, Tweheyo MT, Austad T, et al. Improved Oil Recovery by Low-Salinity Waterflooding. *J Pet Sci Eng* 2014;55:149–66. doi:10.1021/je100198g.
109. Bellmann C, Synytska A, Caspari A, Drechsler A, Grundke K. Electrokinetic investigation of surfactant adsorption. *J Colloid Interface Sci* 2007;309:225–30. doi:10.1016/j.jcis.2007.02.003.
110. Somasundaran P, Huang L. Adsorption/aggregation of surfactants and their mixtures at solid-liquid interfaces. *Adv Colloid Interface Sci* 2000;88:179–208. doi:10.1016/S0001-8686(00)00044-0.
111. Xu QUN, Vasudevan T V, Somasundaran P. Adsorption of Anionic-Nonionic and Cationic-Nonionic Surfactant Mixtures o n Kaolinite 1991;142:528–34.

112. Ahmadall T, Gonzalez MVM V., Harwell JH, Scamehorn JF, Tabatabal A, Gonzalez MVM V., et al. Reducing surfactant adsorption in carbonate reservoirs. *SPE Reserv Eng (Society Pet Eng* 1993;8:117–22. doi:10.2118/24105-PA.
113. Budhathoki M, Barnee SHR, Shiau BJ, Harwell JH. Improved oil recovery by reducing surfactant adsorption with polyelectrolyte in high saline brine. Colloids Surfaces *A Physicochem Eng Asp* 2016;498:66–73. doi:10.1016/j.colsurfa.2016.03.012.
114. Budhathoki M, Barnee SHR, Shiau BJ, Harwell JH. Improved oil recovery by reducing surfactant adsorption with polyelectrolyte in high saline brine. Colloids Surfaces *A Physicochem Eng Asp* 2016;498:66–73. doi:10.1016/j.colsurfa.2016.03.012.
115. Tabary R, Bazin B, Douarche F, Moreau P, Oukhemanou-Destremaut F. Surfactant flooding in challenging conditions: Towards hard brines and high temperatures. SPE Middle East Oil Gas Show Conf MEOS, Proc 2013;3:1637–52. doi:10.2118/164359-ms.
116. Mannhardt K, Schramm LL, Novosad JJ. Effect of rock type and brine composition on adsorption of two foam-forming surfactants. S*PE Adv Technol Ser* 1993;1:212–8. doi:10.2118/20463-pa.
117. Schramm LL, Mannhardt K, Novosad JJ. Electrokinetic properties of reservoir rock particles. *Colloids and Surfaces* 1991;55:309–31. doi:10.1016/0166-6622(91)80102-T.
118. Hunter W. Preface. 2011. doi:10.3138/9781487599768-001.
119. Gulamali MY, Leinov E, Jackson MD. Self-potential anomalies induced by water injection into hydrocarbon reservoirs. *Geophysics* 2011;76:F283. doi:10.1190/1.3596010.
120. Li HCC, de Bruyn PLL. Electrokinetic and adsorption studies on quartz. Surf Sci 1966;5:203–20. doi:10.1016/0039-6028(66)90082-3.
121. Glover P, Revil A. Nature of surface electrical conductivity in natural sands, sandstones, and clays. *Geophys Res Lett* 1998;25:691–4.
122. Knauth LP. Silica: physical behavior, geochemistry and materials applications. Rev Mineral 1994.

123. Lorne B, Perrier F, Avouac J-P. Streaming potential measurements: 1. Properties of the electrical double layer from crushed rock samples. *J Geophys Res Solid Earth* 1999;104:17857–77. doi:10.1029/1999jb900156.
124. Tombácz E, Szekeres M. Surface charge heterogeneity of kaolinite in aqueous suspension in comparison with montmorillonite. *Appl Clay Sci* 2006;34:105–24. doi:10.1016/j.clay.2006.05.009.
125. Bujdák J, Rode BM. The effect of clay structure on peptide bond formation catalysis. *J Mol Catal A Chem* 1999;144:129–36. doi:10.1016/S1381-1169(98)00342-2.
126. Jaafar MZ. Measurement of Streaming Potential for Oilfield Monitoring in Intelligent Wells 2009.
127. Morari G. Clays, Clay Minerals and Ceramic Materials Based on Clay Minerals. 2016.
128. Zeta Potential in Colloid Science: Principles and Applications - Robert J. Hunter (accessed November 23, 2019).
129. Tombácz E, Szekeres M. Surface charge heterogeneity of kaolinite in aqueous suspension in comparison with montmorillonite. *Appl Clay Sc*i 2006;34:105–24. doi:10.1016/j.clay.2006.05.009.
130. Revil A, Pezard PA. Streaming potential in porous media 1 . Theory of the zeta potential 1999;104:21–31.
131. Lorne B, Perrier F. Streaming potential measurements 2 . Relationship between electrical and hydraulic flow patterns from rock samples during deformation (c) (d) k = c S • r2 , 1999;104.
132. 658 Buchbesprechungen 1972:658.
133. Electroplating: Basic Principles, Processes and Practice - Nasser Kanani - (accessed November 23, 2019).
134. Par M. GOUY. De La Charge Électrique a La Surface D'Un Électrolyte. J.de Physs 1910:457–68.
135. Chapman DL. LI. A contribution to the theory of electrocapillarity . London, Edinburgh, *Dublin Philos Mag J Sci* 1913;25:475–81. doi:10.1080/14786440408634187.
136. Bockris JO (John O., Reddy AKN, Gamboa-Aldeco M. Modern electrochemistry. Volume 2A, Fundamentals of electrodics. Kluwer Academic; 2002.

137. Grahame DC. The electrical double layer and the theory of electrocapillarity. *Chem Rev* 1947;41:441–501. doi:10.1021/cr60130a002.
138. Moulin P, Roques H. Zeta potential measurement of calcium carbonate. *J Colloid Interface Sci* 2003;261:115–26. doi:10.1016/S0021-9797(03)00057-2.
139. Zhang S, Moskalenko C, Berguiga L, Elezgaray J, Argoul F. Gouy diffuse layer modelling in phosphate buffers. J Electroanal Chem 2007;603:107–12. doi:10.1016/j.jelechem.2007.01.023.
140. Atkins PW (Peter W, De Paula J, Keeler J. Atkins' Physical chemistry. n.d.
141. Charges S, Do HOW, Arise T. 8. charged interfaces n.d.:194–211.
142. Lützenkirchen J, Preočanin T, Kovačević D, Tomišić V, Lövgren L, Kallay N. Potentiometric titrations as a tool for surface charge determination. Croat Chem Acta 2012;85:391–417. doi:10.5562/cca2062.
143. Dukhin A, Dukhin S, Goetz P. Electrokinetics at high ionic strength and hypothesis of the double layer with zero surface charge. *Langmuir* 2005;21:9990–7. doi:10.1021/la050480d.
144. Isaacs EE, Chow RS. Practical Aspects of Emulsion Stability 1992:51–77. doi:10.1021/ba-1992-0231.ch002.
145. Delgado A V., González-Caballero F, Hunter RJ, Koopal LK, Lyklema J. Measurement and interpretation of electrokinetic phenomena: (IUPAC technical report). *Pure Appl Chem* 2005;77:1753–805. doi:10.1351/pac200577101753.
146. Vinogradov J, Jaafar MZ, Jackson MD. Measurement of streaming potential coupling coefficient in sandstones saturated with natural and artificial brines at high salinity. *J Geophys Res Solid Earth* 2010;115:1–18. doi:10.1029/2010JB007593.
147. Van Der Heyden FHJ, Stein D, Besteman K, Lemay SG, Dekker C. Charge inversion at high ionic strength studied by streaming currents. *Phys Rev Lett* 2006;96:1–4. doi:10.1103/PhysRevLett.96.224502.
148. Bouriat P, Saulnier P, Brochette P, Graciaa A, Lachaise J. A convenient apparatus to determine the zeta potential of grains by electro-osmosis. *J Colloid Interface Sci* 1999;209:445–8. doi:10.1006/jcis.1998.5902.
149. Greenwood R. Review of the measurement of zeta potentials in concentrated aqueous suspensions using electroacoustics. *Adv Colloid Interface Sci* 2003;106:55–81. doi:10.1016/S0001-8686(03)00105-2.

150. Doren A, Lemaitre J, Rouxhet PG. Determination of the zeta potential of macroscopic specimens using microelectrophoresis. *J Colloid Interface Sci* 1989;130:146–56. doi:10.1016/0021-9797(89)90085-4.
151. Comparison of 3 Electrokinetic Methods To Determine the Zeta-potential of Solid-surfaces (accessed November 25, 2019).
152. Hiemenz P, Rajagopalan R. Principles of Colloid and Surface Chemistry, Third Edition, Revised and Expanded, 3rd Edition. n.d.
153. Surfactants and Interfacial Phenomena - Milton J. Rosen, Joy T. Kunjappu - (accessed November 27, 2019).
154. Bellmann C, Synytska A, Caspari A, Drechsler A, Grundke K. Electrokinetic investigation of surfactant adsorption. *J Colloid Interface Sci* 2007;309:225–30. doi:10.1016/j.jcis.2007.02.003.
155. Fuerstenau DW. Streaming potential studies on quartz in solutions of aminium acetates in relation to the formation of hemi-micelles at the quartz-solution interface. J Phys Chem 1956;60:981–5. doi:10.1021/j150541a039.
156. Kosmulski M. Chemical Properties of Material Surfaces 2001. doi:10.1201/9780367800482.
157. Karraker KA, Radke CJ. Disjoining pressures, zeta potentials and surface tensions of aqueous non-ionic surfactant/electrolyte solutions: Theory and comparison to experiment. *Adv Colloid Interface Sci* 2002;96:231–64. doi:10.1016/S0001-8686(01)00083-5.
158. Dimov NK, Kolev VL, Kralchevsky PA, Lyutov LG, Broze G, Mehreteab A. Adsorption of Ionic Surfactants on Solid Particles Determined by Zeta-Potential Measurements : *Competitive Binding of Counterions* 2002;32:23–32. doi:10.1006/jcis.2001.7821.
159. Alargova RG, Vakarelsky IY, Paunov VN, Stoyanov SD, Kralchevsky PA, Mehreteab A, et al. Properties of amphoteric surfactants studied by ζ-potential measurements with latex particles. *Langmuir* 1998;14:1996–2003. doi:10.1021/la970958g.
160. Oruwori AE, Ikiensikimama SS, Engineering G. SPE 136997 Determination of Water Salinities in Hydrocarbon Bearing Reservoirs of Some Niger Delta Fields - Nigeria 2010:1–10.
161. Lake LW, Fanchi JR. Petroleum Engineering Handbook - General Engineering. vol. I. 2006.

162. Hydrocarbon Reservoir - an overview | ScienceDirect Topics (accessed November 25, 2019).
163. Reservoirs S. Sandstone Reservoirs Depositional Environment n.d.
164. Joni IM, Nulhakim L, Vanitha M, Panatarani C. Characteristics of crystalline silica (SiO 2) particles prepared by simple solution method using sodium silicate (Na 2 SiO 3) precursor. *J Phys Conf Ser* 2018;1080. doi:10.1088/1742-6596/1080/1/012006.
165. Dewi R, Agusnar H, Alfian Z, Tamrin. Characterization of technical kaolin using XRF, SEM, XRD, FTIR and its potentials as industrial raw materials. J Phys Conf Ser 2018;1116. doi:10.1088/1742-6596/1116/4/042010.
166. Nayak PS, Singh BK. Instrumental Characterization of Clay by FTIR, XRF, BET and, TPD-NH3. Bull Mater Sci 2007;30:235–8.
167. Characteristics of crystalline silica (SiO2) particles prepared by simple solution method using sodium silicate (Na2SiO3) precursor | Request PDF n.d. https://www.researchgate.net/publication/327790651_Characteristics_of_crystalline_silica_SiO2_particles_prepared_by_simple_solution_method_using_sodium_silicate_Na2SiO3_precursor (accessed December 2, 2019).
168. Bansal V, Rautaray D, Bharde A, Ahire K, Sanyal A, Ahmad A, et al. Fungus-mediated biosynthesis of silica and titania particles. *J Mater Chem* 2005;15:2583–9. doi:10.1039/b503008k.
169. Murray HH. Applied clay mineralogy today and tomorrow. *Clay Mine*r 1999;34:39–49. doi:10.1180/000985599546055.
170. Kobayashi M, Skarba M, Galletto P, Cakara D, Borkovec M. Effects of heat treatment on the aggregation and charging of Stöber-type silica. J Colloid Interface Sci 2005;292:139–47. doi:10.1016/j.jcis.2005.05.093.
171. Li P, Ishiguro M. Adsorption of anionic surfactant (sodium dodecyl sulfate) on silica. Soil Sci Plant Nutr 2016;62:223–9. doi:10.1080/00380768.2016.1191969.
172. Peng L, Qisui W, Xi L, Chaocan Z. Investigation of the states of water and OH groups on the surface of silica. Colloids Surfaces A Physicochem Eng Asp 2009;334:112–5. doi:10.1016/j.colsurfa.2008.10.028.
173. Ferris AP, Jepson WB. The exchange capacities of kaolinite and the preparation of homoionic clays. *J Colloid Interface Sci* 1975;51:245–59. doi:10.1016/0021-9797(75)90110-1.

174. Smith RW, Narimatsu Y. Electrokinetic behavior of kaolinite in surfactant solutions as measured by both the microelectrophoresis and streaming potential methods. *Miner Eng* 1993;6:753–63. doi:10.1016/0892-6875(93)90006-9.
175. Williams DJA, Williams KP. Electrophoresis and zeta potential of kaolinite. J Colloid Interface Sci 1978;65:79–87. doi:10.1016/0021-9797(78)90260-6.
176. Yuan J, Pruett RJ. Zeta potential and related properties of kaolin clays from Georgia. Miner Metall Process 1998;15:50–2. doi:10.1007/bf03402787.
177. Miller JD, Nalaskowski J, Abdul B, Du H. Surface Characteristics of Kaolinite and Other Selected Two Layer Silicate Minerals. Can J Chem Eng 2008;85:617–24. doi:10.1002/cjce.5450850508.
178. Lyklema J. Fundamentals of interface and colloid science. Volume III, Liquid-fluid interfaces. Academic Press; 2000.
179. Kosmulski M, Eriksson P, Brancewicz C, Rosenholm JB. Zeta potentials of monodispersed , spherical silica particles in mixed solvents as a function of cesium chloride concentration 2000;162:37–48.
180. Shi L, Olsson MHM, Hassenkam T, Stipp SLS. A pH-Resolved View of the Low Salinity Effect in Sandstone Reservoirs. Energy and Fuels 2016;30:5346–54. doi:10.1021/acs.energyfuels.6b00338.
181. Thyne G, Brady P. Evaluation of formation water chemistry and scale prediction: Bakken Shale. *Appl Geochemistry* 2016;75:107–13. doi:10.1016/j.apgeochem.2016.10.015.
182. Li Y, Li W, Xiao Q, He N, Ren Z, Lartey C, et al. The influence of common monovalent and divalent chlorides on chalcopyrite flotation. Minerals 2017;7:1–10. doi:10.3390/min7070111.
183. Kollannur NJ, Arnepalli DN. Methodology for Determining Point of Zero Salt Effect of Clays in Terms of Surface Charge Properties. J Mater Civ Eng 2019;31:1–9. doi:10.1061/(ASCE)MT.1943-5533.0002947.
184. Tansub W, Tuitemwong K, Limsuwan P, Theparoonrat S, Tuitemwong P. Synthesis of antibodies-conjugated fluorescent dye-doped silica nanoparticles for a rapid single step detection of campylobacter jejuni in live poultry. J Nanomater 2012;2012. doi:10.1155/2012/865186.

185. Li HR, Li ZQ, Song XW, Li CB, Guo LL, Zhang L, et al. Effect of organic alkalis on interfacial tensions of surfactant/polymer solutions against hydrocarbons. Energy and Fuels 2015;29:459–66. doi:10.1021/ef5019862.
186. Ren ZH. Mechanism of the Salt E ff ect on Micellization of an *Aminosulfonate Amphoteric Surfactant* 2015. doi:10.1021/acs.iecr.5b02169.